OPTIMIZATION DESIGN OF MTH-BAND FIR FILTERS WITH APPLICATION TO IMAGE PROCESSING

GUANQUN CHEN

A THESIS

IN

THE CONCORDIA INSTITUTE FOR ELECTRICAL AND COMPUTER ENGINEERING

PRESENTED IN PARTIAL FULFILLMENT OF THE REQUIREMENTS

FOR THE DEGREE OF MASTER OF APPLIED SCIENCE IN ELECTRICAL AND

COMPUTER ENGINEERING

CONCORDIA UNIVERSITY

MONTRÉAL, QUÉBEC, CANADA

SEPTEMBER 2010

Your file Votre référence
ISBN: 978-0-494-71024-1
Our file Notre référence
ISBN: 978-0-494-71024-1

ABSTRACT

Optimization Design of Mth-Band FIR filters with Application to Image Processing

Guanqun Chen

Cone programming (CP) is a class of convex optimization technique, in which a linear objective function is minimized over the intersection of a set of affine constraints. Such constraints could be linear or convex, equalities or inequalities. Owing to its powerful optimization capability as well as flexibility in accommodating various constraints, the cone programming finds wide applications in digital filter design. In this thesis, fundamentals of linear-phase Mth-band FIR filters are first introduced, which include the time-domain interpolation condition and the desired frequency specifications. The restriction of the interpolation matrix **M** for linear-phase two-dimensional (2-D) Mth-band filters is also discussed by considering both the interpolation condition and the symmetry of the impulse response of the 2-D filter. Based on the analysis of the Mth-band properties, a semidefinite programming (SDP) optimization approach is developed to design linear-phase 1-D and 2-D Mth-band filters. The 2-D SDP optimization design problem is modeled based on both the mini-max and the least-square error criteria. In contrast to the 1-D based design,

the 2-D direct SDP design can offer an optimal equiripple result. A second-order cone programming (SOCP) optimization approach is then presented as an alternative for the design of Mth-band filters. The performances as well as the design complexity of these two design approaches are justified through numerical design examples. Simulation results show that the performance of the SOCP approach is better than that of the SDP approach for 1-D Mth-band filter design due to its reduced computational complexity for the worst-case, whereas the SDP approach is more appropriate for the 2-D Mth-band filter design than the SOCP approach because of its efficient and simple optimization structure. Moreover, the designed Mth-band filters are proved useful in image interpolation according to both the visual quality and the peak signal-to-noise ratio (PSNR) for the images with different levels of details.

Acknowledgments

First and foremost, I would like to express my deepest gratitude and appreciation to my supervisor, Dr. Wei-Ping Zhu, for his guidance and support throughout the span of this research. He is a knowledgeable, nice, energetic and open professor with deep insight into my research. It is an honor to work under his supervision.

I would also like to thank all my friends, especially Chao Wu, Qin Zhu, Chiu-Chih Chen, and Yue Chen, for their friendship, understanding and support.

Above all, my greatest thanks go to my parents, whose consistent encouragement has been my energy and confidence to complete the advanced study. Their unconditional support, care, and love have helped me overcome the difficulties in my life.

Contents

List of Figures

List of Tables

List of Abbreviations

FPD	Fundamental parallelepiped
Fcone	Free vector constraint
Rcone	Rotated quadratic cone constraint
SDP	Semidefinite programming
SOCP	Second-order programming
SPD	Symmetric parallelepiped
Scone	Second-order cone constraint

List of Symbols

A	Amplitude response
A_d	Ideal amplitude response
e_m	Mini-max error
e_l	Least-square error
e_{tm}	Quadratic mini-max error
e_{tl}	Quadratic least-square error
$\mathbf{F}(x)$	Tridiagonal matrix
$\mathbf{G}$	Selection matrix
$\mathbf{G}_t$	2-D selection matrix
H	Frequency response
$\mathbf{H}_c$	Compact expression of 2-D frequency response
H_d	Ideal frequency response
H_{dr}	Real party of ideal frequency response
H_{di}	Imaginary party of ideal frequency response
h	Impulse response

h_a	Linear-phase impulse response
h_{ta}	Transformation of $\mathbf{H}_c$
$\mathbf{I}$	Identity matrix
$\mathbf{M}$	Interpolation matrix
M	1-D Interpolation coefficient (positive integer)
M_1	Interpolation coefficient of horizontal axis (positive integer)
M_2	Interpolation coefficient of vertical axis (positive integer)
M_d	Sampling factor of compressor (positive integer)
M_u	Sampling factor of expander (positive integer)
$\mathbf{N}_c$	Symmetrical center of 2-D impulse response
$\mathcal{N}$	Support region of 2-D impulse response
$\mathbf{x}$	Optimization variable
$\mathbf{O}_n$	All-zero vector
R_p	Number of ω in passband region
R_s	Number of ω in stopband region
$\mathbf{Q}$	Unimodular integer matrix
Λ	Semidefinite positive matrix in least-square design
Υ	Semidefinite positive matrix in mini-max design
Ω	Region of $[-\pi,\ \pi]$
Ω_p	Passband region
Ω_s	Stopband region
Ω_t	Square region of $[-\pi,\ \pi]^2$

Ω_{tp}	Passband of 2-D frequency
Ω_{ts}	Stopband of 2-D frequency
ω_p	Passband cutoff frequency
ω_s	Stopband cutoff frequency
ω_c	Center frequency of transition band
δ_m	Upper bound of square of mini-max error
δ_l	Upper bound of least-square error
δ_{tm}	Upper bound of square of quadratic mini-max error
δ_{tl}	Upper bound of quadratic least-square error
ζ_m	Upper bound of mini-max error
ζ_l	Upper bound of square root of least-square error
ζ_{tm}	Upper bound of quadratic mini-max error
ζ_{tl}	Upper bound of square root of quadratic least-square error

Chapter 1

Introduction

1.1 Background

An ever-increasing trend of research activities in the area of multirate signal processing calls for the development of highly efficient interpolators and decimators. A multirate system including a decimator and an interpolator, which is characterized by sampling rate conversion, can be employed in a wide range of engineering fields, such as linear interpolation, perfect reconstruction filter banks, and speech and image processing. Among such a system, Mth-band filter is the core factor which is utilized before a compressor to avoid the aliasing in the decimation as well as after an expander to reconstruct the sequence in the interpolation. The block diagram of this multirate system is illustrated in Figure 1.1, where M_d and M_u represent the factor of the sampling rate compressor and expander, respectively. $H_1(z)$ and $H_2(z)$ are both low-pass Mth-band filters with cutoff frequencies specified by π/M_d and π/M_u. If the Mth-band filter has an ideal frequency response, a

perfect interpolation and decimation performance would be achieved.

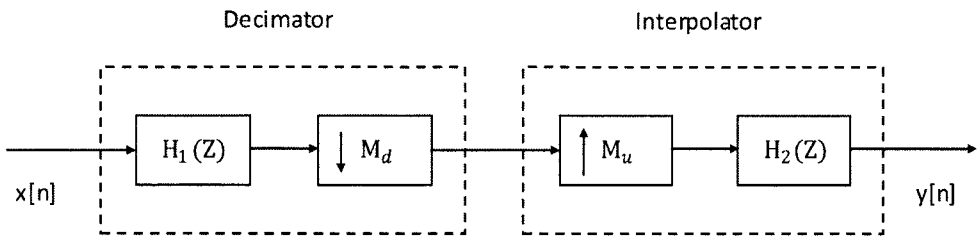

Figure 1.1: The multirate system of decimation and interpolation

An ideal low-pass Mth-band FIR filter has a time-domain property, i.e., its impulse response $h[n]$ gives a zero-crossing every M samples, namely, $h[nM] = \frac{1}{M}\delta[n]$. This property is referred to as the interpolation condition since the output signal of an Mth-band filter is constructed by inserting $M-1$ samples between every two consecutive input samples while leaving the original input samples unchanged. Thus, it can be employed to reconstruct the sequence in the interpolator as shown in Figure 1.1. On the other hand, in the frequency-domain, it is derived from the interpolation condition that the cutoff frequency of an Mth-band filter is exactly at π/M. Due to this cutoff frequency property, if a signal is downsampled by a factor of M, it is necessary to be prefiltered by an Mth-band filter to limit its bandwidth within the interval of $[-\pi/M \ \ \pi/M]$, then the aliasing can be prevented. Although the interpolation condition is a natural characteristic of an ideal Mth-band filter, it is not easy to be realized by a practical filter, since the existing design methods do not support or accommodate this feature. In the last three decades, numerous papers were published on filter design to obtain an approximation to the ideal frequency response. However, most of those findings were hardly useful in satisfying the time-domain constraints of the designed filter, such as the interpolation condition of Mth-band filters.

In late 90s, the cone programming, a relatively new subfield of optimization technique, has been introduced in filter design and quite a few related software packages have been available for research purposes. Since then, some special constraints could be implemented in the design. With the fast development in this area over the past decade, the semidefinite programming (SDP) and the second order cone programming (SOCP) have become a widely-recognized important technique for digital filter design.

1.2 State of the Art Techniques

The FIR filter design can be classified as noniterative or iterative methods [1]. The former usually means the window method which obtains the approximation of an ideal filter by truncating the ideal impulse response with a window function. It is the simplest way of FIR filter design and entails a relatively small amount of computation. However, the window method fails to accommodate the interpolation condition of Mth-band filter since the window function is governed by certain specifications. For example, the Kaiser window has a pair of parameters: the length N and the shape parameter β, which can only provide the designed filter with the trade-off between the transition band width, error ripples and filter length. Moreover, the window method leads to the suboptimal design category where the order of the designed filter that has to satisfy the prescribed specifications may not be the lowest. On the other hand, iterative methods can obtain the optimal approximation to a desired filter based on an optimization criterion. Moreover, this class of design method is particularly important when extra conditions, such as the time-domain condition of the

Mth-band filter, has to be met by the designed filter. As such, we will review some typical optimal design methods for Mth-band filters.

As early as 1970s, the idea of optimal filter design was proposed and developed to a large extent for general FIR filters. In such a design, an error function, also known as objective function, is formulated for the desired frequency response under certain criterion and is then minimized by using an optimization algorithm to get the best approximation to the desired filter. Two commonly employed criteria are the mini-max and the least-square error. In those years, the most frequently used optimization algorithm was Remez exchange algorithm, which led to a great deal of mini-max design methods, including the classical weighted-Chebyshev method [2] and the powerful Parks and Mclellan program [3]. Although this type of methods can offer optimal equiripple solutions for a large family of linear-phase FIR filters, none of them can directly deal with the time-domain constraints. This motivated researchers to seek out the indirect way for the design of Mth-band filters, where the time-domain interpolation condition is realized by the extra operation after obtaining the optimal approximation to the desired filter.

Perhaps, the first attempt for Mth-band filters can be traced back to 1982, when the time-domain interpolation condition and the related frequency property of the Mth-band filter was presented systematically by Mintzer [4]. In Mintzer's design, an optimal approximation $H(e^{j\omega})$ to the desired Mth-band filter is obtained via the Parks and Mclellan program. However, $H(e^{j\omega})$ is actual not the Mth-band filter, since the time-domain interpolation condition cannot be satisfied. In particular, the coefficients represented by $h[nM]$ which are supposed to be zero are very small values. Thus, in order to strictly satisfy the

interpolation condition, Mintzer reset the coefficients $h[nM]$ to zero except $h[0] = 1/M$ while leaving other samples of $h[n]$ unchanged. Thus, the Mth-band filter designed by Mintzer's method is not truly optimal and is in a loss of the equiripple feature. However, as the earliest method for the design of Mth-band filters, Mintzer's work triggered subsequent research in this area.

A more reliable indirect way to satisfy the interpolation condition is on the basis of the precise transformation, as proposed by Vaidyanathan and Nguyen [5] in 1987. The idea of Vaidyanathan's design is to define a lower order prototype filter, from which the Mth-band filter can be constructed. They have deduced a specific relationship between the frequency response of the Mth-band filter and that of the prototype filter. The "trick" of this method is that the impulse response of an Mth-band filter determined by the prototype filter exactly satisfies the interpolation condition. Vaidyanathan gave detailed computation steps from the impulse response of the prototype filter to that of the Mth-band filter, and therefore, the problem is simplified to the design of a lower order prototype filter, which can be achieved easily by the general optimal method such as Parks and Mclellan program. The advantages of the Vaidyanathan's work over the Mintzer's method is that it is considerably faster and provides the equiripple results. However, the designed Mth-band filter also fails to be truly optimal since there exists a distortion in the computation process.

The other significant contribution of Vaidyanathan and Nguyen has been to introduce the eigenfilter approach [6] [7], which is able to cope with the time-domain constraints as well as the frequency-domain specifications. It is an optimal least-square design approach,

in which the objective function formulated as the sum of the quadratic passband and stopband errors is given in the form of $h^T P h$, where h is a vector related to the unknown coefficients of the designed filter, and P is a real, symmetric and positive-definite matrix. By minimizing the objective function, the optimal impulse response coefficients can be obtained as the eigenvector corresponding to the smallest eigenvalue of the matrix. The key factor of this approach is the vector h which is defined according to different time-domain constraints. For example, in the Mth-band filter design presented by Wisutmethangoon in 1999 [8], the vector is composed by unknown impulse response excluding the elements that are structurally zero, then the obtained optimal non-zero coefficients and the zeros are interleaved to construct the designed filter. Although the resulting filter satisfies the interpolation condition exactly, this method is not optimal considering the frequency-domain specifications and the interpolation condition as a whole, since the interpolation condition was not directly involved in the optimization process. As such, the objective of this research is to develop a direct design method in which all the impulse response coefficients of the designed filter are accommodated in the optimization problem such that the resulting filter can satisfy both the desired frequency response and the interpolation condition without any additional processing.

1.3 Research Motivation and Objectives

In the previous two sections, some existing optimal methods for the design of FIR digital filters have been reviewed. It was shown that neither the Parks and Mclellan program

nor the eigenfilter approach can offer a direct design of Mth-band filters, since the time-domain interpolation condition cannot be satisfied exactly. In these methods, actually, an Mth-band filter can only be obtained indirectly, where the filter coefficients related to the interpolation condition are reset to zero in the post-processing when the filter is designed. Hence, it is imperative to develop efficient optimal approaches that can design Mth-band filters directly. Fortunately, with the development of advanced optimization algorithms, some optimal design methods have been proposed to make the designed filter satisfy various requirements. Among them, the semidefinite programming [9] [10] [11] is primarily concerned with the design of FIR digital filters owing to the following features. (1) It is a generic tool for the design of a wide variety of digital filters, regardless of 1-D or 2-D, FIR or IIR, mini-max or least-square design. (2) It can accommodate extra constraints, such as the interpolation condition and flatness in the form of a linear inequality or equality. (3) It is sufficiently accurate since highly efficient and user-friendly software is available for the design. In addition, second order cone programming [12] [13] as a special case of the SDP has also attracted lots of researchers. Although it is less general than SDP, it also has all of the above advantages. Thus, it seems that both SDP and SOCP are suitable for the design of Mth-band filters.

Having the above observation in mind, the present thesis will focus on a direct optimal design of Mth-band filters. The SDP approach is presented first with an emphasis on its flexility of accommodating the time-domain interpolation condition. Next, the SOCP approach will be studied and compared with the SDP approach towards the design complexity. Moveover, both methods are extended for the design of two-dimensional (2-D)

Mth-band FIR filters. Finally, the Mth-band filters designed by the proposed approaches will be applied to image interpolation.

1.4 Organization of the Thesis

The thesis is organized as follows:

Chapter 1: The proceeding chapter provides an overview on the existing optimization methods for the design of FIR digital filters. It is shown that neither the Parks and Mclellan program nor the eigenfilter approach can offer a direct design of Mth-band FIR filters, which supports the motivation of the proposed work.

Chapter 2: Fundamentals of three classes of Mth-band filters are introduced, including 1-D, 2-D rectangular and 2-D diamond-shaped Mth-band filters. Both the time- and frequency-domain constraints for each case are given in detail. Moveover, the restriction of the interpolation matrix $\mathbf{M}$ for the 2-D linear-phase diamond-shaped Mth-band filters is discussed by considering the constraint and symmetry of 2-D impulse responses.

Chapter 3: An efficient optimazation approach, known as the semidefinite programming (SDP) approach, is investigated for the design of linear-phase Mth-band FIR filters with an emphasis on the 2-D direct SDP design. Both mini-max and lease-square error criteria are employed in the SDP optimization design problem. The performance of the SDP approach is evaluated in terms of the maximum error as well as the execution time by several design examples. The designed Mth-band filters are finally applied to image interpolation to confirm their interpolation property.

Chapter 4: A second-order cone programming (SOCP) approach is studied as an alternative for the design of linear-phase Mth-band FIR filters based on both the mini-max and the least-square error criteria. The SOCP approach is compared with the SDP approach towards the design performances as well as the computational complexity through numerical examples. The Mth-band filters designed via the SOCP approach are also applied as interpolation filters for image resizing.

Chapter 5: The final chapter summaries all the research work of this thesis and points out the possible research directions for future work.

1.5 Contributions

The main contributions of the the thesis are summarized as follows:

1. The possible choices of the interpolation matrix **M** for 2-D linear-phase diamond-shaped Mth-band filter are addressed by incorporating the interpolation condition and the quadrantal symmetry of the 2-D impulse response.

2. Two optimization approaches are investigated for the design of linear-phase 1-D and 2-D nonseparable Mth-band filters. The way of accommodating the interpolation condition in the optimization design problem is proposed in detail. It is shown that both of the two approaches are useful in offering equiripple optimal or nearly optimal linear-phase Mth-band filters. More specifically, the performance of the SOCP approach is better than that of the SDP approach for 1-D Mth-band filter design due to its reduced computational

complexity for the worst-case, whereas the SDP approach is more appropriate for 2-D Mth-band filter design than the SOCP approach because of its efficient and simple optimization structure.

3. The Mth-band filter designed via the SDP and SOCP approaches are applied to image resizing. The high interpolation quality of the resized images indicates that both of the two approaches can make the designed filters, regardless of 1-D or 2-D, exactly satisfy the time-domain interpolation condition.

Chapter 2

Fundamentals of Mth-band FIR Filters

2.1 Introduction

In the area of digital signal processing, FIR filter plays a key role in view of its inherent stability, linear-phase and no feedback property. It has found extensive applications in various engineering fields such as telecommunications, electronics, speech and image processing. Among these applications, some FIR filters are required to achieve much more complex and selective designs, for example, filters applied in the decimator and interpolator are Mth-band FIR filters which should satisfy the time-domain constraint $h(nM) = \frac{1}{M}\delta(n)$ besides its frequency property. The time-domain property makes Mth-band filters particularly useful in image interpolation and perfect reconstruction. However, the interpolation condition is in general difficult to be realized directly by most of the existing optimal design methods, including the famous Parks and Mclellan program and eigenfilter approach, since it cannot be involved in the optimization process. Thus, the properties of Mth-band filters

are proposed in this chapter to prepare for the development of two optimization algorithms for Mth-band filters in the following chapters.

In this chapter, we will first review the properties of 1-D Mth-band filters, where its frequency-domain constraint is derived explicitly from the property $h(nM) = \frac{1}{M}\delta(n)$. Subsequently, the 2-D rectangular Mth-band filter is proposed as an direct extension of the 1-D case. Since the rectangular pattern is a specific interpolated version, we then develop a more general case, the 2-D diamond-shaped Mth-band filter, which is appropriate for a wide range of interpolation matrix **M**. However, we will show that the frequency-domain constraint of this case is much more complicated than the rectangular one.

2.2 Linear-Phase Mth-Band FIR Filters

2.2.1 Linear-Phase Property

In general, linear-phase is the desirable property of a FIR filter, where the group delay of the filter is constant. This property implies that all frequencies have equal delay times, resulting in no phase distortion. The lack of phase distortion is a major advantage in many engineering applications. Thus, only the linear-phase Mth-band FIR filter is considered in this thesis. Before the in depth study of Mth-band filters, it is necessary to briefly review the linear-phase property at first. It is well known that the linear-phase property can be realized by ensuring that the impulse response is symmetrical about the center point [1]. Denote $h(n)$ to be the impulse response of an N-tap FIR filter, then its corresponding

frequency response is given by

$$H(e^{j\omega}) = \sum_{n=0}^{N-1} h(n)e^{-j\omega n} = \mathbf{h}^T[\mathbf{c}(\omega) - j\mathbf{s}(\omega)] \tag{2.1}$$

where $\mathbf{h} = [h(0)\ h(1)\ \cdots\ h(N-1)]^T$, $\mathbf{c}(\omega) = [1\ \cos\omega\ \cdots\ \cos(N-1)\omega]^T$, and $\mathbf{s}(\omega) = [0\ \sin\omega\ \cdots\ \sin(N-1)\omega]^T$. If this FIR filter has the linear-phase property and N is an odd number, $h(n)$ should be symmetrical about the sample $L = (N-1)/2$, namely, $h(n) = h(N-1-n)$. Therefore, $H(e^{j\omega})$ can be simplified as

$$H(e^{j\omega}) = e^{-j\omega L}\sum_{k=0}^{L} h_a(k)\cos\omega k \tag{2.2a}$$

where

$$h_a(0) = h(L), \quad h_a(k) = 2h(L-k), \tag{2.2b}$$

Obviously, the group delay is a constant equaled to L, and the amplitude response can be expressed individually as

$$\mathbf{A}(\omega) = \sum_{k=0}^{L} h_a(k)\cos\omega k = \mathbf{h}_a^T\,\mathbf{c}_a(\omega) \tag{2.3}$$

where $\mathbf{h}_a = [h(L)\ \ 2h(L-1)\ \ \cdots\ \ 2h(0)]^T$, and $\mathbf{c}_a(\omega) = [1\ \ \cos\omega\ \ \cdots\ \ \cos(\frac{N-1}{2})\omega]^T$.

2.2.2 Mth-Band FIR Filters

The discussion in the previous chapter has shown that a zero-phase Mth-band filter $h(n)$ should satisfy the time-domain constraint, namely, $h(n)$ gives a zero-crossing every M samples, i.e.,

$$h(nM) = \frac{1}{M}\delta(n). \tag{2.4}$$

Owing to this property, Mth-band filter is employed in signal interpolation, where the output signal is generated by inserting M-1 new samples between every two consecutive input samples but the original set of input samples is preserved in the interpolated signal. Hence, the property in (2.4) is also denoted as the interpolation condition.

Corresponding to the interpolation condition (2.4), there should be some restrictions on the frequency-domain which can be directly derived from (2.4). We start our derivation with the definition of Fourier transform [4] [14],

$$\sum_{k=0}^{M-1} H(e^{j(\omega-2\pi k/M)}) = \sum_{k=0}^{M-1}\sum_{n} h(n)e^{-j(\omega-2\pi k/M)n}. \tag{2.5}$$

By exchanging the order of summations, (2.5) can be rewritten as

$$\sum_{k=0}^{M-1} H(e^{j(\omega-2\pi k/M)}) = \sum_{n} h(n)e^{-j\omega n}\left[\sum_{k=0}^{M-1} e^{j2\pi kn/M}\right]. \tag{2.6}$$

It can be verified that the term inside the square brackets is always zero except that n is an integer multiple of M. Meanwhile, according to the interpolation condition $h(nM) = \frac{1}{M}\delta(n)$, when n is the integer multiple of M, $h(n)$ equals to zero except for $h(0)$. Thus,

$n = 0$ is the only term that makes the above equation hold. By substituting $n = 0$ in (2.6), it follows that

$$\sum_{k=0}^{M-1} H(e^{j(\omega - 2\pi k/M)}) = M \times h(0) = 1, \tag{2.7}$$

which is the frequency-domain constraint of Mth-band filter. However, (2.7) can not be easily formulized by the designed methods, therefore, it is further processed via the specific examples to obtain an equivalent but more convenient condition. Consider the simplest case, half-band filter of which M equals 2, then (2.7) becomes

$$H(e^{j\omega}) + H(e^{j(\omega-\pi)}) = 1. \tag{2.8}$$

This shows that the summation of $H(e^{j\omega})$ and its shifted copy from the origin to the point

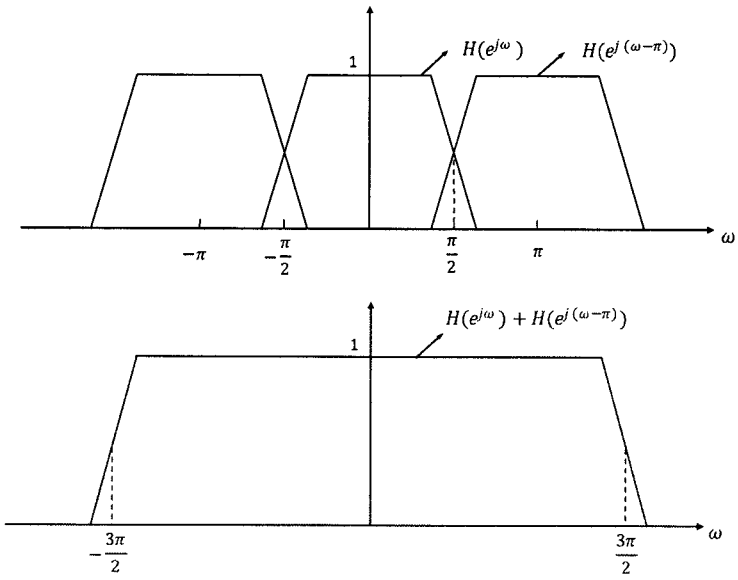

Figure 2.1: Frequency responses of the half-band filter $H(e^{j\omega})$ and its shifted version $H(e^{j(\omega-\pi)})$, as well as their summation.

π is unity for all ω. In other words, if $H(e^{j\omega})$ refers to a low-pass filter, (2.8) implies that the frequency response has an antisymmetry with respect to $\pi/2$ shown in Fig. 2.1, i.e., the center frequency of transition band is the half-band frequency $\pi/2$ [14] [15]. Certainly, there should exist similar condition for an arbitrary Mth-band filter when $M > 2$. Let us consider an extension of our analysis to the fourth-band filter, where $M = 4$, then (2.7) becomes

$$H(e^{j\omega}) + H(e^{j(\omega-\pi/2)}) + H(e^{j(\omega-\pi)}) + H(e^{j(\omega-3\pi/2)}) = 1. \tag{2.9}$$

It is intuitive in Fig. 2.2 that the frequency response of the fourth-band filter is antisymmetric around the point $\pi/4$, that is, the center frequency of the transition band is the fourth-band frequency $\pi/4$. By parity of reasoning, we can summarize that the frequency-

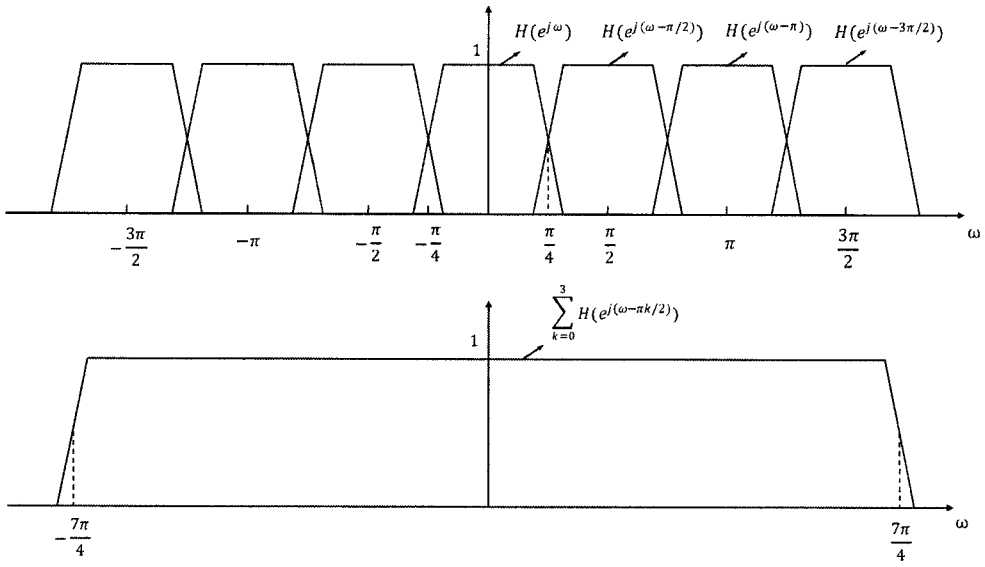

Figure 2.2: Frequency responses of the fourth-band filter $H(e^{j\omega})$ and its shifted versions $H(e^{j(\omega-\pi k/2)})$, as well as their summation.

domain constraint of a zero-phase Mth-band low-pass filter can be satisfied by making its

transition-band center frequency exactly at the Mth-band frequency π/M. Suppose that ω_c represents the center frequency of the transition band, and ω_p and ω_s represent the cutoff frequencies of the passband and the stopband, respectively. From the preceding discussion, ω_c, ω_p and ω_s have the following relationship

$$\omega_c = \frac{\omega_p + \omega_s}{2} = \frac{\pi}{M}, \tag{2.10}$$

which is often denoted as the cutoff frequency constraint. In a specific design problem, ω_c is obtained by predefining the ω_p and ω_s to be equally away from π/M. Although the cutoff frequency constraint (2.10) obeys to the zero-phase property, its derivation procedure is easy to understand and also appropriate for the linear-phase case. It will be shown that the same cutoff frequency constraint can be obtained even though the time-domain interpolation condition is imposed together with the linear-phase property.

Recall that the impulse response $h_{lin}(n)$ of a linear-phase Mth-band filter is the actual L-shifted version of $h(n)$ in (2.4). Thus, it is easy to obtain the linear-phase frequency response $H_{lin}(e^{j\omega})$ from $H(e^{j\omega})$ in (2.7) according to the Fourier shifting theorem, that is, $H_{lin}(e^{j\omega}) = e^{-j\omega L}H(e^{j\omega})$. Then, the frequency-domain constraint of a linear-phase Mth-band filter can be given by

$$\sum_{k=0}^{M-1} e^{j(\omega-2\pi k/M)L} H_{lin}(e^{j(\omega-2\pi k/M)}) = \sum_{k=0}^{M-1} H(e^{j(\omega-2\pi k/M)}) = 1, \tag{2.11}$$

It is equivalent to

$$\sum_{k=0}^{M-1} e^{-j(2\pi k/M)L} H_{lin}(e^{j(\omega-(2\pi k/M))}) = e^{-j\omega L}. \tag{2.12}$$

In order to know if (2.12) can lead to the same cutoff frequency constraint as the zero-phase case, it is better to observe the amplitude response constraint which is obtained by taking the absolute value of (2.12), i.e.,

$$\sum_{k=0}^{M-1} A_{lin}(\omega - (2\pi k/M)) = 1. \tag{2.13}$$

Comparing (2.13) with (2.7), we can conclude that the center frequency of the transition band of a linear-phase Mth-band low-pass filter is exactly at π/M, i.e., $\omega_c = (\omega_p+\omega_s)/2 = \pi/M$. For this case, the time-domain interpolation condition is in general given by

$$h(Mn + L) = \frac{1}{M}\delta(n). \tag{2.14}$$

Moreover, the above derivation about the cutoff frequency constraint is extended to the high-pass and band-pass Mth-band filter [16]. With a similar processing from (2.5) to (2.7)

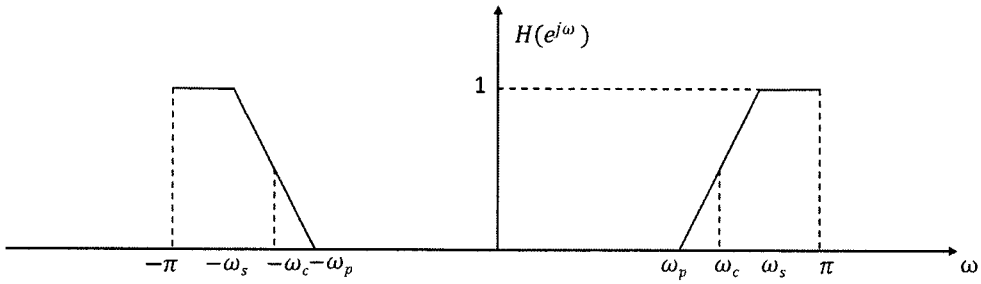

Figure 2.3: Frequency response of the high-pass Mth-band filter

and from (2.11) to (2.13), we find that both high-pass and band-pass Mth-band filters have

the same frequency-domain constraint (2.13) as the low-pass case. However, they employ different cutoff frequency constraint to realize (2.13). For a high-pass Mth-band filter in Fig. 2.3, it is easy to verify from (2.13) that the transition-band center frequency is exactly at $(M-1)\pi/M$, i.e.,

$$\omega_c = \frac{\omega_p + \omega_s}{2} = \frac{(M-1)}{M}\pi. \tag{2.15}$$

The band-pass case is more complicated since it has two transition bands. The center frequency of the first transition band, ω_{c_1}, depicted in Fig. 2.4, is obtained by using the same cutoff frequency principle as the low-pass case. Then, the center frequency of the second transition band, ω_{c_2}, can be determined by the bandwidth principle that the bandwith of a band-pass Mth-band filter should be equal to π/M. The desired linear-phase band-pass filter is illustrated in Fig. 2.4, where ω_{p_1}, ω_{p_2}, ω_{s_1} and ω_{s_2} are cutoff frequencies, and ω_{c_1} and ω_{c_2} are center frequencies of the two transition-bands, respectively. If the summation

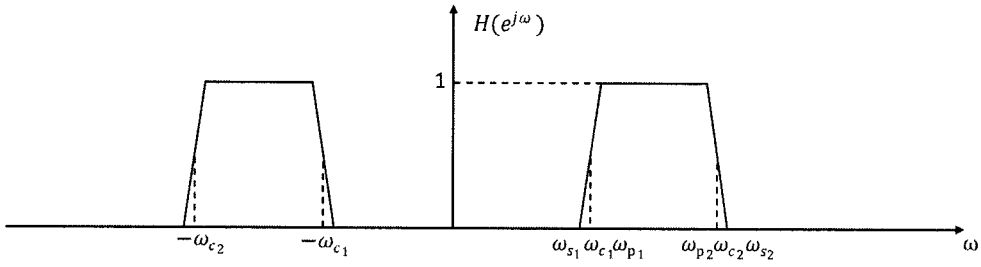

Figure 2.4: Frequency response of the band-pass Mth-band filter

of $H(e^{j\omega})$ and its M-1 shifting versions is equal to 1, then we have the cutoff frequency

constraint of band-pass Mth-band filters, i.e.,

$$\omega_{c1} = \frac{\omega_{p1} + \omega_{s1}}{2} = \frac{\pi}{M}, \tag{2.16a}$$

$$\omega_{c2} = \frac{\omega_{p2} + \omega_{s2}}{2} = \omega_{c1} + \frac{\pi}{M} \tag{2.16b}$$

Same as the low-pass filter, the equations (2.15) and (2.16) can be held by predefining the values of ω_p and ω_s in the specific deign problem.

2.3 2-D Linear-Phase Rectangular Mth-Band FIR Filters

2.3.1 Quadrantal Symmetry Property

Before giving the specific interpolation condition of linear-phase 2-D rectangular Mth-band filters, we first derive the transfer function of the filter we would like to design. It is well known that the impulse sequence of 2-D filters can have various types of symmetry to reduce the design and implementation complexity [17] [18]. In this thesis, we will consider to design the case of which the impulse sequence $h(\mathbf{n})$ has quadrantal symmetry. If the center of symmetry is at original, i.e., the designed filter is zero-phase, then we have

$$h(\mathbf{n}) = h(\mathbf{T}_1\,\mathbf{n}) = h(\mathbf{T}_2\,\mathbf{n}) = h(\mathbf{T}_1\,\mathbf{T}_2\,\mathbf{n}) \tag{2.17a}$$

where

$$\mathbf{T}_1 = \begin{bmatrix} 1 & 0 \\ 0 & -1 \end{bmatrix}, \qquad \mathbf{T}_2 = \begin{bmatrix} -1 & 0 \\ 0 & 1 \end{bmatrix}$$

Note that $\mathbf{T}_1\mathbf{T}_2 = -\mathbf{I}$. An example of such a $h(\mathbf{n})$ is illustrated in Fig. 2.5. It is clear

•	•	•	•	•	•	•
•	9	8	7	8	9	•
•	6	5	4	5	6	•
•	3	2	1	2	3	•
•	6	5	4	5	6	•
•	9	8	7	8	9	•
•	•	•	•	•	•	•

Figure 2.5: Quadrantally symmetric $h(\mathbf{n})$

from Fig. 2.5 that the quadrantal symmetry is a combination of the n_1-axis reflection, the n_2-axis reflection and the centro symmetries [19] [20], therefore, $h(\mathbf{n})$ can be expressed by the quatre quadrant of itself. This compact expression is particularly useful in the 2-D filter design. Recall that in general the frequency response of a 2-D FIR filter with impulse sequence supported on region $\mathbf{R}^{(2N_1+1)\times(2N_2+1)}$ is given by

$$H(j\omega_1, j\omega_2) = \sum_{n_1=0}^{2N_1} \sum_{n_2=0}^{2N_2} h(n_1,\, n_2) \exp(-j\omega_1 n_1 - j\omega_2 n_2) = \mathbf{g}_1^T \mathbf{H} \mathbf{g}_2 \tag{2.18}$$

where $\mathbf{g}_1 = [1 \; e^{-j\omega_1} \; e^{-j2\omega_1} \; \cdots \; e^{-j(2N_1)\omega_1}]^T$, $\mathbf{g}_2 = [1 \; e^{-j\omega_2} \; e^{-j2\omega_2} \; \cdots \; e^{-j(2N_2)\omega_2}]^T$, and $\mathbf{H} \in \mathbf{R}^{(2N_1+1)\times(2N_2+1)}$ is the matrix expression of $h(n_1,\, n_2)$. In order to derive the compact

expression of $h(n_1,\ n_2)$, $\mathbf{H}$ is partitioned as

$$\mathbf{H} = \begin{bmatrix} \mathbf{H}_{lu} & \mathbf{h}_u & \mathbf{H}_{ru} \\ \mathbf{h}_l & h_{cn} & \mathbf{h}_r \\ \mathbf{H}_{ld} & \mathbf{h}_d & \mathbf{H}_{rd} \end{bmatrix} \tag{2.19}$$

If the designed impulse sequence $\mathbf{H}$ is assumed to possess the quadrantal symmetry, referred as shown in Fig. 2.5, it is easy to find that the vectors $\mathbf{h}_u$ and $\mathbf{h}_d \in \mathbf{R}^{N_1 \times 1}$ are reflection symmetrical about the n_1-axis, the vectors $\mathbf{h}_l$ and $\mathbf{h}_r \in \mathbf{R}^{1 \times N_2}$ are reflection symmetrical about the n_2-axis, and the matrices $\mathbf{H}_{ru}$, $\mathbf{H}_{ld}$, $\mathbf{H}_{lu}$, and $\mathbf{H}_{rd} \in \mathbf{R}^{N_1 \times N_2}$ possess the n_1-axis reflection , the n_2-axis reflection, and the centro symmetry, respectively. As a consequence, the compact expression of $h(n_1,\ n_2)$ is obtained as

$$\mathbf{H}_c = \begin{bmatrix} h_{cn} & 2\mathbf{h}_r \\ 2\mathbf{h}_d & 4\mathbf{H}_{rd} \end{bmatrix} \tag{2.20}$$

Then, the frequency response of a linear-phase 2-D quadrantally symmetric FIR filter, i,e,. the center of the quadrantal symmetry at the point $(N_1,\ N_2)$ [21], can be expressed as

$$\mathbf{H}(j\omega_1, j\omega_2) = e^{-j(N_1\omega_1 + N_2\omega_2)} \mathbf{c}_1(\omega_1)^T \mathbf{H}_c \mathbf{c}_2(\omega_2) \tag{2.21}$$

where $\mathbf{c}_i(\omega_i) = [1 \ \cos\omega_i \ \cdots \ \cos N_i\omega_i]^T$, for $i = 1,\ 2$. Furthermore, we would like to present $\mathbf{c}_1(\omega_1)^T \mathbf{H}_c \mathbf{c}_2(\omega_2)$ as the form of $\mathbf{h}_{ta}^T \mathbf{c}_{ta}(\omega_1,\ \omega_2)$, which will efficiently reduce the complexity of the design as well as the implementation of 2-D filters. If $\mathbf{h}_{ta} \in \mathbf{R}^{(N_1+1)(N_2+1)\times 1}$

is a column vector generated by stacking the columns of $\mathbf{H}_c$ [21], then $\mathbf{c}_{ta}(\omega_1, \omega_2)$ should be the same dimensional-column vector as $\mathbf{h}_{ta}$, which is given by stacking $\mathbf{c}_p$ given below from $p = 0$ to $p = N_2$, i.e.,

$$\mathbf{c}_{ta}(\omega_1, \omega_2) = \left[\mathbf{c}_0(\omega_1, \omega_2)\ \mathbf{c}_1(\omega_1, \omega_2)\ \cdots\ \mathbf{c}_{N_2}(\omega_1, \omega_2)\right]^T \tag{2.22a}$$

where

$$\mathbf{c}_p(\omega_1, \omega_2) = \cos\, p\omega_2 \cdot \left[1\ \cos\omega_1\ \cos 2\omega_1\ \cdots\ \cos N_1\omega_1\right] \tag{2.22b}$$

$$\text{for } 0 \le p \le N_2$$

As a consequence, the frequency response is finally simplified to

$$\mathbf{H}(j\omega_1, j\omega_2) = e^{-j(N_1\omega_1 + N_2\omega_2)}\mathbf{h}_{ta}^T\mathbf{c}_{ta}(\omega_1, \omega_2) \tag{2.23}$$

This compact expression is particular useful and widely applied in the design problems. Based on the above analysis, we will give the interpolation condition and its related frequency-domain constraint for linear-phase rectangular Mth-band filters.

2.3.2 Properties of 2-D Linear-Phase Rectangular Mth-Band Filters

In analogy with the 1-D Mth-band, we start our analysis with the zero-phase filters. It is easily to verify from the above analysis that the impulse responses $\mathbf{h}(n_1, n_2)$ of a 2-D zero-phase rectangular Mth-band filter with quadratical symmetry can be obtained as the

vector product of two 1-D impulse responses, i.e.,

$$\mathbf{h}(n_1,\, n_2) = \mathbf{h}_r(n_1)\, \mathbf{h}_c^T(n_2) \tag{2.24}$$

where $\mathbf{h}_r(n_1)$ and $\mathbf{R}$ represent the impulse responses of two 1-D zero-phase Mth-band filters with the different interpolated coefficients M_1 and M_2, respectively. Thus, the interpolation condition of $\mathbf{h}(n_1,\, n_2)$ is given by

$$\begin{cases} h(M_1 n_1,\, n_2) = 0 & \text{for } (n_1,\, n_2) \neq (0,\, 0) \\ h(n_1,\, M_2 n_2) = 0 & \text{for } (n_1,\, n_2) \neq (0,\, 0) \\ h(n_1,\, n_2) = 1/(M_1 \times M_2) & \text{for } (n_1,\, n_2) = (0,\, 0) \end{cases} \tag{2.25}$$

Fig. 2.6 demonstrates the case for $M_1 = 3$ and $M_2 = 2$, where black dots represent the zero-crossings. According to this interpolation condition, the frequency-domain constraint

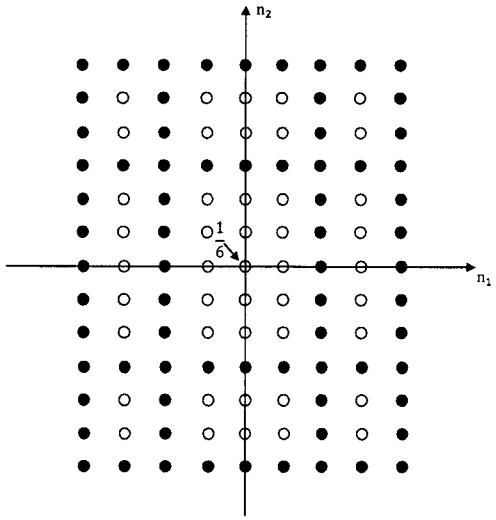

Figure 2.6: Rectangular interpolation for the designed impulse signal

can be derived by the definition of the 2-D Fourier transform (2.18),

$$\sum_{k_1=0}^{M_1-1}\sum_{k_2=0}^{M_2-1} H\big(j(\omega_1-\frac{2\pi k_1}{M_1}),\, j(\omega_2-\frac{2\pi k_2}{M_2})\big) \tag{2.26}$$
$$= \sum_{k_1=0}^{M_1-1}\sum_{k_2=0}^{M_2-1}\sum_{n_1}\sum_{n_2} h(n_1,\, n_2)e^{-j[(\omega_1-2\pi k_1/M_1)n_1+(\omega_2-2\pi k_2/M_2)n_2]}$$

By changing the order of sums, it follows that

$$\sum_{k_1=0}^{M_1-1}\sum_{k_2=0}^{M_2-1} H\big(j(\omega_1-\frac{2\pi k_1}{M_1}),\, j(\omega_2-\frac{2\pi k_2}{M_2})\big) \tag{2.27}$$
$$= \sum_{n_1}\sum_{n_2} h(n_1,\, n_2)e^{-j(\omega_1 n_1+\omega_2 n_2)}\left[\sum_{k_1=0}^{M_1-1} e^{j2\pi k_1 n_1/M_1}\sum_{k_2=0}^{M_2-1} e^{j2\pi k_2 n_2/M_2}\right]$$

Obviously, the terms in the square brackets are always zero except that n_1 and n_2 are the integer multiples of M_1 and M_2, simultaneously. Meanwhile, considering the interpolation condition (2.25), the only term that makes the equation (2.29) hold is $h(0,\, 0)$. Substituting $h(0,\, 0) = 1/(M_1 \times M_2)$ into (2.29) yields

$$\sum_{k_1=0}^{M_1-1}\sum_{k_2=0}^{M_2-1} H\big(j(\omega_1-\frac{2\pi k_1}{M_1}),\, j(\omega_2-\frac{2\pi k_2}{M_2})\big) = 1 \tag{2.28}$$

Similarly, the frequency-domain constraint of a 2-D linear-phase rectangular Mth-band filter with quadratical symmetry can be obtained from (2.28) by employing the relationship

$H_{lin}(j\omega_1,\, j\omega_2) = e^{-j(N_1\omega_1+N_2\omega_2)}H(j\omega_1,\, j\omega_2)$, namely,

$$\sum_{k_1=0}^{M_1-1}\sum_{k_2=0}^{M_2-1} e^{-j(2\pi k_1 N_1/M_1+2\pi k_2 N_2/M_2)} H_{lin}\big(j(\omega_1 - \frac{2\pi k_1}{M_1}),\, j(\omega_2 - \frac{2\pi k_2}{M_2})\big) \quad (2.29)$$
$$= \quad e^{-j(N_1\omega_1+N_2\omega_2)}$$

By taking the absolute value of (2.29), it follows that

$$\sum_{k_1=0}^{M_1-1}\sum_{k_2=0}^{M_2-1} A_{lin}\big((\omega_1 - 2\pi k_1/M_1),\, (\omega_2 - 2\pi k_2/M_2)\big) = 1 \quad (2.30)$$

This means that the amplitude response $A(\omega_1,\, \omega_2)$ and its shifted versions add up to unity for the entire plane of $(\omega_1,\, \omega_2)$. Intuitively, a possible choice for the passband and stopband cutoff frequencies can be obtained based on (2.30) as follows

$$\omega_{1c} = \frac{\omega_{1p} + \omega_{1s}}{2} = \frac{\pi}{M_1}, \quad (2.31a)$$

$$\omega_{2c} = \frac{\omega_{2p} + \omega_{2s}}{2} = \frac{\pi}{M_2} \quad (2.31b)$$

With the interpolation condition (2.25) and the related cutoff frequency constraint (2.31), we will develop a SDP-based design for the nonseparable 2-D linear-phase rectangular Mth-band FIR filters.

2.4 2-D Linear-Phase Diamond-Shaped Mth-Band FIR Filters

2.4.1 Restriction of Interpolation Matrix

It is well known that the 2-D signal has many different sampling versions. Due to this property, a more generalized definition of 2-D Mth-band filter is given by defining a nonsigular matrix $\mathbf{M} = \begin{bmatrix} m_1 & m_2 \\ m_3 & m_4 \end{bmatrix}$. Thus, a 2-D filter with impulse response $h(\mathbf{n})$ is referred as to an Mth-band filter [22] if

$$h(\mathbf{M}\,\mathbf{n}) = 0, \qquad \mathbf{n} \neq 0 \tag{2.32}$$

where $\mathbf{n} \in \mathcal{N} = \{(n_1, n_2) : -N_1 \leq n_1 \leq N_1, -N_2 \leq n_2 \leq N_2\}$. The set of all vectors $\mathbf{Mn}$ for $\mathbf{n} \in \mathcal{N}$ in (2.32) is called the lattice $LAT(\mathbf{M})$. It is generated by the integer linear combinations of the column vectors of $\mathbf{M}$. $LAT(\mathbf{M})$ show different interpolation shapes for various $\mathbf{M}$. For example, the lattices in Fig. 2.7(a) and 2.7(b) represent the well-known hexagonal pattern when $\mathbf{M} = \begin{bmatrix} 1 & 1 \\ 2 & -2 \end{bmatrix}$, or the quincunx pattern when $\mathbf{M} = \begin{bmatrix} 1 & 1 \\ -1 & -1 \end{bmatrix}$. In analogy with the rectangular case, this kind of filter can also be employed to interpolation, where the original set of input simples is preserved as the lattice points in the interpolated version. Thus, $\mathbf{M}$ is also called the interpolation matrix of a 2-D Mth-band filter. However, not every nonsingular $\mathbf{M}$ is appropriate for the 2-D linear-phase Mth-band filter with quadrantal symmetry. The quadrantal symmetry property can be regarded as a restriction on $\mathbf{M}$. In other words, possible choices of $\mathbf{M}$ should ensure that the impulse sequence $h(\mathbf{n})$

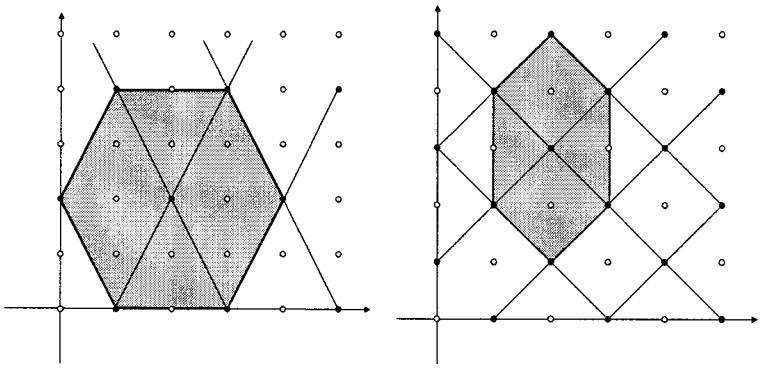

(a) (b)

Figure 2.7: (a) Hexagonal interpolation. (b) Quincunx interpolation

satisfy the interpolation condition and the quadrantal symmetry simultaneously [23], i.e.,

$$h(\mathbf{M}\,\mathbf{n}+\mathbf{N}_c) = h(\mathbf{T}_1\,\mathbf{M}\,\mathbf{n}+\mathbf{N}_c) = h(\mathbf{T}_2\,\mathbf{M}\,\mathbf{n}+\mathbf{N}_c) = h(-\mathbf{M}\,\mathbf{n}+\mathbf{N}_c) = 0 \qquad (2.33)$$

where $\mathbf{N}_c = \begin{bmatrix} N_1 \\ N_2 \end{bmatrix}$ is the symmetrical center of linear-phase property. In order for the above equation to hold, regardless of the linear shift $\mathbf{N}_c$, it is observed that four matrices $\mathbf{M}$, $\mathbf{T}_1\mathbf{M}$, $\mathbf{T}_2\mathbf{M}$, and $-\mathbf{M}$ are requested to generate the same lattice for $\mathbf{n} \in \mathcal{N}$, i.e., $LAT(\mathbf{M})$= $LAT(\mathbf{T}_1\mathbf{M})$= $LAT(\mathbf{T}_2\mathbf{M})$= $LAT(-\mathbf{M})$. From the lemma about the nonuniqueness of the lattice-generator [22], it is well known that $LAT(\mathbf{M})$ is identical to $LAT(\mathbf{M}\,\mathbf{Q})$ if, $\mathbf{Q}$ is a 2×2 unimodular integer matrix. Here, a matrix is defined as unimodular one if its determinant equals ± 1. Obviously, $-\mathbf{M}$ always satisfies the lemma for arbitrary $\mathbf{M}$. As such, $\mathbf{M}$ can be determined from

$$\mathbf{T}_1\,\mathbf{M} = \mathbf{M}\,\mathbf{Q}_1, \qquad (2.34a)$$

$$\mathbf{T}_2\,\mathbf{M} = \mathbf{M}\,\mathbf{Q}_2 \qquad (2.34b)$$

where $\mathbf{Q}_1$ and $\mathbf{Q}_2$ are unimodular integer matrices. Premultiplying the matrix $\mathbf{T}_1$ on the both sides of (2.34a), we can have

$$\mathbf{T}_1\mathbf{T}_1\mathbf{M} = \mathbf{T}_1\mathbf{M}\mathbf{Q}_1 \tag{2.35}$$

Then, substituting $\mathbf{M} = \begin{bmatrix} m_1 & m_2 \\ m_3 & m_4 \end{bmatrix}$ and $\mathbf{T}_1 = \begin{bmatrix} 1 & 0 \\ 0 & -1 \end{bmatrix}$ in (2.35) yields

$$\begin{bmatrix} m_1 & m_2 \\ m_3 & m_4 \end{bmatrix} = \begin{bmatrix} m_1 & m_2 \\ -m_3 & -m_4 \end{bmatrix} \mathbf{Q}_1 \tag{2.36}$$

Since the determinant of $\mathbf{Q}_1$ should be ± 1, it is easy to find two possible choices of $\mathbf{Q}_1$ that ensure the matrix $\mathbf{M}$ to be nonsingular, namely, the anti-diagonal matrices $\begin{bmatrix} 0 & 1 \\ 1 & 0 \end{bmatrix}$ and $\begin{bmatrix} 0 & -1 \\ -1 & 0 \end{bmatrix}$. The former leads to $m_1 = m_2$, and $m_3 = -m_4$, while the latter gives $m_1 = -m_2$, and $m_3 = m_4$. This implies that when the elements of $\mathbf{M}$ has the property of $\begin{bmatrix} \phi & \phi \\ \psi & -\psi \end{bmatrix}$, or $\begin{bmatrix} \psi & -\psi \\ \phi & \phi \end{bmatrix}$, the lattices generated by $\mathbf{M}$ and $\mathbf{T}_1\mathbf{M}$ are identical. Fortunately, this class of matrices $\mathbf{M}$ is also proven appropriate for (2.34b), where we have $\mathbf{T}_2\mathbf{M} = \mathbf{M}\begin{bmatrix} 0 & 1 \\ 1 & 0 \end{bmatrix}$, or $\mathbf{T}_2\mathbf{M} = \mathbf{M}\begin{bmatrix} 0 & -1 \\ -1 & 0 \end{bmatrix}$. As such, we can conclude that an nonsingular matrix $\mathbf{M}$ can be used as the interpolation matrix for the design of 2-D linear-phase Mth-band filters with quadrantal symmetry if $\mathbf{M}$ is chosen as

$$\begin{bmatrix} \phi & \phi \\ \psi & -\psi \end{bmatrix}, \quad \text{or} \quad \begin{bmatrix} \psi & -\psi \\ \phi & \phi \end{bmatrix}. \tag{2.37}$$

It is interesting note that several commonly used sampling matrices satisfy the condition (2.37). For instance, both the hexagonal sampling matrix $\mathbf{M} = \begin{bmatrix} 1 & 1 \\ 2 & -2 \end{bmatrix}$, and the quincunx sampling matrix $\mathbf{M} = \begin{bmatrix} 1 & 1 \\ 1 & -1 \end{bmatrix}$ can be employed as the interpolation matrix in the design of such a filter.

2.4.2 Frequency Specification

The frequency specification derived from the interpolation condition (2.4) is denoted as the cutoff frequency constraint of the 1-D Mth-band filter. In the 2-D case, we have a similar cutoff frequency constraint such that the passband is restricted to a certain region to avoid the aliasing. We already study the Mth-band filter with the rectangular passband. Now we would like to find an appropriate passband of the 2-D Mth-band filter with $\mathbf{M}$ defined in (2.37).

Besides the rectangular pattern, it is well known that the other typical class of 2-D low-pass filters has a diamond-shaped passband. In such a filter, the passband is in general bandlimited to the region of the symmetric parallelepiped *SPD* $\pi\mathbf{V}^T$, where $\mathbf{V}$ is the sampling matrix. It is proved in [22] [24] that an ideal 2-D filter with passband on *SPD* $(\pi\mathbf{M}^{-T})$ has the Mth-band property. In other words, the region *SPD* $(\pi\mathbf{M}^{-T})$ generated by the interpolation matrix $\mathbf{M}$ can be used as the passband in the design of Mth-band filters. In order to better understand the symmetric parallelepiped (*SPD*), we first impose the definition of fundamental parallelepiped (*FPD*). For a given 2×2 nonsingular matrix $\mathbf{U}$, *FPD*($\mathbf{U}$) denotes an parallelogram area including all the points of the set $\mathbf{Ux}$ where $\mathbf{x} = \begin{bmatrix} x_1 \\ x_2 \end{bmatrix}$, with $0 \leq x_1, x_2 < 1$.Thus, the edges of the parallelogram area are determined by the column

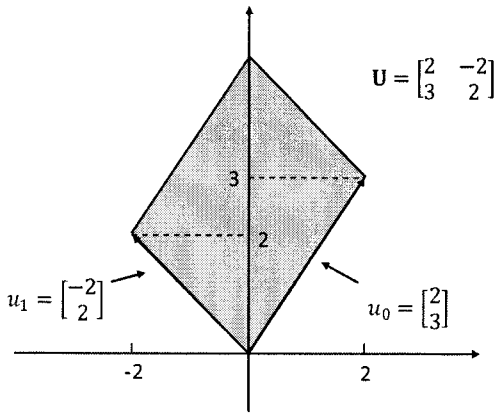

Figure 2.8: The fundamental parallelepiped *FPD*(**U**)

vectors of **U**. For example, a sketch of *FPD*(**U**) for a specific sampling matrix $\mathbf{U} = \begin{bmatrix} 2 & -2 \\ 3 & 2 \end{bmatrix}$ is demonstrated in Fig. 2.8. Compared to *FPD*(**U**), the symmetric parallelepiped *SPD*(**U**) is defined to include all the points of the set **Ux** for $-1 \leq x_0,\ x_1 < 1$. Hence, it is obtained as the union of *FPD*(**U**) and its shifted copies around the origin. The relation between *SPD*(**U**) and *FPD*(**U**) is demonstrated in Fig. 2.9 for $\mathbf{U} = \begin{bmatrix} -1 & 1 \\ 2 & 2 \end{bmatrix}$. Bearing this idea in

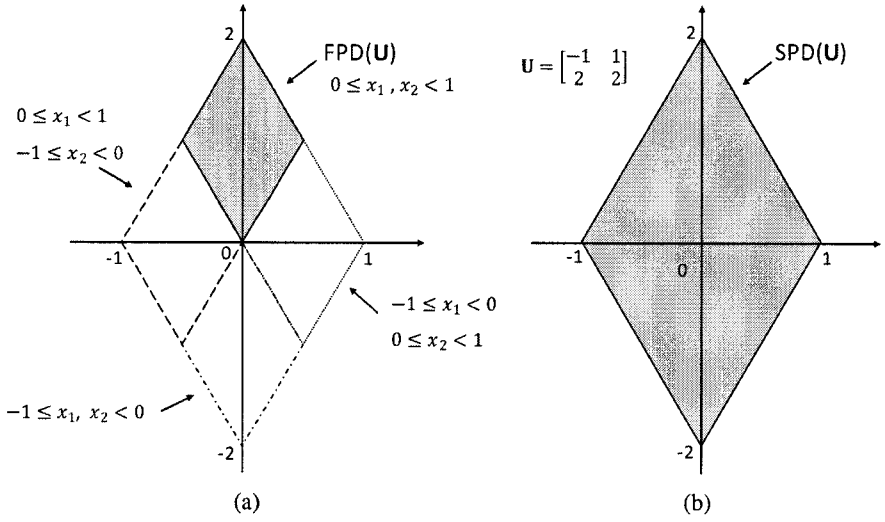

Figure 2.9: The relation between *SPD*(**U**) and *FPD*(**U**)

mind, it is easy to determine the passband of a 2-D diamond-shape Mth-band filter for a specific $\mathbf{M}$. Recall that both the hexagonal sampling matrix $\mathbf{M} = \begin{bmatrix} 1 & 1 \\ 2 & -2 \end{bmatrix}$, and the quincunx sampling matrix $\mathbf{M} = \begin{bmatrix} 1 & 1 \\ 1 & -1 \end{bmatrix}$ are appropriate to be the interpolation matrix in our design. Hence, we choose these two sampling matrices as the examples here to demonstrate their *SPD* $(\pi\mathbf{M}^T)$ region in Fig. 2.10(a) and 2.10(b), respectively. It is worth mentioning that

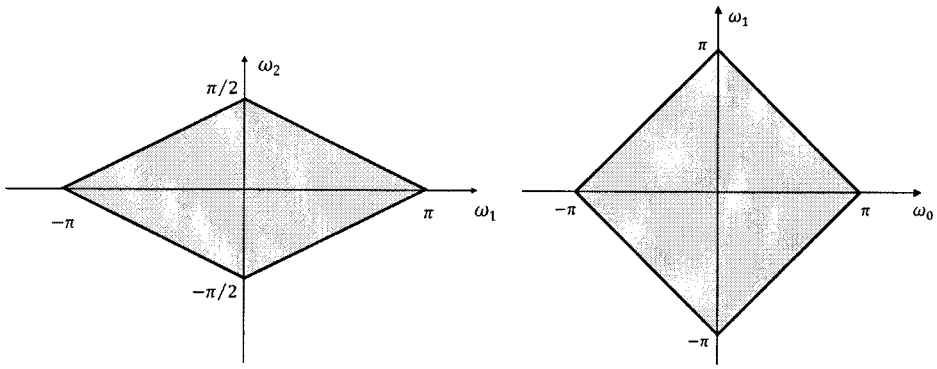

Figure 2.10: (a) *SPD*$(\pi\mathbf{M}^{-T})$ for hexagonal interpolation. (b) *SPD*$(\pi\mathbf{M}^{-T})$ for quincunx interpolation

the passband determined by *SPD* $(\pi\mathbf{M}^{-T})$ reduces to the interval of $[\pi, -\pi]$ when $\mathbf{M}$ is a scalar. This is consistent with the 1-D cutoff frequency constraint, which indirectly proves the feasibility and correctness of employing *SPD* $(\pi\mathbf{M}^{-T})$ as the passband. In summary, the region determined by *SPD* $(\pi\mathbf{M}^{-T})$ plays a crucial role in the 2-D Mth-band design.

2.5 Conclusion

In this chapter, we started with an analysis of 1-D linear-phase Mth-band filters, which focuses on the derivation of the cutoff frequency constraint from the time-domain interpolation condition. As an direct extension of the 1-D case, the 2-D linear-phase rectangular Mth-band filter is then deduced to prepare for the nonseparable filter design. The 2-D linear-phase diamond-shaped Mth-band filter with quadrantal symmetry is finally proposed, where the possible choices of the interpolation matrix $\mathbf{M}$ and the related passband region have been given explicitly. In the following chapters, we will investigate to design the Mth-band filters via the SDP and the SOCP approach.

Chapter 3

Design of Mth-band FIR Filters via the SDP Approach

The conventional optimization methods for the design of Mth-band filters are aimed at the frequency-domain constraint and hardly take into account the time-domain interpolation condition. However, by realizing the interpolation condition, one can design a high-quality Mth-band filter and thus enhance its performance in the interpolation and decimation applications.

In this chapter, an efficient optimization approach is investigated for the design of linear-phase Mth-band FIR filters, known as the semidefinite programming (SDP) approach. It can efficiently accommodate both inequality and equality constraints. The interpolation condition $h(nM) = \frac{1}{M}\delta(n)$ is therefore incorporated in the design problem as the equality constraint, while the error function between the designed filter and desired one is formulated as the inequality constraint. By considering the equality and the inequality

constraint as a whole in the optimization problem, the SDP will give an filter with both the optimal frequency response and the exact interpolation condition satisfied.

The SDP optimization problem for the Mth-band filter design will be modeled based-on the mini-max and the lease-square error criteria, respectively. Moreover, two types of methods are developed for the design of the 2-D rectangular Mth-band filter, termed as the direct and indirect design. The direct design, which is also applicable to the 2-D filters with other shapes, generates an nonseparable 2-D filter as the best approximation to the 2-D desired filter via the SDP approach. In contrast, the indirect design results in a 2-D filter that is synthesized by two 1-D constituent filters. The performance of the SDP approach will be demonstrated by numerical examples in terms of the maximum error as well as the design complexity. Besides, the designed Mth-band filters will be applied to image interpolation.

3.1 Semidefinite Programming (SDP) and Its Application to Filter Design

3.1.1 SDP Basics

Semidefinite programming (SDP) is a convex optimization technique, where a linear objective function is minimized over the intersection of an affine set and the cone of positive

semidefinite matrices [9] [12]. In general, the linear programming (LP) and quadratic programming (QP) can be modeled as the special cases of SDPs. Many primal-dual interior-point methods [25] have been proven efficient for solving the SDP problems over the past decade.

The standard form of a SDP problem can be expressed as [10] [26]

$$\text{minimize} \quad \mathbf{C} \cdot \mathbf{X} \tag{3.1a}$$

$$\text{subject to} \quad \mathbf{A}_g \cdot \mathbf{X} = b_g \qquad \text{for } g = 1, 2, \cdots, m \tag{3.1b}$$

$$\mathbf{X} \succeq 0 \tag{3.1c}$$

where $\mathbf{X} \in \mathbf{R}^{n \times n}$ is the optimization variable, and $\mathbf{C} \in \mathbf{R}^{n \times n}$, $\mathbf{A}_g \in \mathbf{R}^{n \times n}$ and $b_g \in \mathbf{R}$ are given parameters. Moveover, $\mathbf{X}$, $\mathbf{C}$, $\mathbf{A}_g$ are symmetric matrices, the inequality $\mathbf{X} \succeq 0$ denotes that $\mathbf{X}$ is positive semidefinite, and $\cdot$ denotes the matrix inner product defined by

$$\mathbf{C} \cdot \mathbf{X} = \sum_{i=1}^{n} \sum_{j=1}^{n} C_{ij} X_{ij}. \tag{3.2}$$

(In some other papers, the inner product is also expressed as $\mathbf{C} \cdot \mathbf{X} = \text{tr}(\mathbf{CX})$, where $\text{tr}(\mathbf{CX})$ denotes the trace of the matrix product $\mathbf{CX}$). Obviously, $\mathbf{C} \cdot \mathbf{X}$ is a linear function of the elements X_{ij}. Hence, we conclude that (3.1) is totally represented as a SDP problem in which a linear objective function of variable $\mathbf{X}$ is minimized over the intersection of m affine linear equality constraints $\mathbf{A}_g \cdot \mathbf{X} = b_g$, for $g = 1, \cdots, m$ and the positive semidefinite matrix $\mathbf{X} \succeq 0$. In general, (3.1) is referred to as the primal SDP problem. Similar to

the linear programming, there exists a dual SDP problem corresponding to (3.1), which is given by [10]

$$\text{maximize} \quad \mathbf{b}^T\mathbf{y} \tag{3.3a}$$

$$\text{subject to} \quad \mathbf{C} - \sum_{g=1}^{m} y_g \mathbf{A}_g \succeq 0 \qquad \text{for } g = 1, 2, \cdots, m \tag{3.3b}$$

where $\mathbf{b} = [b_1, b_2, \cdots, b_m]^T$ and $\mathbf{y} = [y_1, y_2, \cdots, y_m]^T$. The duality theorem [27] [28] states that if the primal SDP problem has an optimal solution $\mathbf{X}^*$, then the dual SDP problem also has an optimal solution $\mathbf{y}^*$, and moveover $\mathbf{C} \cdot \mathbf{X}^* = \mathbf{b}^T\mathbf{y}^*$. In general, a SDP optimization problem can be solved from two perspectives, the primal or the dual problem.

3.1.2 Typical SDP Problem for Filter Design

The minimization problem corresponding to (3.3) can be written as

$$\text{minimize} \quad -\mathbf{b}^T\mathbf{y} \tag{3.4a}$$

$$\text{subject to} \quad \mathbf{C} - \sum_{g=1}^{m} y_g \mathbf{A}_g \succeq 0 \qquad \text{for } g = 1, 2, \cdots, m \tag{3.4b}$$

Then, with substitutions $-\mathbf{b} \rightarrow \mathbf{c}$, $\mathbf{y} \rightarrow \mathbf{x}$, $\mathbf{C} \rightarrow \mathbf{F}_0$, and $-\mathbf{A}_g \rightarrow \mathbf{F}_i$, the typical SDP problem for the filter design purpose is given by

$$\text{minimize} \quad \mathbf{c}^T\mathbf{x} \tag{3.5a}$$

$$\text{subject to} \quad \mathbf{F}(\mathbf{x}) \succeq 0 \tag{3.5b}$$

$$\mathbf{F}(\mathbf{x}) = \mathbf{F}_0 + \sum_{i=1}^{n} x_i\mathbf{F}_i \tag{3.5c}$$

where the optimization variable is $\mathbf{x} \in \mathbf{R}^n$, the vector $\mathbf{c} \in \mathbf{R}^n$ and the symmetrical matrices $\mathbf{F}_i \in \mathbf{R}^{m\times n}$ $(i = 0, 1, 2 \cdots, n)$ are the given parameters. Noticing that $\mathbf{F}(\mathbf{x})$ is an affine set of $\mathbf{x}$, and $\mathbf{F}(\mathbf{x}) \succeq 0$ implies that $\mathbf{F}(\mathbf{x})$ is positive semidefinite at $\mathbf{x}$. In (3.5), a linear function of the optimization variable $\mathbf{x}$ is minimized subject to the convex constraint that a combination of the affine symmetrical matrices is positive semidefinite [9]. For a specific filter design problem, since the optimization variable $\mathbf{x}$ in (3.5) is related to the impulse response of the designed filter, the convex constraint $\mathbf{F}(\mathbf{x}) \succeq 0$ can be determined by the error function between the designed filter and the desired one. Depending on the error criteria used in the optimization, the SDP problem has different forms. We will consider the mini-max and lease-square SDP design of the linear-phase Mth-band FIR filters.

3.2 Design of Mth-Band FIR Filter via SDP

3.2.1 Mini-Max Error Criterion Based Design

In an equiripple mini-max type design, the error function e_m is defined by

$$e_m = \left|H(e^{j\omega}) - H_d(e^{j\omega})\right| \tag{3.6}$$

where $H(e^{j\omega})$ is the frequency response of the filter to be designed, and $H_d(e^{j\omega})$ is the desired frequency response. Recall that $H(e^{j\omega}) = \mathbf{h}^T[\mathbf{c}(\omega) - j\mathbf{s}(\omega)]$ as shown in (2.1). Our aim is to find the optimal $\mathbf{h}$ which minimizes the maximum value of the weighted error e_m, with $-\pi \leq \omega \leq \pi$ [29], namely,

$$\underset{\mathbf{h}}{\text{minimize}} \quad \left[W(\omega)\left|H(e^{j\omega}) - H_d(e^{j\omega})\right|\right]_{\max} \quad \text{for } \omega \in [-\pi, \pi] \tag{3.7}$$

where $W(\omega)$ represents the weighting function. If we denote by δ_m the maximum value of the square of weighted e_m, then (3.7) can be rewritten as

$$\underset{\mathbf{h}}{\text{minimize}} \quad \delta_m \tag{3.8a}$$

$$\text{subject to} \quad \delta_m - W(\omega)^2\left|H(e^{j\omega}) - H_d(e^{j\omega})\right|^2 \geq 0 \tag{3.8b}$$

$$\omega \in [-\pi, \pi]$$

Comparing (3.8a) with (3.5a), it is observed that δ_m is the objective function of the optimization problem, i.e., $\mathbf{c}^T\mathbf{x} = \delta_m$. If we define $\mathbf{x} = [\delta_m \quad \mathbf{h}^T]$, and $\mathbf{c} = [1 \quad 0 \quad \cdots \quad 0]^T$, the inequality constraint (3.8b) is naturally affine with respect to $\mathbf{x}$. Next, we would like to express (3.8b) as a positive semidefinite matrix. Denoting the desired frequency response $H_d(e^{j\omega})$ as

$$H_d(e^{j\omega}) = H_{dr}(\omega) - jH_{di}(\omega) \tag{3.9}$$

where $H_{dr}(\omega)$ and $jH_{di}(\omega)$ are the real and imaginary parts of $H_d(e^{j\omega})$, respectively, it follows that

$$W(\omega)^2\left|H(e^{j\omega}) - H_d(e^{j\omega})\right|^2 = W(\omega)^2\left[\mathbf{h}^T\mathbf{c}(\omega) - H_{dr}(\omega)\right]^2 + \left[\mathbf{h}^T\mathbf{s}(\omega) - H_{di}(\omega)\right]^2 \tag{3.10}$$

Then, $\delta_m - W(\omega)^2\left|H(e^{j\omega}) - H_d(e^{j\omega})\right|^2 \geq 0$ is equivalent to [29] [30]

$$\Upsilon(\omega) = \begin{bmatrix} \delta_m & \mathbf{h}^T\mathbf{c}_w(\omega) - H_{drw}(\omega) & \mathbf{h}^T\mathbf{s}_w(\omega) - H_{diw}(\omega) \\ \mathbf{h}^T\mathbf{c}_w(\omega) - H_{drw}(\omega) & 1 & 0 \\ \mathbf{h}^T\mathbf{s}_w(\omega) - H_{diw}(\omega) & 0 & 1 \end{bmatrix} \succeq 0 \tag{3.11}$$

where $\mathbf{c}_w(\omega) = W(\omega)\mathbf{c}(\omega)$, $\mathbf{s}_w(\omega) = W(\omega)\mathbf{s}(\omega)$, $H_{drw}(\omega) = W(\omega)H_{dr}(\omega)$, and $H_{diw}(\omega) = W(\omega)H_{di}(\omega)$. It is clear from (3.11) that $\Upsilon(\omega)$ is a 3×3 symmetric matrix, and $\Upsilon(\omega) \succeq 0$ means that $\Upsilon(\omega)$ is positive semidefinite matrix on $\mathbf{x}$. Note that (3.11) is hold for all ω which belongs to $-\pi \leq \omega \leq \pi$. In this thesis, the range of ω is defined as a set of points distributed uniformly in the interval of $[-\pi, \pi]$, i.e., $\omega \in \{\omega_r = 2\pi r/R, r = 1, 2, \cdots, R\}$. When R is large enough, ω_r are sufficiently dense in $[-\pi, \pi]$. Since $\Upsilon(\omega)$ at each ω_r should

be semidefinite positive, then the mini-max SDP problem can be summarized as

$$\text{minimize} \quad \mathbf{c}^T\mathbf{x} \tag{3.12a}$$

$$\text{subject to} \quad \mathbf{F}(\mathbf{x}) \succeq 0 \tag{3.12b}$$

where $\mathbf{c} = [1\ 0\ \cdots\ 0]^T$, $\mathbf{x} = [\delta_m\ \mathbf{h}^T]^T$, and $\mathbf{F}(\mathbf{x}) = \text{diag}\left\{\boldsymbol{\Upsilon}(\omega_1),\ \boldsymbol{\Upsilon}(\omega_2),\ \cdots,\ \boldsymbol{\Upsilon}(\omega_R)\right\}$. $\mathbf{F}(\mathbf{x})$ is called the tridiagonal matrix [29] which ensures the realization of every positive semidefinite matrix constraint $\boldsymbol{\Upsilon}(\omega_r) \succeq 0$ for $r = 1, 2, \cdots, R$. Obviously, $\mathbf{F}(\mathbf{x})$ is affine with respect to $\mathbf{x}$. The problem in (3.12) is a general mini-max SDP problem for filter design.

Furthermore, we impose the linear-phase property on the general mini-max SDP problem. The frequency response $H_d(e^{j\omega})$ of an idea linear-phase filter is defined as

$$H_d(e^{j\omega}) = e^{-j\omega(N-1)/2}\, A_d(\omega) \tag{3.13a}$$

with

$$A_d(\omega) = \begin{cases} 1, & \omega \in (0,\ \omega_p) \\ 0, & \omega \in (\omega_s,\ \pi) \end{cases} \tag{3.13b}$$

where N is an odd number representing the length of the filter, ω_p and ω_s are the passband and stopband cutoff frequencies, and their relationship should satisfy that $\omega_p + \omega_s = 2\pi/M$.

Then, substituting (3.13b) and (2.2) into error function (3.6) yields

$$e_m = A(\omega) - A_d(\omega) = \mathbf{h}_a^T \mathbf{c}_a(\omega) - A_d(\omega) \tag{3.14}$$

In such a design, the optimization variable in (3.12a) is simplified to $\mathbf{x} = [\delta_m \;\; h(\frac{N-1}{2}) \;\; 2h(\frac{N-1}{2}-1) \;\; \cdots \;\; 2h(0)]^T$, and the constraint matrix $\mathbf{F}(x)$ in (3.12b) is thus given by

$$\mathbf{F}(x) = \mathrm{diag}\{\boldsymbol{\Upsilon}_{lin}(\omega_1),\ \boldsymbol{\Upsilon}_{lin}(\omega_2),\ \cdots,\ \boldsymbol{\Upsilon}_{lin}(\omega_R)\} \tag{3.15a}$$

$$\boldsymbol{\Upsilon}_{lin}(\omega) = \begin{bmatrix} \delta_m & W(\omega)\big(\mathbf{h}_a\, \mathbf{c}_a(\omega) - A_d(\omega)\big) \\ W(\omega)\big(\mathbf{h}_a\, \mathbf{c}_a(\omega) - A_d(\omega)\big) & 1 \end{bmatrix} \succeq 0 \tag{3.15b}$$

It should be noticed that the SDP problem (3.15) is regarded as incomplete when it is used to design the Mth-band filters, since the time-domain interpolation condition (2.14) has not been incorporated. In general, the interpolation condition is formulated as a linear matrix equality constraint in the design problem [31], therefore, it can be formulated as

$$\mathbf{G}\mathbf{x} = \mathbf{q} \tag{3.16}$$

where $\mathbf{q}$ is a vector representing the right side of the interpolation condition $h_a(Mn) = \delta(n)/M$, and $\mathbf{G}$ is a selection matrix which is used to pick up the vector representing the left side of the interpolation condition, i.e., $[h_a(0),\ h_a(M),\ h_a(2M),\ \cdots]$, from the optimization variable $\mathbf{x}$. Since the size and content of $\mathbf{q}$ and $\mathbf{G}$ vary with M, it is better to

illustrate $\mathbf{q}$ and $\mathbf{G}$ for a specific M. For instance, the interpolation condition of an linear-phase half-band filter is realized through the following expression

$$\begin{bmatrix} 0 & 1 & 0 & 0 & \cdots & \cdots & & & \\ 0 & 0 & 0 & 1 & 0 & \cdots & \cdots & & \\ & & & & \ddots & & & & \\ \cdots & & & 0 & 0 & 1 & 0 & \cdots & \\ \cdots & \cdots & & & & 0 & 0 & 1 & 0\cdots \\ & & & & & & & & \ddots \end{bmatrix} \begin{bmatrix} \delta_m \\ h_a(0) \\ \vdots \\ h_a(1) \\ h_a(L) \end{bmatrix} = \begin{bmatrix} \frac{1}{M} \\ 0 \\ \vdots \\ 0 \\ \vdots \\ 0 \end{bmatrix} \tag{3.17}$$

Without the loss of generality, the time-domain constraint of a linear-phase fourth-band filter is given by

$$\begin{bmatrix} 0 & 1 & 0 & 0 & \cdots & \cdots & & & & \\ 0 & 0 & 0 & 0 & 0 & 1 & \cdots & \cdots & & \\ \vdots & \vdots & & & & & \ddots & & & \\ \vdots & \vdots & & & & & 0 & 0 & 1 & \cdots \\ \vdots & & & & & & & & & \ddots \end{bmatrix} \begin{bmatrix} \delta_m \\ \mathbf{h}_a \end{bmatrix} = \begin{bmatrix} \frac{1}{M} \\ 0 \\ \vdots \\ 0 \end{bmatrix} \tag{3.18}$$

Similarly, the interpolation condition of an arbitrary linear-phase Mth-band filter can be

easily derived. Thus far, the mini-max SDP optimization problem for the design of linear-phase Mth-band filters is established as

$$\text{minimize} \quad \mathbf{c}^T\mathbf{x} \tag{3.19a}$$

$$\text{subject to} \quad \mathbf{F}(x) \succeq 0 \tag{3.19b}$$

$$\mathbf{Gx} = \mathbf{q} \tag{3.19c}$$

where $\mathbf{x} = [\delta_m \ \ \mathbf{h}_a^T]^T$ is the optimization variable, $\mathbf{c} = [1 \ \ 0 \ \ \cdots \ \ 0]^T$, $\mathbf{F}(x) \succeq 0$ is the matrix inequality constraint in (3.15), and $\mathbf{Gx} = \mathbf{q}$ is the matrix equality constraint similar to those in (3.17)and (3.18).

3.2.2 Least-Square Error Criterion Based Design

In an equiripple least-square type design, the weighted least-square error function e_L is defined as [32]

$$e_l = \int_\Omega W(\omega)\left|H(e^{j\omega}) - H_d(e^{j\omega})\right|^2 d\omega \tag{3.20}$$

where $\Omega \in [-\pi \ \pi]$. Letting δ_l be the maximum value of e_l, we can obtain the first inequality constraint in the least-square SDP problem [29],

$$\delta_l - \int_\Omega W(\omega)\left|H(e^{j\omega}) - H_d(e^{j\omega})\right|^2 \geq 0 \tag{3.21a}$$

where

$$H(e^{j\omega}) = \sum_{n=0}^{N-1} h(n)e^{-j\omega n} = \mathbf{h}^T \mathbf{g}(e^{j\omega}) \tag{3.21b}$$

with $\mathbf{g}(e^{j\omega}) = [1 \;\; e^{-j\omega} \;\; e^{-j2\omega} \;\; \cdots \;\; e^{-j(N-1)\omega}]^T$. By defining

$$\mathbf{U} = \int_{\Omega} W(\omega)\mathbf{g}(e^{j\omega})\mathbf{g}^T(e^{j\omega})d\omega \tag{3.22a}$$

$$\mathbf{u} = \int_{\Omega} W(\omega)\mathbf{g}(e^{j\omega})H_d(e^{j\omega})d\omega \tag{3.22b}$$

$$a = \int_{\Omega} W(\omega)\left|H_d(e^{j\omega})\right|^2 d\omega \tag{3.22c}$$

(3.21) can be rewritten as

$$\delta_l - (\mathbf{h}^T\mathbf{U}\mathbf{h} - 2\mathbf{h}^T\mathbf{u} + a) \geq 0 \tag{3.23}$$

Since $\mathbf{U}$ is positive semidefinite on Ω, there exists a symmetric square root $\mathbf{U}^{1/2} = \mathbf{U}^{T/2}$, such that $\mathbf{U} = \mathbf{U}^{1/2}\mathbf{U}^{1/2}$. Hence, (3.23) is equivalent to

$$\delta_l - \left\|\mathbf{U}^{1/2}\mathbf{h} - \mathbf{U}^{-1/2}\mathbf{u}\right\|^2 + \lambda \geq 0 \tag{3.24a}$$

where

$$\left\|\mathbf{U}^{1/2}\mathbf{h} - \mathbf{U}^{-1/2}\mathbf{u}\right\|^2 = (\mathbf{h}^T\mathbf{U}^{1/2} - \mathbf{u}^T\mathbf{U}^{-1/2})(\mathbf{U}^{1/2}\mathbf{h} - \mathbf{U}^{-1/2}\mathbf{u}) \tag{3.24b}$$

$$\lambda = \mathbf{u}^T\mathbf{U}^{-1}\mathbf{u} - a \tag{3.24c}$$

Furthermore, (3.24) is equivalent to a positive semidefinite matrix, i.e.,

$$\mathbf{\Lambda}(\omega) = \begin{bmatrix} \delta_l + \lambda & \mathbf{h}^T\mathbf{U}^{1/2} - \mathbf{u}^T\mathbf{U}^{-1/2} \\ \mathbf{U}^{1/2}\mathbf{h} - \mathbf{U}^{-1/2}\mathbf{u} & \mathbf{I} \end{bmatrix} \succeq 0 \tag{3.25}$$

where $\mathbf{I}$ is an identity matrix. It is clear that $\mathbf{\Lambda}(\omega)$ is affine w.r.t. δ_l and $\mathbf{h}$. When the filter is of linear-phase, (3.25) can be modified as

$$\mathbf{\Lambda}_{lin}(\omega) = \begin{bmatrix} \delta_l + \lambda_{lin} & \mathbf{h}_a^T\mathbf{U}_{lin}^{1/2} - \mathbf{u}_{lin}^T\mathbf{U}_{lin}^{-1/2} \\ \mathbf{U}_{lin}^{1/2}\mathbf{h}_a - \mathbf{U}_{lin}^{-1/2}\mathbf{u}_{lin} & \mathbf{I} \end{bmatrix} \succeq 0 \tag{3.26}$$

where $\mathbf{U}_{lin} = \int_\Omega W(\omega)\mathbf{c}_a(\omega)\mathbf{c}_a(\omega)^T d\omega$, $\mathbf{u}_{lin} = \int_{\Omega_p} W(\omega)A_d(\omega)\mathbf{c}_a(\omega)d\omega$, $a_{lin} = \int_{\Omega_p} W(\omega)$ $A_d(\omega)^2 d\omega$, and $\lambda_{lin} = \|\mathbf{U}_{lin}^{-1/2}\mathbf{u}_{lin}\|^2 - a_{lin}$. Note that Ω_p represents the passband interval $[-\omega_p \ \omega_p]$.

Besides, in order to achieve the equiripple design, the passband and stopband errors should also be taken into consideration. If we denote by δ_p and δ_s the maximum values of the squared amplitude response errors of the passband and stopband, respectively, then the other two inequality constraints for the least-square SDP design can be obtained as

$$\delta_p - W(\omega)^2\big[A(\omega) - A_d(\omega)\big]^2 \geq 0 \qquad \text{for } \omega \in [-\omega_p \ \omega_p] \tag{3.27a}$$

$$\delta_s - W(\omega)^2 A(\omega)^2 \geq 0 \qquad \text{for } \omega \in [-\pi \ \omega_s] \cup [\omega_s \ \pi] \tag{3.27b}$$

Similar to the manner we process (3.8b), it can be shown that (3.27) is equivalent to

$$\boldsymbol{\Upsilon}_p(\omega) = \begin{bmatrix} \delta_p & W(\omega)\big(\mathbf{h}_a\,\mathbf{c}_a(\omega) - A_d(\omega)\big) \\ W(\omega)\big(\mathbf{h}_a\,\mathbf{c}_a(\omega) - A_d(\omega)\big) & 1 \end{bmatrix} \succeq 0 \tag{3.28a}$$

$$\boldsymbol{\Upsilon}_s(\omega) = \begin{bmatrix} \delta_s & W(\omega)\big(\mathbf{h}_a\,\mathbf{c}_a(\omega)\big) \\ W(\omega)\big(\mathbf{h}_a\,\mathbf{c}_a(\omega)\big) & 1 \end{bmatrix} \succeq 0 \tag{3.28b}$$

Obviously, $\boldsymbol{\Lambda}(\omega)$, $\boldsymbol{\Upsilon}_p(\omega)$, and $\boldsymbol{\Upsilon}_s(\omega)$ are all affine w.r.t $\mathbf{h}_a$. We now determine the objective function for the eqiripple least-square design in order to find the optimal $\mathbf{h}_a$ that minimizes the errors δ_l, δ_p, and δ_s, simultaneously. Considering that δ_l, δ_p, and δ_s are all positive real numbers, we employ the summation of δ_l, δ_p, and δ_s as the objective function for the optimization problem.

Similar to the mini-max design, the interpolation condition should be incorporated in the least-square design as the equality constraint. Combining all the inequality and equality constraints, the equiripple least-square SDP optimization problem for the design of linear-phase Mth-band filters can be summarized as

$$\begin{aligned} &\text{minimize} && \mathbf{c}^T\mathbf{x} \\ &\text{subject to} && \mathbf{F}(x) \succeq 0 \\ & && \mathbf{G}\mathbf{x} = \mathbf{q} \end{aligned} \tag{3.29}$$

where $\mathbf{c} = [1\ \ 1\ \ 1\ \ 0\ \ \cdots\ \ 0]^T$, $\mathbf{x} = [\delta_l\ \ \delta_p\ \ \delta_s\ \ \mathbf{h}_a^T]^T$, and $\mathbf{F}(x) = \text{diag}\left\{\boldsymbol{\Lambda}_{lin}(\omega),\ \boldsymbol{\Upsilon}_p(\omega_1),\right.$ $\boldsymbol{\Upsilon}_p(\omega_2),\ \cdots, \boldsymbol{\Upsilon}_p(\omega_{R_p}),\ \boldsymbol{\Upsilon}_s(\omega_1),\ \boldsymbol{\Upsilon}_s(\omega_2),\ \cdots,\ \left.\boldsymbol{\Upsilon}_s(\omega_{R_s})\right\}$. Note that R_p and R_s denote the

number of ω in passband and stopband, respectively. In the next section, we will extend the SDP approach for the design of 2-D Mth-band filters.

3.3 Design of 2-D Linear-Phase Mth-Band Filters via SDP

3.3.1 Design of 2-D Rectangular Mth-Band Filters Based on 1-D Filters

By a simple analysis, it is known that 2-D rectangular Mth-band filters can be obtained by designing 1-D filters. In such a design, two Mth-band filters (M could be different in the two 1-D filters) are designed separately via the SDP approach in Section 3.2. Then, as we mentioned in Section 2.3.2, the 2-D impulse responses can be obtained as the vector product of the two 1-D impulse responses, i.e.,

$$\mathbf{h}(n_1,\, n_2) = \mathbf{h}_r(n_1)\, \mathbf{h}_c^T(n_2) \tag{3.30}$$

where $\mathbf{h}_r(n_1) \in \mathbf{R}^{(2N_1+1)\times 1}$ and $\mathbf{R}^{(2N_2+1)\times 1}$represent the impulse responses of two 1-D Mth-band filters, respectively. The filter designed by this manner is also known as the separable filter. Note that if both $\mathbf{h}_r(n_1)$ and $\mathbf{h}_c(n_2)$ have the linear-phase property, i.e, they are symmetrical about their center point N_1 and N_2, respectively, then $\mathbf{h}(n_1,\, n_2) \in \mathbf{R}^{(2N_1+1)\times(2N_2+1)}$ has a quadrantal symmetry about its center point $(N_1,\, N_2)$. Although the 1-D based design is easy to implement, it is impossible to get an equiripple frequency response since the error functions of the two 1-D Mth-band filters are minimized separately

via the SDP approach. Moreover, it can not be used to design a 2-D Mth-band filter with arbitrary shapes of passband. As such, we would like to investigate the direct 2-D SDP design for arbitrary shaped 2-D Mth-band filters.

3.3.2 Direct SDP Design of Arbitrary 2-D Mth-Band Filters

A. Mini-Max Design

The direct SDP design for the nonseparable 2-D Mth-band filter is much more complicated than the 1-D based design because the optimization process is subject to the constraint composed by the quadratic error function between the desired and the designed 2-D filters [33] [34]. Following a simple analysis of the 2-D linear-phase property, the frequency response of an ideal linear-phase 2-D quadrantally symmetric Mth-band FIR filter is given by

$$H_d(e^{\omega_1,\omega_2}) = e^{-j(N_1\omega_1+N_2\omega_2)}\, A_d(\omega_1,\, \omega_2) \tag{3.31a}$$

with

$$A_d(\omega_1,\, \omega_2) = \begin{cases} 1, & (\omega_1,\, \omega_2) \in \Omega_{tp} \\ 0, & (\omega_1,\, \omega_2) \in \Omega_{ts} \end{cases} \tag{4.26b}$$

where R_p denotes the passband region and R_p denotes the stopband region. Note that for the rectangular filter $\Omega_{tp} = \{\omega : -\omega_{ip} \leq \omega_i \leq \omega_{ip},\, i = 1,2\}$ and $\Omega_{ts} = \{\omega : (-\pi \leq \omega_i \leq -\omega_{is}) \cup (\omega_{is} \leq \omega_i \leq \pi),\, i = 1,2\}$, while for the diamond-shaped case the passband

region is determined by the interpolation matrix $\mathbf{M}$, i.e., $SPD\ (\pi\mathbf{M}^{-T})$. This reflects the first "arbitrariness" of the direct approach in the sense that it can be used to design a filter with an arbitrary passband region. Recall that the ideal 2-D frequency response with an arbitrary passband can be expressed as $\mathbf{H}(j\omega_1, j\omega_2) = e^{-j(N_1\omega_1+N_2\omega_2)}\mathbf{h}_{ta}^T\mathbf{c}_{ta}(\omega_1, \omega_2)$, therefore, the weighted quadratic error function of the mini-max design is given by

$$e_{tm} = A(\omega_1, \omega_2) - A_d(\omega_1, \omega_2) = \mathbf{h}_{ta}^T\mathbf{c}_{ta}(\omega_1, \omega_2) - A_d(\omega_1, \omega_2) \tag{3.32}$$

Let δ_{tm} be an upper bound of the square of weighed error e_{tm}. Then, the SDP problem aimed at minimizing δ_{tm} can be written as

$$\underset{\mathbf{h}_{ta}}{\text{minimize}} \quad \mathbf{c}^T\mathbf{x} \tag{3.33a}$$

$$\text{subject to} \quad \delta_{tm} - W(\omega_1,\omega_2)^2\left[\mathbf{h}_{ta}^T\mathbf{c}_{ta}(\omega_1, \omega_2) - A_d(\omega_1,\omega_2)\right]^2 \geq 0 \tag{3.33b}$$

$$\omega_i \in [-\pi\ \pi] \quad \text{for } i = 1, 2$$

where $\mathbf{c} = [1\ \ 0\ \ \cdots\ \ 0]^T$ and $\mathbf{x} = [\delta_{tm}\ \ \mathbf{h}_{ta}^T]^T$. Note that the search for δ_{tm} is on the region of $\Omega_t = \{\omega :\ -\pi \leq \omega_i \leq \pi,\ i = 1, 2\}$. In our design, (ω_1, ω_2) is replaced by a set of grid points distributed uniformly in Ω_t, i.e., $\Omega_t = \left\{(\omega_1^{(r)}, \omega_2^{(r)}), \omega_{1,2}^{(r)} = 2\pi r/R, r = 1, 2, \cdots, R\right\}$. Therefore, the constraint (3.33b) has the following discrete form,

$$\mathbf{F}_t(\mathbf{x}) = \text{diag}\left\{\boldsymbol{\Upsilon}(\omega_1^{(1)},\omega_2^{(1)}),\ \cdots,\ \boldsymbol{\Upsilon}(\omega_1^{(R)},\omega_2^{(R)})\right\} \succeq 0 \tag{3.34a}$$

where

$$\Upsilon(\omega_1,\omega_2)=\begin{bmatrix} \delta_{tm} & \mathbf{h}_{ta}^T\mathbf{c}_{ta}(\omega_1,\,\omega_2)-A_d(\omega_1,\omega_2) \\ \mathbf{h}_{ta}^T\mathbf{c}_{ta}(\omega_1,\,\omega_2)-A_d(\omega_1,\omega_2) & 1 \end{bmatrix}\succeq 0 \quad (3.34b)$$

Clearly, $\mathbf{F}_t(\mathbf{x})$ is affine w.r.t $\mathbf{x}$, and it is positive semidefinite. Note that the weighted function is defined as $W(\omega_1,\omega_2)=1$ in the above expression for all available ω_1 and ω_2. In analogy with the 1-D case, the interpolation condition should be incorporated in the SDP problem as a linear matrix equality constraint, i.e.,

$$\mathbf{G}_t\mathbf{x}=\mathbf{q}_t \quad (3.35)$$

Since $\mathbf{x}=[\delta_{tm}\ \ \mathbf{h}_{ta}^T]^T$, the purpose of (3.35) is to pick up the coefficients of $\mathbf{h}_{ta}\in\mathbf{R}^{(N_1+1)(N_2+1)\times 1}$, which are supposed to be zero, and reset them to zero. Recall that $\mathbf{h}_{ta}$ is a column vector generated by stacking the columns of the compact impulse response $\mathbf{H}_c\in\mathbf{R}^{(N_1+1)\times(N_2+1)}$ in (2.21). If $\mathbf{H}_c$ represents a rectangular Mth-band filter, it should satisfy the interpolation condition in (2.25). Otherwise, for the diamond-shaped filter, the 2-D interpolation condition in terms of $\mathbf{H}_c$ can be expressed as $\mathbf{H}_c(\mathbf{Mn})=0$, for $\mathbf{n}\neq 0$. Thus, we can employ a series of selection matrices $\mathbf{G}_{ti}$ for $i=0,\ 1\ \cdots,\ N_2$ to determine the coefficients which are supposed to be zero of each column of $\mathbf{H}_c$, then the same coefficients in $\mathbf{h}_{ta}$ are determined by stacking these matrices as a block diagonal matrix, i.e., $\mathbf{G}_t=\mathrm{diag}\{\mathbf{G}_{t0},\ \mathbf{G}_{t1},\ \cdots,\ \mathbf{G}_{tN_2}\}$. $\mathbf{q}_t$ in (3.35) is obviously an all-zero vector except for the rectangular case with $q_t(0)=1/|\det(\mathbf{M})|$. Now we explain how to define $\mathbf{G}_t$ through

the specific example. Consider the interpolation condition of a 17×17 2-D linear-phase rectangular Mth-band filter with $M_1 = 4$ and $M_2 = 2$. The graphical illustration of the compact impulse response $\mathbf{H}_c$ is demonstrated in Fig. 3.1, where black dots represent the coefficients which are supposed to be zero. According to Fig. 3.1, (3.35) becomes

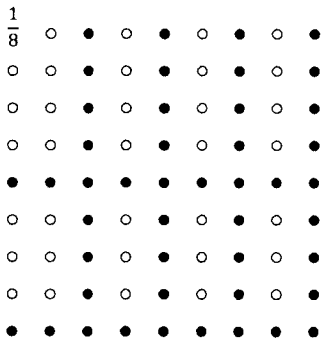

Figure 3.1: Interpolation sample points of $\mathbf{H}_c$

$$\begin{bmatrix} \mathbf{G}_{t0} & 0 & \cdots & & \\ 0 & \mathbf{G}_{t1} & 0 & \cdots & \\ & & & \ddots & \\ \cdots & & & 0 & \mathbf{G}_{t8} \end{bmatrix} \begin{bmatrix} \delta_{tm} \\ \mathbf{h}_{ta} \end{bmatrix} = \begin{bmatrix} \frac{1}{8} \\ 0 \\ \vdots \\ 0 \end{bmatrix} \tag{3.36a}$$

where $\mathbf{G}_{t0}$ is used to determine the first column of $\mathbf{H}_c$ which includes $\mathbf{H}_c(1,1) = 1/8$, where

$$\mathbf{G}_{t0} = \begin{bmatrix} 0 & 1 & 0 & 0 & 0 & 0 & 0 & 0 & 0 & 0 \\ 0 & 0 & 0 & 0 & 0 & 1 & 0 & 0 & 0 & 0 \\ 0 & 0 & 0 & 0 & 0 & 0 & 0 & 0 & 0 & 1 \end{bmatrix} \tag{3.36b}$$

It is observed that the columns 1, 3, 5, and 7 have the same interpolation version that the periodic zero-coefficients are separated by 4 samples. Therefore, their selection matrices $\mathbf{G}_{ti}$ for $i = 1,\ 3,\ 5,\ 7$ are of the same form,

$$\mathbf{G}_{ti} = \begin{bmatrix} 0 & 0 & 0 & 0 & 1 & 0 & 0 & 0 & 0 \\ 0 & 0 & 0 & 0 & 0 & 0 & 0 & 0 & 1 \end{bmatrix} \quad \text{for } i = 1,\ 3,\ 5,\ 7 \tag{3.36c}$$

Similarly, the columns 2, 4, 6, and 8 in Fig. 3.1 are all-zero columns, thus the corresponding selection matrices $\mathbf{G}_{ti}$ for $i = 2,\ 4,\ 6,\ 8$ are identity matrices, i.e.,

$$\mathbf{G}_{ti} = \begin{bmatrix} 1 & 0 & 0 & \cdots & & \\ 0 & 1 & 0 & \cdots & & \\ & & & \ddots & & \\ 0 & 0 & & \cdots & 0 & 1 \end{bmatrix} \quad \text{for } i = 2,\ 4,\ 6,\ 8 \tag{3.36d}$$

For the diamond-shaped Mth-band filter, the interpolation conditions of some interpolation patterns are the same as that of the 1-D Mth-band filter, where the coefficients which are supposed to be zero are separated by a fix number of the samples, such as the hexagonal interpolation, while other interpolation patterns have the similar situation as the rectangular filter. Here, we can find the second "arbitrariness" of the direct approach that the arbitrary interpolation condition can be realized by (3.35). Thus far, the mini-max SDP optimization

problem for the design of linear-phase 2-D Mth-band FIR filters can be formulated as

$$\text{minimize} \quad \mathbf{c}^T\mathbf{x} \tag{3.37a}$$

$$\text{subject to} \quad \mathbf{F}_t(\mathbf{x}) \succeq 0 \tag{3.37b}$$

$$\mathbf{G}_t\mathbf{x} = \mathbf{q}_t \tag{3.37c}$$

where $\mathbf{x} = [\delta_{tm} \ \mathbf{h}_{ta}^T]^T$is the optimization variable, $\mathbf{c} = [1 \ 0 \ \cdots \ 0]^T$, $\mathbf{F}_t(\mathbf{x}) \succeq 0$ is the matrix inequality constraint in (3.34), and $\mathbf{G}_t\mathbf{x} = \mathbf{q}_t$ is the interpolation condition realized by the similar form of (3.36).

B. Least-Square Design

The weighted L_2 error function for 2-D linear-phase filters is defined as

$$e_{tl} = \int\int_{\Omega_t} W(\omega_1, \omega_2)\left[\mathbf{h}_{ta}^T\mathbf{c}_{ta}(\omega_1, \omega_2) - A_d(\omega_1, \omega_2)\right]^2 d\omega_1 d\omega_2 \tag{3.38}$$

where Ω_t is a square region denoted as $[-\pi, \ \pi]^2$. By some simple manipulations, (3.38) can be rewritten as

$$e_{tl} = \mathbf{h}_{ta}^T\mathbf{U}_t\mathbf{h}_{ta} - 2\mathbf{h}_{ta}\mathbf{u}_t + a_t \tag{3.39a}$$

where

$$\mathbf{U}_t = \int\int_{\Omega_t} W(\omega_1, \omega_2)\mathbf{c}_{ta}(\omega_1, \omega_2)\mathbf{c}_{ta}(\omega_1, \omega_2)^T d\omega_1 d\omega_2 \tag{3.39b}$$

$$\mathbf{u}_t = \int\int_{\Omega_{tp}} W(\omega_1, \omega_2)A_d(\omega_1, \omega_2)\mathbf{c}_{ta}(\omega_1, \omega_2)d\omega_1 d\omega_2 \tag{3.39c}$$

$$a_t = \int\int_{\Omega_{tp}} W(\omega)A_d(\omega_1, \omega_2)^2 d\omega_1 d\omega_2 \tag{3.39d}$$

If we denote by δ_{tl} the maximum value of e_{tl}, then the L_2 error inequality constraint is defined by $\delta_{tl} - e_{tl} \geq 0$, which is equivalent to

$$\mathbf{\Lambda}_t(\omega_1, \omega_2) = \begin{bmatrix} \delta_{tl} + \lambda_t & \mathbf{h}_{ta}^T\mathbf{U}_t^{1/2} - \mathbf{u}_t^T\mathbf{U}_t^{-1/2} \\ \mathbf{U}_t^{1/2}\mathbf{h}_{ta} - \mathbf{U}_t^{-1/2}\mathbf{u}_t & \mathbf{I} \end{bmatrix} \succeq 0 \tag{3.40}$$

where $\mathbf{U}_t^{1/2}$ is the symmetric square root of $\mathbf{U}_t$, $\mathbf{I}$ space is the identity matrix, and $\lambda_t = \|\mathbf{U}_t^{-1/2}\mathbf{u}_2\| - a_t$. Besides, the equiripple property can be achieved by imposing the following constraints

$$\delta_{tp} - W(\omega_1, \omega_2)^2\left[A(\omega_1, \omega_2) - A_d(\omega_1, \omega_2)\right]^2 \geq 0 \quad (\omega_1, \omega_2) \in \Omega_{tp} \tag{3.41a}$$

$$\delta_{ts} - W(\omega_1, \omega_2)^2 A(\omega_1, \omega_2)^2 \geq 0 \quad (\omega_1, \omega_2) \in \Omega_{ts} \tag{3.41b}$$

Note that the frequencies in passband and stopband are defined as $\left\{(\omega_1^{(r_p)}, \omega_2^{(r_p)}),\ 1 \leq r_p \leq R_p\right\}$ and $\left\{(\omega_1^{(r_s)}, \omega_2^{(r_s)}),\ 1 \leq r_s \leq R_s\right\}$, respectively. Analogously, (3.41) can be expressed

as the matrix form

$$\Upsilon_{tp}(\omega_1,\,\omega_2) = \begin{bmatrix} \delta_{tp} & \mathbf{h}_{ta}\,\mathbf{c}_{ta}(\omega_1,\,\omega_2) - A_d(\omega_1,\,\omega_2) \\ \mathbf{h}_{ta}\,\mathbf{c}_{ta}(\omega_1,\,\omega_2) - A_d(\omega_1,\,\omega_2) & 1 \end{bmatrix} \succeq 0 \tag{3.42a}$$

$$\Upsilon_{ts}(\omega_1,\,\omega_2) = \begin{bmatrix} \delta_{ts} & \mathbf{h}_{ta}\,\mathbf{c}_{ta}(\omega_1,\,\omega_2) \\ \mathbf{h}_{ta}\,\mathbf{c}_{ta}(\omega_1,\,\omega_2) & 1 \end{bmatrix} \succeq 0 \tag{3.42b}$$

where the weighted function is denoted as $W(\omega_1, \omega_2) = 1$ for all available ω_i for $i = 1,\ 2$. Since there are three inequality constraints corresponding to δ_{tl}, δ_{tp} and δ_{ts}, respectively, the optimization variable in the SDP problem should contain the three errors, thus, the objective of this optimization problem is to find $\mathbf{h}_{ta}$ that minimizes the sum of these three errors. In summary, the equiripple SDP design for the 2-D linear-phase Mth-band filters based on the L^2 error criterion can be described as the same optimization model of (3.37), but with the optimization variable and the related parameters given by

$$\mathbf{x} = [\delta_{tl}\ \ \delta_{tp}\ \ \delta_{ts}\ \ \mathbf{h}_{ta}^T]^T \tag{3.43a}$$

$$\mathbf{c} = [1\ \ 1\ \ 1\ \ 0\ \ \cdots\ \ 0]^T \tag{3.43b}$$

$$\begin{aligned} \mathbf{F}(\mathbf{x}) = \mathrm{diag}\Big\{ & \Lambda_t(\omega_1,\,\omega_2), \\ & \Upsilon_{tp}(\omega_1^{(1)},\omega_2^{(1)}),\ \cdots,\ \Upsilon_{tp}(\omega_1^{(R_p)},\omega_2^{(R_p)}), \\ & \Upsilon_{ts}(\omega_1^{(1)},\omega_2^{(1)}),\ \cdots,\ \Upsilon_{ts}(\omega_1^{(R_s)},\omega_2^{(R_s)}) \Big\} \succeq 0 \end{aligned} \tag{3.43c}$$

where $\mathbf{\Lambda}(\omega_1, \omega_2)$ in (3.40), $\mathbf{\Upsilon}_{tp}$ and $\mathbf{\Upsilon}_{ts}$ are in (3.42). Besides, the interpolation condition can be met the same as the 2-D mini-max design through the similar form of (3.36).

Compared to 1-D based design, the complexity of the direct SDP approach is much higher and thus needs longer computational time. However, the direct 2-D design is a general method that can design arbitrarily shaped 2-D Mth-band filters. Moveover, it can offer equiripple frequency response for the designed filter.

3.4 Numerical Examples

In this section, several linear-phase Mth-band filters are designed via the proposed SDP approach. The performance of our design is evaluated in terms of the maximum error as well as the computational time. Our examples show the superiority of the SDP approach in different aspects.

All the SDP optimization problems in this chapter are implemented by a user-friendly MATLAB package Self-Dual-Minimization (SeDuMi) [35]. A complete SDP optimization problem in SeDuMi can be defined through five functions, which are the initialization of the SDP problem, the declaration of the optimization variables, the declaration of the liner matrix equality constraints, the declaration of the linear matrix inequality constraints, and the declaration of the linear objective function. For a feasible SDP problem, SeDuMi often generates both the primal and the dual optimal solutions.

Example 3.1

In the first example, a linear-phase low-pass half-band FIR filter with an odd length

of 113 is designed based on the mini-max SDP problem (3.37). According to the cutoff frequency constraint of the low-pass Mth-band filter (2.10) that $(\omega_p + \omega_s)/2 = \pi/2$, we set an narrow transition band of 0.05π, i.e., $\omega_p = 0.475\pi$ and $\omega_s = 0.525\pi$. The ideal amplitude response is thus given by

$$A_d(e^{j\omega}) = \begin{cases} 1, & \omega \in (0,\ 0.475\pi) \\ 0, & \omega \in (0.525\pi,\ \pi) \end{cases} \tag{3.44}$$

The resulting amplitude response of the designed filters are depicted along with this ideal amplitude response in Fig. 3.2(a). Since the maximum error is minimized, it is observed from Fig.3.2(b) that our design yields equiripple error both in passband and stopband. The amplitude response in dB and the linear phase response in rad are plotted in Fig. 3.3(a) and 3.3(b), respectively. The maximum amplitude approximation error of this design is 0.0028 and the execution time is 1.7969 seconds, which demonstrate that our design can offer a really optimal performance with a relatively small computational time, even for the critical frequency specifications.

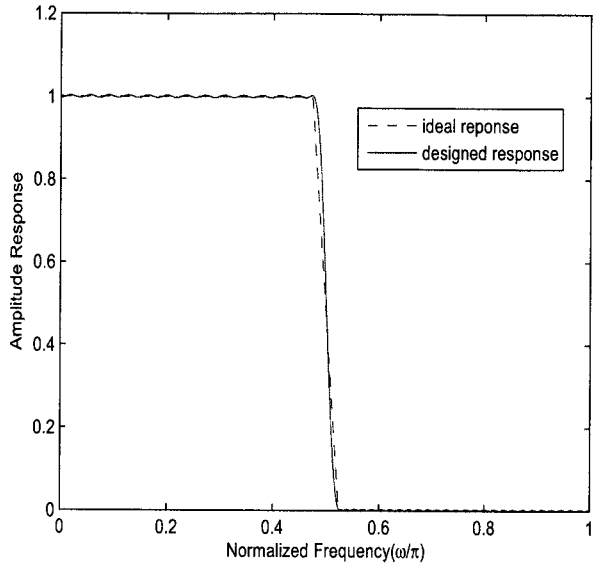

(a)

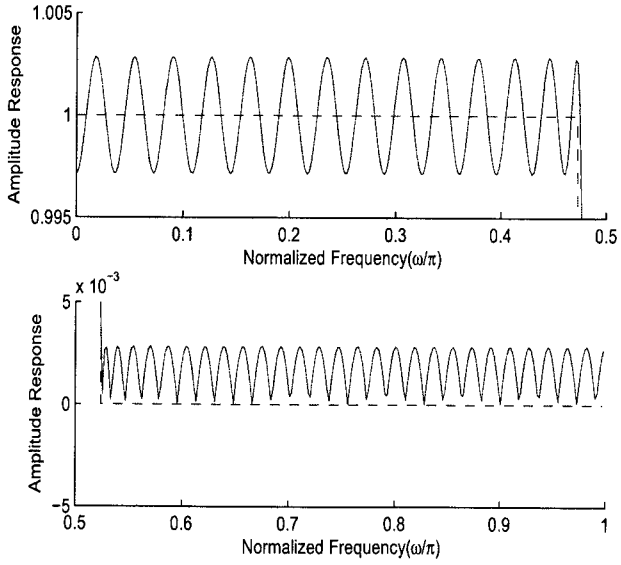

(b)

Figure 3.2: The half-band filter designed in *Example 3.1*. (a) Actual amplitude response vs. the ideal specification. (b) Passband and stopband amplitude errors.

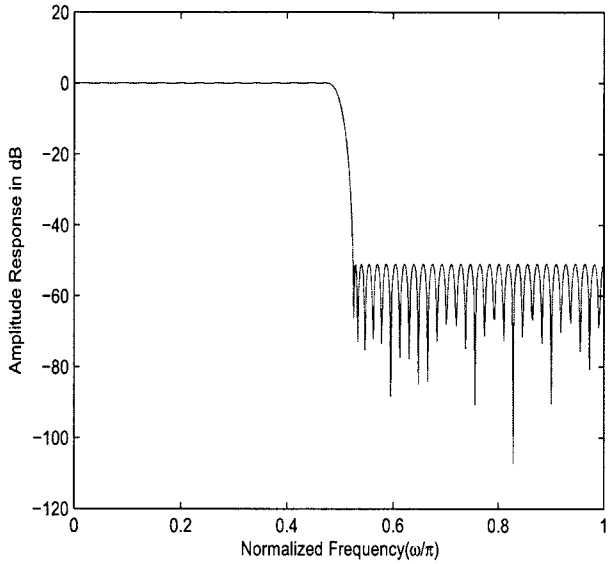

(a)

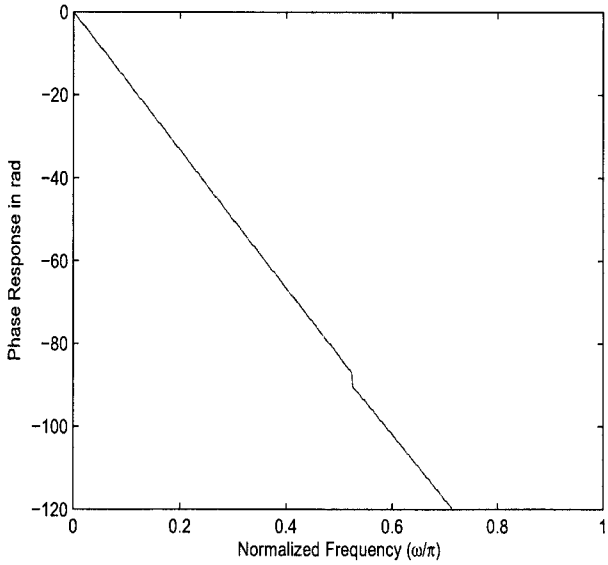

(b)

Figure 3.3: The half-band filter designed in *Example 3.1*. (a) Amplitude response in dB. (b) Linear-phase response in rad.

Example 3.2

In this example, we design a 53-tap fourth-band high-pass filter. The objective is to demonstrate an equiripple SDP design in the least-square sense. According to the cutoff frequency constraint of the high-pass Mth-band filter (2.15), i.e., $(\omega_p + \omega_s)/2 = 3\pi/4$, the frequency specifications are set as $\omega_p = 0.7\pi$ and $\omega_s = 0.8\pi$. The related simulation results are shown in Fig. 3.4(a), 3.4(b), 3.5(a) and 3.5(b). It is observed from Fig. 3.4(b) that both passband and stopband have the nearly equiripple property. The maximum least-square error of this high-pass filter is 0.5424 and the maximum pass-band and stop-band approximation errors are 0.012 and 0.017, respectively. The execution time is 1.7035 seconds.

Example 3.3

Now, we investigate the design of a 51×43 2-D rectangular Mth-band filter with the interpolation coefficients given as $M_1 = 3$ and $M_2 = 5$. According to 2-D cutoff frequency constraint (2.26), we set that $\omega_{1_p} = \pi/3 - 0.05$, $\omega_{1_s} = \pi/3 + 0.05$, $\omega_{2_p} = \pi/5 - 0.05$, and $\omega_{2_s} = \pi/5 + 0.05$. The frequency response of the ideal 2-D linear-phase Mth-band filter is defined by

$$\mathbf{H}(j\omega_1, j\omega_2) = \begin{cases} e^{-j(N_1\omega_1 + N_2\omega_2)}, & (\omega_1, \omega_2) \in \Omega_p \\ 0, & (\omega_1, \omega_2) \in \Omega_s \end{cases} \tag{3.45}$$

Both the 1-D based design and the direct 2-D design are employed in this example. The amplitude responses plots of the 2-D filters designed by the two methods are shown in Fig. 3.6(a) and 3.6(b), respectively. Table 3.1 summarizes the design results and execution time

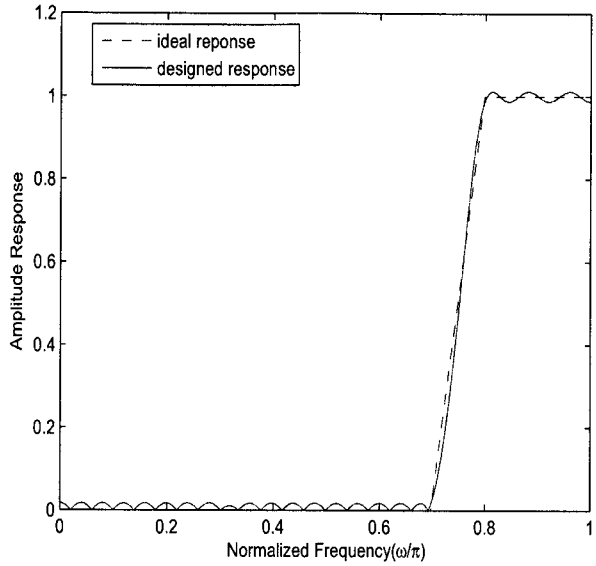

(a)

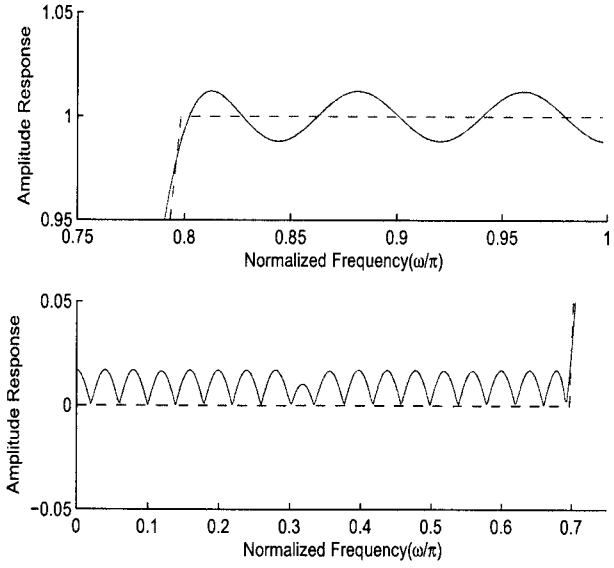

(b)

Figure 3.4: The fourth-band high-pass filter designed in *Example 3.2*. (a) Actual amplitude response vs. the ideal specification. (b) Passband and stopband amplitude errors.

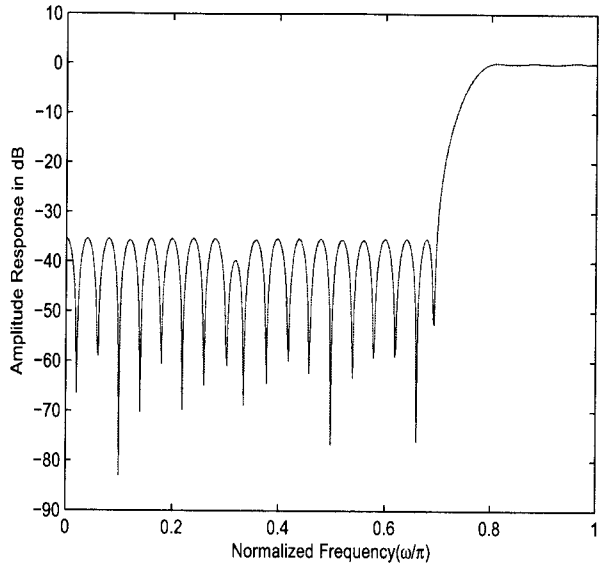

(a)

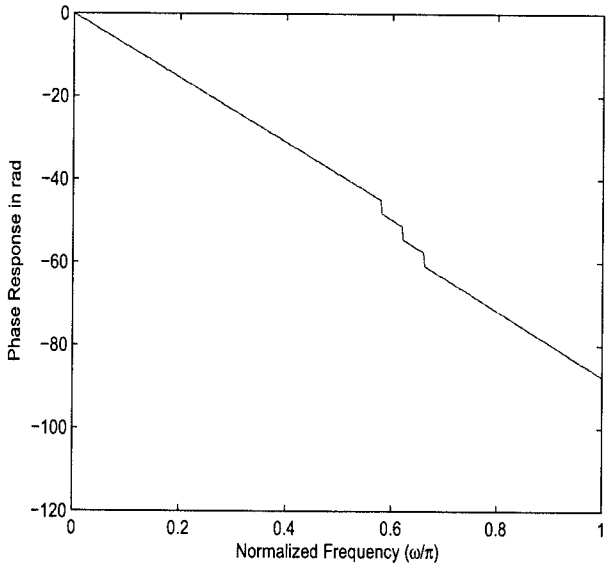

(b)

Figure 3.5: The fourth-band high-pass filter designed in *Example 3.2*. (a) Amplitude response in dB. (b) Linear-phase response in rad.

of the two approaches. Although the overall result of the 1-D based design is obtained as the synthesis of the optimal constituent 1-D filters, it is not considered optimal in the mini-max sense. Moveover, the maximum error of the overall frequency response is $0.0051 + 0.0044$ which is much bigger than 0.0058. However, the execution time of 1-D based design is much smaller than the direct approach.

Table 3.1: Comparison of maximum errors and execution time for the 2-D Mth-band filter in *Example 3.3* designed via the direct and the 1-D based approaches

	Maximum error			Execution time (seconds)	
Filter size	Direct approach	1-D based design		Direct approach	1-D based design
$N_1 = 15, N_2 = 15$	0.0563	0.0290	0.0273	14.7056	2.3601
$N_1 = 25, N_2 = 21$	0.0096	0.0049	0.0096	41.2541	2.5310
$N_1 = 35, N_2 = 27$	0.0037	8.8111e-004	0.0034	126.0973	2.7040

Example 3.4

Now, we design a 23×19 2-D rectangular Mth-band filter with $M_1 = 4$ and $M_2 = 2$ by the direct SDP approach in the least-square sense. As such, the frequency specifications are $\omega_{1_p} = 0.2\pi$, $\omega_{1_s} = 0.3\pi$ and $\omega_{2_p} = 0.4\pi$, $\omega_{2_s} = 0.6\pi$. The maximum least-square, passband and stopband errors are 3.0786, 0.0721 and 0.0412, respectively. The execution time is 41.8860 seconds. The amplitude response is plotted in Fig. 3.7. This simulation result confirms the feasibility of the SDP least-square approach for the direct design of 2-D Mth-band filter.

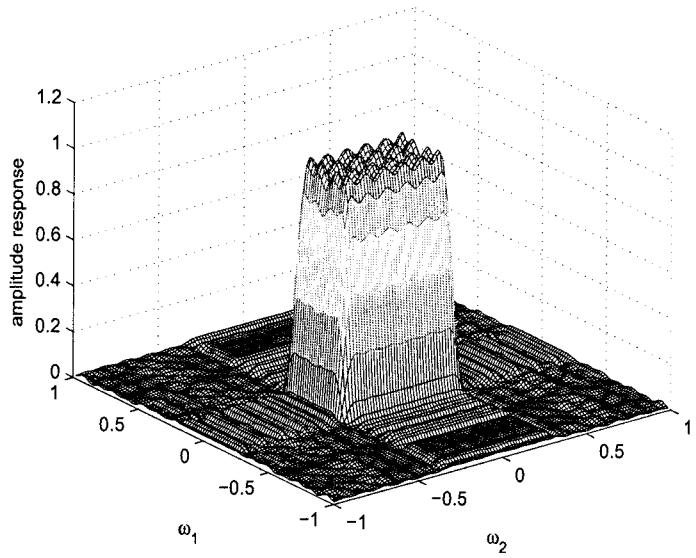

(a)

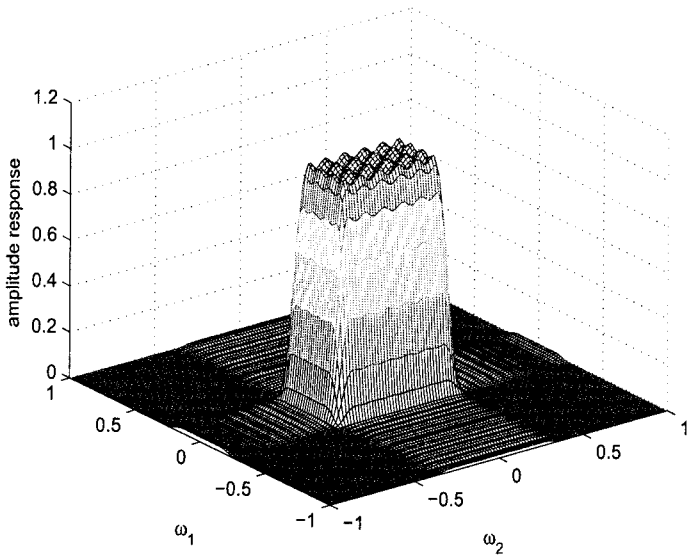

(b)

Figure 3.6: Amplitude responses of the 2-D rectangular Mth-band filter in *Example 3.3*. (a) Using the direct approach. (b) Using the 1-D based design.

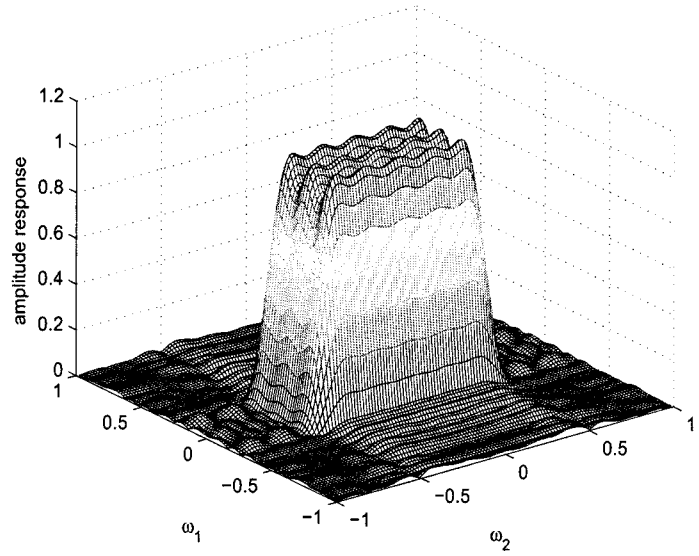

(a)

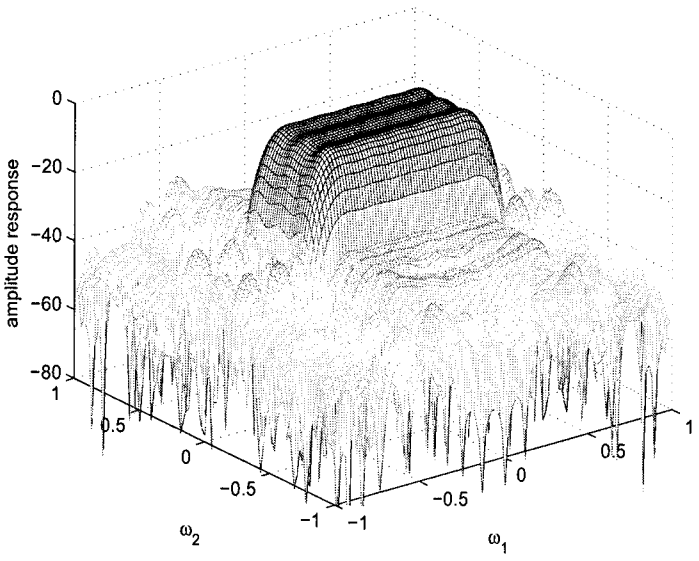

(b)

Figure 3.7: The Mth-band filter designed in *Example 3.4*. (a) Amplitude response in linear value. (b) Amplitude response in dB.

Example 3.5

Here, a 2-D diamond-shaped Mth-band filter with the hexagonal interpolation, i.e., $\mathbf{M} = \begin{bmatrix} 1 & 1 \\ 2 & -2 \end{bmatrix}$, is directly designed via the SDP mini-max design. Recall that the passband of such a filter is determined by $SPD\ (\pi \mathbf{M}^{-T})$. We choose the edge of $SPD\ (\pi \mathbf{M}^{-T})$ as the center of the transition band which is given as the gray region in Fig. 3.8. The simulation results are shown in Fig. 3.9. The maximum error of this example is 0.0117 and the computational time is 4.5157 seconds, which prove that the SDP approach can be employed to directly design the 2-D Mth-band filter with other shapes besides the rectangular pattern.

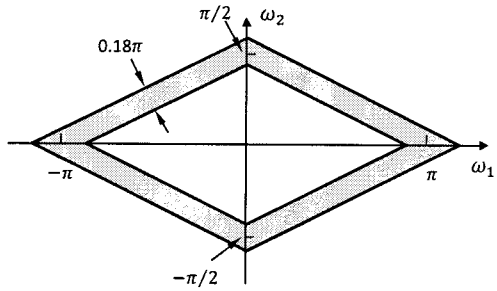

Figure 3.8: Transition band (gray region) for the 2-D diamond-shaped Mth-band filter with hexagonal interpolation

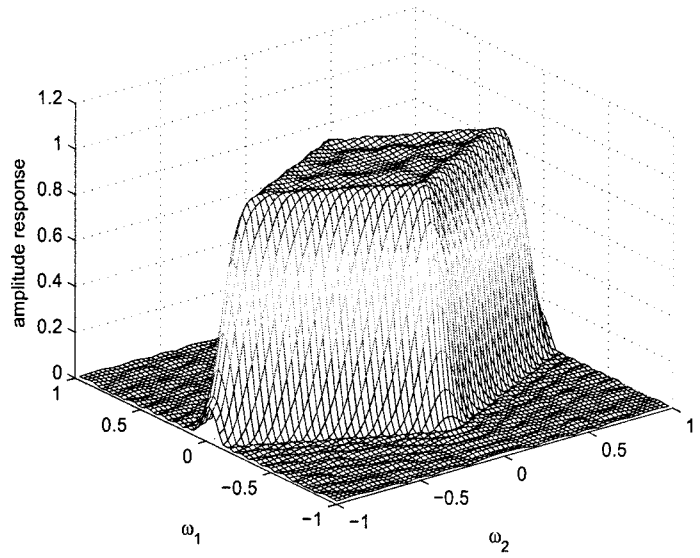

(a)

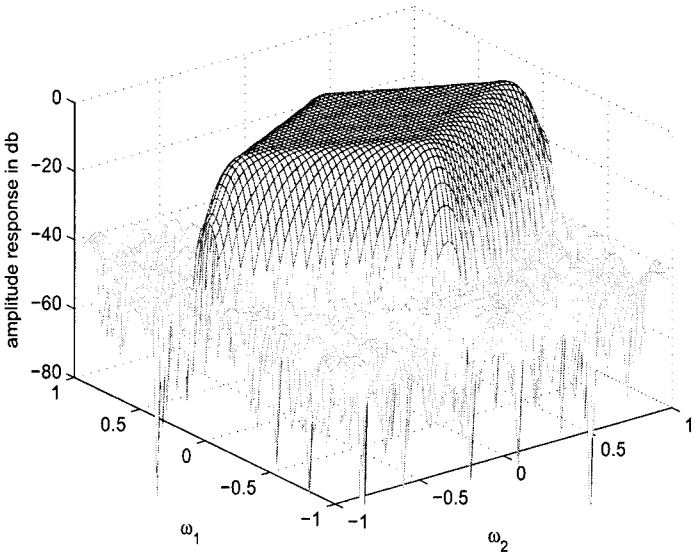

(b)

Figure 3.9: The Mth-band filter designed in *Example 3.5*. (a) Amplitude response in linear value. (b) Amplitude response in dB.

3.5 Application in Image Interpolation

Digital images are often zoomed or shrunk for various purposes by scaling its spatial resolution/ size. The spatial resolution of a digital image is represented by the number of pixels. Image shrinking can be achieved easily by deleting the related pixels, whereas image zooming is a difficult task since the processed image needs to be interpolated with unknown pixels [36]. The well known methods for image zooming are the nearest neighbor interpolation and the bilinear interpolation, both of which cause considerable blurring in the image. Here, the Mth-band filter is applied in image interpolation and is expected to yield a better resolution due to its interpolation condition [37] [38]. As well as shown, the Mth-band filter designed via the SDP approach exactly satisfy the interpolation condition.

In order to ensure a high accuracy, we now use the multirate system in Fig. 1.1 to resize a test image. More specifically, in decimator, a test image with the resolution of 512×512 is first prefiltered by a half-band filter with the unity amplitude response to avoid the aliasing, and then downsampled by a factor of 2 to generate an image with the resolution of 256×256. The lower resolution image is subsequently processed in the interpolator for upsampling by 2, plus a half-band interpolation filtering with the amplitude response of 4 to obtain an interpolated image with the original resolution. Note that the test images which have different level of detail are respectively resized by a 1-D 35-tap half-band filter and 2-D 35×35 nonseparable half-band filter. The passband and stopband cutoff frequencies of these half-band filters are all set as 0.4π and 0.6π. Note that the interpolation process by employing the 1-D half-band filter involves two steps, i.e., (1) a 1-D half-band filter is

first employed to interpolate the pixels of a test image in the horizontal direction; (2) the same 1-D half-band filter is then applied to get the pixels in the vertical direction. This process acts as a 2-D separable half-band interpolation filtering. The interpolated images are depicted in Fig. 3.10, 3.11 and 3.12, respectively. The qualities of the interpolated images are evaluated in terms of the peak signal-to-noise ratio (PSNR), as shown in Table 3.2. It is observed that both 1-D and 2-D Mth-band filters designed via the SDP approach can provide a high interpolation quality.

Table 3.2: Comparison of PSNR for the interpolated images achieved through the 1-D and 2-D Mth-band filter designed via the SDP approach

	The peak signal-to-noise ratio (PSNR)	
Test image	1-D Mth-band filter	2-D Mth-band filter
Lena	35.1429	34.8058
Girl (Elaine)	32.9976	32.7953
Fishing Boat	30.9908	30.8304

3.6 Conclusions

The SDP approach for the design of linear-phase Mth-band filters has been proposed in this chapter. Both the mini-max and the least-square criteria have been studied for the SDP design of 1-D and 2-D Mth-band filters with an emphasis on the formulation of the interpolation condition. It has been shown through various design examples that the SDP approach has the sufficient accuracy and flexibility. More specifically, we can conclude that (1) it gives the nearly optimal performance even for the design of filters with critical

(a)

(b)

Figure 3.10: The interpolated image with a low level of detail. (a) Using 1-D Mth-band filter. (b) Using 2-D Mth-band filter.

(a)

(b)

Figure 3.11: The interpolated image with a medium level of detail. (a) Using 1-D Mth-band filter. (b) Using 2-D Mth-band filter.

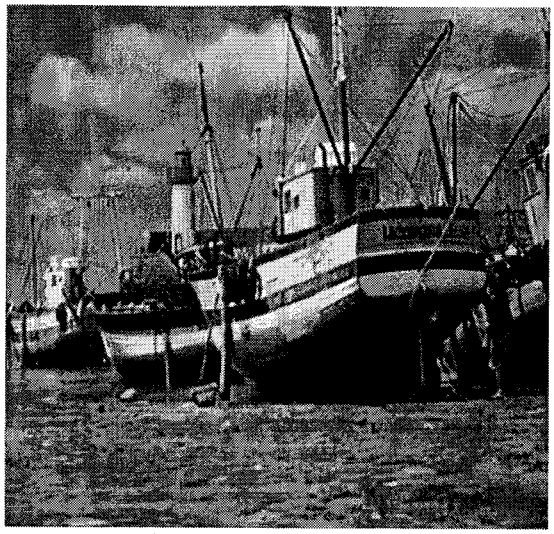

(a)

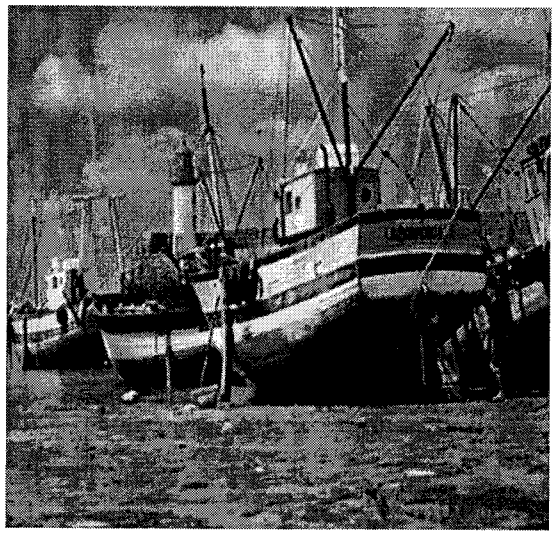

(b)

Figure 3.12: The interpolated image with a relatively large amount of detail. (a) Using 1-D Mth-band filter. (b) Using 2-D Mth-band filter.

frequency specifications; (2) it can design the equiripple 2-D Mth-band filters with arbitrary passband shape and amplitude response in the mini-max and or the lease-square sense. The designed Mth-band filters have also been applied to image interpolation, showing the application value of the proposed design approach.

Chapter 4

Design of Mth-band FIR Filters via the SOCP Approach

In this chapter, another optimization technique, known as the second order cone programming (SOCP), is investigated to design the Mth-band FIR filters. As a special case of the SDP, the SOCP has been proven less general but more efficient than the SDP in some applications. This chapter is organized as follows. We will first review the basic theory of the SOCP, including its relation to the SDP. The specific SOCP problems for the design of linear-phase Mth-band filters, in which the equality or inequality constraints are expressed as the form of the second-order cone constraints, are then developed in detail. Finally, numerical examples for Mth-band filter design via the SOCP approach are provided and compared to those from the SDP approach in terms of the design performance as well as the computational complexity.

4.1 Second-Order Cone Programming

4.1.1 Second-Order Cone Constraint

Second-order cone is a simple type of closed convex pointed cone, which is also called the quadratic, ice-cream, or Lorentz cone. A second-order cone constraint of dimension n is defined to restrict a vector formed by n variables to the second-order cone [39]. Specifically, the first variable of the vector is greater than or equal to the Euclidean norm of the subsequent $n-1$ variables, with the standard form shown as

$$\text{Scone}_n = \left\{ [e \quad \mathbf{y}]^T, e \in \mathbf{R}, \mathbf{y} \in \mathbf{R}^{n-1} \;\middle|\; e \geq \| \mathbf{y} \| \right\} \tag{4.1}$$

where $[e \quad \mathbf{y}]^T$ denotes the vector including n variables, and $\| \cdot \|$ denotes the standard Euclidean (L^2) norm, i.e., $\|\mathbf{y}\| = \sqrt{y^T y}$. Fig. 4.1 demonstrates the geometry of the second-order cone of dimension three. Note that when the dimension is less than three, there exist two special cases. For $n = 2$, the second-order cone constraint reduces to a linear

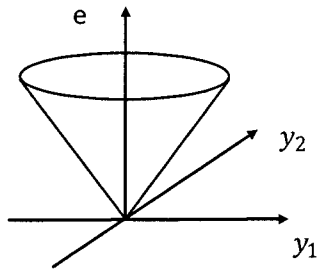

Figure 4.1: Second-order cone constraint of dimension 3

inequality constraint, i.e.,

$$\text{Scone}_2 = \left\{ [\, e \;\; y \,]^T,\, e, y \in \mathbf{R} \;\middle|\; e \geq y \right\}. \tag{4.2}$$

We will show that this case is particularly useful in the mini-max design. Furthermore, when $n = 1$, the second-order cone constraint is degenerated to restrict the variable to be nonnegative, i.e.,

$$\text{Scone}_1 = \{\, e \in \mathbf{R} \mid e \geq 0 \,\}. \tag{4.3}$$

An alternative form of the second-order cone is also commonly used in the SOCP, known as the rotated quadratic cone, which is obtained by rotating the second-order cone over an angle of forty-five degrees [13]. The rotated quadratic cone constraint of dimension n is given by

$$\text{Rcone}_n = \left\{ [\, e_1 \;\; e_2 \;\; \mathbf{y} \,]^T,\, e_1, e_2 \in \mathbf{R},\, \mathbf{y} \in \mathbf{R}^{n-2} \;\middle|\; e_1 + e_2 \geq 0,\; e_1 e_2 \geq \frac{1}{2} \| \mathbf{y} \|^2 \right\} \tag{4.4}$$

This means that the vector $[\, e_1 \;\; e_2 \;\; \mathbf{y} \,]^T$ has the property that the summation of its fist two variables are greater than or equal to zero, and the product of them is greater than or equal to the subsequent $n - 2$ variables. The expressions (4.1) and (4.4) reflect the variety of the second-order cone constraint, which makes the SOCP problems sufficiently flexible.

4.1.2 SOCP and Its Relation to SDP

SOCP is a class of convex optimization technique that minimizes a linear objective function over the intersection of an affine set and the Cartesian product of second-order (quadratic) cones [12] [13]. Due to the variety of the second-order cone constraint, several common convex optimization problems can be cast as SOCPs, such as the linear programming (LP), quadratic programming (QP), quadratically constrained convex quadratic programming (QCQP) and so on. The SOCPs can also be efficiently solved by the primal-dual interior-point methods, the same as SDP.

The standard form of a SOCP problem can be described as

$$\text{minimize} \quad \mathbf{q}^T\mathbf{x} \tag{4.5a}$$

$$\text{subject to} \quad \|\mathbf{A}_i\mathbf{x} + \mathbf{s}_i\| \leq \mathbf{r}_i^T\mathbf{x} + t_i \qquad \text{for } i = 1, \cdots, N, \tag{4.5b}$$

where $\mathbf{x} \in \mathbf{R}^n$ is the optimization variable, and the given parameters are $\mathbf{q} \in \mathbf{R}^n$, $\mathbf{A}_i \in \mathbf{R}^{(m_i-1)\times n}$, $\mathbf{s}_i \in \mathbf{R}^{m_i-1}$, $\mathbf{r}_i \in \mathbf{R}^n$, and $t_i \in \mathbf{R}$. An equivalent cone expression of (4.5b) is then given by

$$\begin{bmatrix} \mathbf{r}_i^T \\ \mathbf{A}_i \end{bmatrix} \mathbf{x} + \begin{bmatrix} t_i \\ \mathbf{s}_i \end{bmatrix} \in \text{Scone}_{m_i} \tag{4.6}$$

where m_i denotes the dimension of the second-order cone for $i = 1, \cdots, N$.

In general, the SOCP is regarded as a special case of the SDP since it is included by the SDP [12] [40]. This is because the second order cone is equivalent to a cone of positive

semidefinite matrix, i.e.,

$$e \geq \|\mathbf{x}\| \iff \begin{bmatrix} e & \mathbf{x}^T \\ \mathbf{x} & e\boldsymbol{I} \end{bmatrix} \succeq 0 \tag{4.7}$$

According to (4.7), the SOCP problem in (4.5) can be converted to an SDP problem with the following form,

$$\text{minimize} \quad \mathbf{q}^T\mathbf{x} \tag{4.8a}$$

$$\text{subject to} \quad \begin{bmatrix} \mathbf{r}_i^T\mathbf{x} + t_i & (\mathbf{A}_i\mathbf{x} + \mathbf{s}_i)^T \\ \mathbf{A}_i\mathbf{x} + \mathbf{s}_i & (\mathbf{r}_i^T\mathbf{x} + t_i)\boldsymbol{I} \end{bmatrix} \succeq 0 \tag{4.8b}$$

However, it is not advisable to solve the SOCP problem via the SDP due to the computational complexity concern. The interior-point methods often provide a much better worst-case complexity for a SOCP problem (4.5) than its SDP counterpart (4.8) [41]. Besides, it is proven that the computational amount per iteration required by the interior-point methods to solve the SOCP is less than that required to solve the SDP [12]. The computational savings of the SOCP over the SDP becomes more significant when the dimension n of the second-order cone constraint is larger. An independent study of the SOCP approach for the design of Mth-band filters is therefore necessary.

4.2 Design of Mth-Band FIR Filters via SOCP

4.2.1 Mini-Max Error Criteria Based Design

Recall that the objective of the mini-max filter design is to find the optimal $\mathbf{h}$ that minimizes the maximum error representing the difference between the designed filter and the ideal filter [42], namely,

$$\underset{\mathbf{h}}{\text{minimize}} \quad \Big[W(\omega) \big| H(e^{j\omega}) - H_d(e^{j\omega}) \big| \Big]_{\substack{\max \\ \omega \in [-\pi, \pi]}} \tag{4.9}$$

where $W(\omega)$ is the weighting function. Here, we denote by ζ_m an upper bound of the weighted error, and consider that the designed N-tap filter has the frequency response $H(e^{j\omega}) = \mathbf{h}^T[\mathbf{c}(\omega) - j\mathbf{s}(\omega)]$, and the ideal filter has $H_d(e^{j\omega}) = H_{dr}(\omega) - jH_{di}(\omega)$, then we can have

$$\underset{\mathbf{h}}{\text{minimize}} \quad \zeta_m \tag{4.10a}$$

$$\text{subject to} \quad \zeta_m \geq W(\omega)\big\{ \big[\mathbf{h}^T\mathbf{c}(\omega) - H_{dr}(\omega)\big]^2 + \big[\mathbf{h}^T\mathbf{s}(\omega) - H_{di}(\omega)\big]^2 \big\}^{1/2} \tag{4.10b}$$

$$\omega \in [-\pi, \pi]$$

Defining a vector,

$$\mathbf{C}(\omega) = W(\omega) \begin{bmatrix} \mathbf{h}^T\mathbf{c}(\omega) - H_{dr}(\omega) \\ \mathbf{h}^T\mathbf{s}(\omega) - H_{di}(\omega) \end{bmatrix} \tag{4.11}$$

then we can obtain $W(\omega)\left\{[(\mathbf{h}^T\mathbf{c}(\omega)-H_{dr}(\omega)]^2+[(\mathbf{h}^T\mathbf{s}(\omega)-H_{di}(\omega)]^2\right\}^{1/2}=\left\|\mathbf{C}(\omega)\right\|$. The constraint in (4.10b) is thus equivalent to $\zeta_m \geq \left\|\mathbf{C}(\omega)\right\|$, which is a standard second-order cone constraint. Note that this second-order cone constraint holds for all available ω within the interval $[-\pi\ \ \pi]$. Similar to the SDP design ω is replaced by a set of discrete points distributed uniformly in $[-\pi, \pi]$, i.e., $\omega \in \{\omega_r = 2\pi r/R,\, r = 1,\, 2,\, \cdots,\, R\}$. As such, the mini-max SOCP problem for the design of a general FIR filter is given by

$$\text{minimize} \quad \mathbf{q}^T\mathbf{x} \tag{4.12a}$$

$$\text{subject to} \quad \mathbf{q}^T\mathbf{x} \geq \left\| \begin{bmatrix} \mathbf{h}^T\mathbf{c}(\omega_r) - H_{dr}(\omega_r) & \mathbf{h}^T\mathbf{s}(\omega_r) - H_{di}(\omega_r) \end{bmatrix}^T \right\| \tag{4.12b}$$

$$\text{for } r = 1,\, 2,\, \cdots,\, R$$

where $\mathbf{x} = [\zeta_m\ \ h(0)\ \ h(1)\ \ \cdots\ \ h(N-1)]^T$ are the optimization variable, and the given parameters are $\mathbf{q} = [1\ 0\ \cdots\ 0]^T$, $\mathbf{c}(\omega_r) = [1\ \ \cos\omega_r\ \ \cdots\ \ \cos(N-1)\,\omega_r]^T$, and $\mathbf{s}(\omega_r) = [0\ \ \sin\omega_r\ \ \cdots\ \ \sin(N-1)\,\omega_r]^T$. In order to explicitly indicate the second-order cone property, we give an equivalent cone expression of (4.12), namely,

$$\text{minimize} \quad \mathbf{q}^T\mathbf{x} \tag{4.13a}$$

$$\text{subject to} \quad \begin{bmatrix} \mathbf{q}^T \\ [0\ \ \mathbf{c}^T(\omega_r)] \\ [0\ \ \mathbf{s}^T(\omega_r)] \end{bmatrix} \mathbf{x} - \begin{bmatrix} 0 \\ H_{dr}(\omega_r) \\ H_{di}(\omega_r) \end{bmatrix} \in \text{Scone}_3 \tag{4.13b}$$

$$\text{for } r = 1,\, 2,\, \cdots,\, R$$

By imposing the linear-phase property, that is $H(e^{j\omega}) = e^{-j\omega(N-1)/2}\mathbf{h}_a^T\mathbf{c}_a(\omega)$ and $H_d(e^{j\omega}) = e^{-j\omega(N-1)/2}A(\omega)$ ($A(\omega)$ could be the arbitrary amplitude response), (4.13) is simplified to

$$\text{minimize} \quad \mathbf{q}^T\mathbf{x} \tag{4.14a}$$

$$\text{subject to} \begin{bmatrix} \mathbf{q}^T \\ [0 \;\; \mathbf{c}_a^T(\omega_r)] \end{bmatrix} \mathbf{x} - \begin{bmatrix} 0 \\ A(\omega_r) \end{bmatrix} \in \text{Scone}_2 \tag{4.14b}$$

$$\text{for } r = 1, 2, \cdots, R$$

where $\mathbf{x} = [\zeta_m \;\; h_a(0) \;\; h_a(1) \;\; \cdots \;\; h_a(\frac{N-1}{2})]^T$, $\mathbf{q} = [1 \; 0 \; \cdots \; 0]^T$, and $\mathbf{c}_a(\omega) = [1 \;\; \cos\omega \;\; \cdots \;\; \cos(\frac{N-1}{2})\,\omega]^T$. Notice that (4.14b) is actually an inequality constraint as we discussed before.

Next, we consider to incorporate the interpolation condition in the above SOCP problem. Similar to the SDP, the coefficients of $h_a(Mn)$ can be selected from the optimization variable $\mathbf{x}$ by a selection matrix $\mathbf{G}$ (which is introduced explicitly in Section (3.2.1)) determined by M. Then, these selected coefficients should be set to be zero except $h_a(0) = 1/M$. This case is in general classified as the free vector constraint in the SOCP problem. The free vector constraint of dimension n specifies that the n variables formed this vector are restricted to be zero. In order to be consistent with the above cone expression, the free vector constraint in this thesis is defined as follows

$$\text{Fcone}_n = \{\, \mathbf{f} \in \mathbf{R}^n \mid \mathbf{f} = \mathbf{O}_n \,\}. \tag{4.15}$$

where $\mathbf{O}_n = [0\ 0\ \cdots\ 0]^T$ denotes an n-dimensional all-zero vector [43]. The free vector constraint is not only used to restrict the variables to be zero, it also allows for arbitrary equality constraints. For example, $h_a(0) = 1/M$ can be regarded as an free variable constraint from the perspective of $h_a(0) - 1/M = 0$. Thus, the interpolation condition of a linear-phase M-band filter in the SOCP problem can be described as

$$\mathbf{Gx} \in \text{Fcone}_m \tag{4.16}$$

where $\mathbf{G} \in \mathbf{R}^{m\times(N-1)/2+2}$ is the selection matrix. For example, when $M = 3$, it has the form of

$$\mathbf{G} = \begin{bmatrix} 0 & 1 & 0 & 0 & \cdots & \cdots & & & & \\ 0 & 0 & 0 & 0 & 1 & 0 & \cdots & \cdots & & \\ \vdots & \vdots & & & & & \ddots & & & \\ \vdots & \vdots & & & & & 0 & 0 & 1 & \cdots \\ \vdots & & & & & & & & & \ddots \end{bmatrix} \tag{4.17}$$

By incorporating the free vector and the second-order cone constraints, the mini-max SOCP optimization problem for the design of linear-phase Mth-band filters can be defined as

$$\text{minimize} \quad \mathbf{q}^T\mathbf{x} \tag{4.18a}$$

$$\text{subject to} \quad \begin{bmatrix} \mathbf{G} \\ \mathbf{C} \end{bmatrix} \mathbf{x} - \begin{bmatrix} \mathbf{O}_n \\ \mathbf{A} \end{bmatrix} \in \left(\text{Fcone}_m \times \text{Scone}_2^{(R)}\right) \tag{4.18b}$$

where

$$\mathbf{C} = \begin{bmatrix} \mathbf{q}^T \\ [0 \ \mathbf{c}_a^T(\omega_1)] \\ \mathbf{q}^T \\ [0 \ \mathbf{c}_a^T(\omega_2)] \\ \vdots \\ \mathbf{q}^T \\ [0 \ \mathbf{c}_a^T(\omega_R)] \end{bmatrix}, \quad \mathbf{A} = \begin{bmatrix} 0 \\ A_d(\omega_1) \\ 0 \\ A_d(\omega_2) \\ \vdots \\ 0 \\ A_d(\omega_R) \end{bmatrix} \tag{4.18c}$$

It is observed from (4.18) that the SOCP problem has a property that the free vector and the second-order cone constraints are stacked in a structure, in which they are distinguished by specifying the dimensions and the cones they belong to [44] [45].

4.2.2 Least-Square Error Criteria Design

In the SOCP least-square design, if we denote by ζ_l an upper bound of the square root of the weighted least-square error, then we can obtain the the first inequality constraint based on this error criterion as follows

$$\zeta_l \geq \left(\int_{\Omega} W(\omega) \left| H(e^{j\omega}) - H_d(e^{j\omega}) \right|^2 d\omega \right)^{1/2} \tag{4.19}$$

where $\Omega \in [-\pi \ \pi]$, and $H(e^{j\omega}) = \mathbf{h}^T \mathbf{g}(e^{j\omega})$ in (3.21b). We already proved in the SDP design that (4.19) can be equivalent to [46]

$$\zeta_l \geq \sqrt{\left\|\mathbf{U}^{1/2}\mathbf{h} - \mathbf{U}^{-1/2}\mathbf{u}\right\|^2 - \lambda} \tag{4.20}$$

where $\mathbf{U}^{1/2} \in \mathbf{R}^{N\times N}$, $\mathbf{u} \in \mathbf{R}^N$, and λ are shown in (3.22) and (3.24). Since λ is a scalar, (4.20) can be further written as

$$\zeta_l \geq \left\| \left[(\mathbf{U}^{1/2}\mathbf{h} - \mathbf{U}^{-1/2}\mathbf{u})^T \quad (-\lambda)^{1/2}\right]^T \right\| \tag{4.21}$$

Through the above a series of manipulations, we can now see that the least-square error constraint (4.19) is a second-order cone, which has the cone expression as

$$\begin{bmatrix} \zeta_l \\ \mathbf{U}^{1/2}\mathbf{h} \\ 0 \end{bmatrix} - \begin{bmatrix} 0 \\ \mathbf{U}^{-1/2}\mathbf{u} \\ (-\lambda)^{1/2} \end{bmatrix} \in \text{Scone}_{N+2} \tag{4.22}$$

Since our designs focus on the linear-phase filter, then (4.22) is further simplified to

$$\begin{bmatrix} \zeta_l \\ \mathbf{U}_{lin}^{1/2}\mathbf{h}_a \\ 0 \end{bmatrix} - \begin{bmatrix} 0 \\ \mathbf{U}_{lin}^{-1/2}\mathbf{u}_{lin} \\ (-\lambda_{lin})^{1/2} \end{bmatrix} \in \text{Scone}_{N+2} \tag{4.23}$$

where $\lambda_{lin} = \|\mathbf{U}_{lin}^{-1/2}\mathbf{u}_{lin}\|^2 - a_{lin}$, $\mathbf{U}_{lin} = \int_{\Omega} W(\omega)\mathbf{c}_a(\omega)\mathbf{c}_a(\omega)^T d\omega$, $\mathbf{u}_{lin} = \int_{\Omega_p} W(\omega)A_d(\omega)\mathbf{c}_a(\omega)d\omega$, and $a_{lin} = \int_{\Omega_p} W(\omega)A_d(\omega)^2 d\omega$.

Besides, both the passband and stopband errors should be taken into consideration to achieve the equiripple property. The second-order cone constraints based on the passband and stopband errors according to (4.13) are given by

$$\begin{bmatrix} \zeta_p \\ \begin{bmatrix} 0 & \mathbf{h}_a^T\mathbf{c}_a(\omega_{pr}) \end{bmatrix} \\ \zeta_s \\ \begin{bmatrix} 0 & \mathbf{h}_a^T\mathbf{c}_a(\omega_{sr}) \end{bmatrix} \end{bmatrix} - \begin{bmatrix} 0 \\ A_d(\omega_{pr}) \\ 0 \\ A_d(\omega_{sr}) \end{bmatrix} \in \text{Scone}_2 \times \text{Scone}_2 \tag{4.24}$$

where ω_{pr} for $r = 1,\ 2,\ \cdots,\ R_1$ and ω_{sr} for $r = 1,\ 2,\ \cdots,\ R_2$ denote the passband and stopband frequencies, respectively. The objective of the eqiripple least-square design is to find the optimal $\mathbf{h}_a$ which minimizes the errors ζ_l, ζ_p, and ζ_s, simultaneously. Since ζ_l, ζ_p, and ζ_s are all positive real scalars, the minimization of each of them accounts to the minimization of their sum. By incorporating these three second-order cone constraints and the interpolation condition, we obtain the equiripple least-square SOPC optimization problem for the design of linear-phase Mth-band filters below,

$$\text{minimize} \quad \mathbf{q}^T\mathbf{x} \tag{4.25a}$$

$$\text{subject to} \quad \begin{bmatrix} \mathbf{G} \\ \mathbf{C}_l \\ \mathbf{C}_m \end{bmatrix} \mathbf{x} - \begin{bmatrix} \mathbf{O}_n \\ \mathbf{V} \\ \mathbf{A} \end{bmatrix} \in \left(\text{Fcone}_m \times \text{Scone}_{N+2} \times \text{Scone}_2^{(R_1+R_2)}\right) \tag{4.25b}$$

where $\mathbf{x} = [\zeta_l \ \ \zeta_p \ \ \zeta_s \ \ \mathbf{h}_a^T]^T$ is the optimization variable, and $\mathbf{q} = [1 \ 1 \ 1 \ 0 \ \cdots \ 0]^T$, and $\mathbf{O}_n = [0 \ 0 \ \cdots \ 0]^T$. The second-order constraint based on the least-square error is given by

$$\mathbf{C}_l = \begin{bmatrix} \mathbf{q}_1^T \\ [\mathbf{O}_3 \ \mathbf{U}_{lin}^{1/2}] \\ 0 \end{bmatrix}, \qquad \mathbf{V} = \begin{bmatrix} 0 \\ \mathbf{U}_{lin}^{-1/2}\mathbf{u}_{lin} \\ (-\lambda_{lin})^{1/2} \end{bmatrix} \tag{4.25c}$$

where $\mathbf{q}_1 = [1 \ 0 \ 0 \ \cdots \ 0]^T$, $\mathbf{O}_3 = [0 \ 0 \ 0]$, $\mathbf{U}_{lin}^{1/2}$, $\mathbf{u}_{lin}$ and λ_{lin} are given in (4.35). The second-order constraints based on the passband and stopband errors are given by

$$\mathbf{C}_m = \begin{bmatrix} \mathbf{q}_2^T \\ [\mathbf{O}_3 \ \mathbf{c}_a^T(\omega_{p1})] \\ \vdots \\ \mathbf{q}_2^T \\ [\mathbf{O}_3 \ \mathbf{c}_a^T(\omega_{pR_1})] \\ \mathbf{q}_3^T \\ [\mathbf{O}_3 \ \mathbf{c}_a^T(\omega_{s1})] \\ \vdots \\ \mathbf{q}_3^T \\ [\mathbf{O}_3 \ \mathbf{c}_a^T(\omega_{sR_2})] \end{bmatrix}, \qquad \mathbf{A} = \begin{bmatrix} 0 \\ A_d(\omega_{p1}) \\ \vdots \\ 0 \\ A_d(\omega_{pR_1}) \\ 0 \\ A_d(\omega_{s1}) \\ \vdots \\ 0 \\ A_d(\omega_{sR_2}) \end{bmatrix} \tag{4.25d}$$

where $\mathbf{q}_2 = [0 \ 1 \ 0 \ \cdots \ 0]^T$, $\mathbf{q}_3 = [0 \ 0 \ 1 \ \cdots \ 0]^T$. In the next section, we would like extend the SOCP approach to the design of 2-D linear-phase Mth-band filters.

4.3 Design of 2-D Linear-Phase Mth-Band Filters via SOCP

4.3.1 2-D Mini-Max SOCP Design

The SOCP can also be employed to directly design the 2-D linear-phase Mth-band filters with the quadratical symmetry. Recall that the ideal response of such a filter in general is given by

$$H_d(e^{\omega_1,\omega_2}) = e^{-j(N_1\omega_1+N_2\omega_2)}\, A_d(\omega_1,\, \omega_2) \tag{4.26a}$$

where

$$A_d(\omega_1,\, \omega_2) = \begin{cases} 1, & (\omega_1,\, \omega_2) \in \Omega_{tp} \\ 0, & (\omega_1,\, \omega_2) \in \Omega_{ts} \end{cases} \tag{4.26b}$$

where Ω_{tp} and Ω_{ts} denote the passband and the stopband, respectively. Let $\mathbf{H}(j\omega_1, j\omega_2)$ be the frequency response of a $(2N_1+1) \times (2N_2+1)$ filter to be designed. By using the quadratical symmetry, we have $\mathbf{H}(j\omega_1, j\omega_2) = e^{-j(N_1\omega_1+N_2\omega_2)}\mathbf{h}_{ta}^T\mathbf{c}_{ta}(\omega_1,\, \omega_2)$. Let ζ_{tm} be an upper bound of the quadratic error function between the desired and the designed frequency

responses, then the SOCP optimization problem without considering the interpolation condition can be described as [47]

$$\underset{\mathbf{h}_{ta}}{\text{minimize}} \quad \zeta_{tm} \tag{4.27a}$$

$$\text{subject to} \quad \zeta_{tm} \geq W(\omega_1, \omega_2)\left[\mathbf{h}_{ta}^T \mathbf{c}_{ta}(\omega_1,\, \omega_2) - A_d(\omega_1, \omega_2)\right] \tag{4.27b}$$

$$\omega_i \in [-\pi, \pi] \quad \text{for } i = 1,\ 2$$

Since (4.27b) is a simple inequality constraint, it is equivalent to

$$\underset{\mathbf{h}_{ta}}{\text{minimize}} \quad \mathbf{q}^T\mathbf{x} \tag{4.28a}$$

$$\text{subject to} \quad \begin{bmatrix} \zeta_{tm} \\ \mathbf{h}_{ta}^T \mathbf{c}_{ta}(\omega_1,\, \omega_2) \end{bmatrix} - \begin{bmatrix} 0 \\ A_d(\omega_1, \omega_2) \end{bmatrix} \in \text{Scone}_2 \tag{4.28b}$$

where $W(\omega_1, \omega_2) = 1$, $\mathbf{q} = [1\ 0\ \cdots\ 0]^T$, and $\mathbf{x} = [\zeta_{tm}\ \mathbf{h}_{ta}^T]^T$. Note that the seconder-order cone constraint (4.28b) should hold for every available set of $(\omega_1,\, \omega_2)$. As usual, $(\omega_1,\, \omega_2)$ is represented by $\Omega = \left\{(\omega_1^{(r)},\, \omega_2^{(r)}),\ r = 1,\, 2,\, \cdots,\, R\right\}$. In analogy with the 1-D design, the interpolation condition can be realized by defining the coefficients which are supposed to be zero of $\mathbf{h}_{ta}$ belong to the free variables, namely,

$$\mathbf{G}_t\mathbf{x} \in \text{Fcone}_m \tag{4.29}$$

where $\mathbf{G}_t$ is the selection matrix, of which the formulation is described explicitly in Section 3.3.2 and a specific example is given in (3.36). In summary, the mini-max SOCP optimization problem for the design of linear-phase 2-D Mth-band FIR filters can be formulated as

$$\text{minimize} \quad \mathbf{q}^T\mathbf{x} \tag{4.30a}$$

$$\text{subject to} \quad \begin{bmatrix} \mathbf{G}_t \\ \mathbf{C}_t \end{bmatrix} \mathbf{x} - \begin{bmatrix} \mathbf{O}_n \\ \mathbf{A}_t \end{bmatrix} \in \left(\text{Fcone}_m \times \text{Scone}_2^{(R^2)}\right) \tag{4.30b}$$

where

$$\mathbf{C}_t = \begin{bmatrix} \mathbf{q}^T \\ \left[0 \;\; \mathbf{c}_{ta}^T(\omega_1^{(r)}, \omega_2^{(r)})\right] \end{bmatrix}, \quad \mathbf{A}_t = \begin{bmatrix} 0 \\ A_d(\omega_1^{(r)}, \omega_2^{(r)}) \end{bmatrix} \tag{4.30c}$$

$$\text{for } r = 1, 2, \cdots, R.$$

4.3.2 2-D Least-Square SOCP Design

In the 2-D equiripple least-square SOCP problem, the objective is to determine the impulse response $\mathbf{h}_{ta}$ such that the total squared error in the passband and stopband is minimized. The total weighted squared error can be written as

$$\begin{aligned} e_{tl} &= \int\int_{\Omega_t} W(\omega_1, \omega_2)\left[\mathbf{h}_{ta}^T\mathbf{c}_{ta}(\omega_1, \omega_2) - A_d(\omega_1, \omega_2)\right]^2 d\omega_1 d\omega_2 \\ &= \mathbf{h}_{ta}^T\mathbf{U}_t\mathbf{h}_{ta} - 2\mathbf{h}_{ta}^T\mathbf{u}_t + a_t \end{aligned} \tag{4.31a}$$

where $a_t \in \mathbf{R}$, $\mathbf{U}_t \in \mathbf{R}^{N_s \times N_s}$, $\mathbf{u}_t \in \mathbf{R}^{N_s}$ are in (3.39) with $N_s = (N_1+1)(N_2+1)$. Since $\mathbf{U}_t$ has a symmetric square root $\mathbf{U}^{1/2} \in \mathbf{R}^{N_s \times N_s}$, i.e., $\mathbf{U} = \mathbf{U}^{1/2}\mathbf{U}^{1/2}$ and $\mathbf{U}^{1/2} = \mathbf{U}^{T/2}$, (4.31a) can be further converted to

$$e_{tl} = \left\|\mathbf{U}_t^{1/2}\mathbf{h}_{ta} - \mathbf{U}_t^{-1/2}\mathbf{u}_t\right\|^2 - \lambda_t \tag{4.32}$$

where $\lambda_t = \|\mathbf{U}_t^{-1/2}\mathbf{u}_2\|^2 - a_t$. In the SOCP design, we denote ζ_{tl} as an upper bound of the square root of the e_{tl} to form the first second-order cone constraint, i.e.,

$$\zeta_{tl} \geq \sqrt{\left\|\mathbf{U}_t^{1/2}\mathbf{h}_{ta} - \mathbf{U}_t^{-1/2}\mathbf{u}_t\right\|^2 + (-\lambda_t)} \tag{4.33}$$

which leads to

$$\zeta_{tl} \geq \left\| \left[(\mathbf{U}_t^{1/2}\mathbf{h}_{ta} - \mathbf{U}_t^{-1/2}\mathbf{u}_t)^T \quad (-\lambda_t)^{1/2}\right]^T \right\| \tag{4.34}$$

Then, the equivalent cone express is given by

$$\begin{bmatrix} \zeta_{tl} \\ \mathbf{U}_t^{1/2}\mathbf{h}_{ta} \\ 0 \end{bmatrix} - \begin{bmatrix} 0 \\ \mathbf{U}_t^{-1/2}\mathbf{u}_t \\ (-\lambda)_t^{1/2} \end{bmatrix} \in \text{Scone}_{N_s+2} \tag{4.35}$$

Let ζ_p and ζ_p be the upper bounds of the passband and the stopband errors, respectively. The second-order cone constraints which are formulated based on the passband and stopband

errors can be written as

$$\begin{bmatrix} \zeta_{tp} \\ \begin{bmatrix} 0 & \mathbf{h}_{ta}^T \mathbf{c}_{ta}(\omega_1^{(r_p)}, \omega_2^{(r_p)}) \end{bmatrix} \\ \zeta_{ts} \\ \begin{bmatrix} 0 & \mathbf{h}_{ta}^T \mathbf{c}_{ta}(\omega_1^{(r_s)}, \omega_2^{(r_s)}) \end{bmatrix} \end{bmatrix} - \begin{bmatrix} 0 \\ A_d(\omega_1^{(r_p)}, \omega_2^{(r_p)}) \\ 0 \\ A_d(\omega_1^{(r_s)}, \omega_2^{(r_s)}) \end{bmatrix} \in \text{Scone}_2 \times \text{Scone}_2 \tag{4.36}$$

where the frequencies in passband and stopband are defined as $\{(\omega_1^{(r_p)}, \omega_2^{(r_p)}),\ 1 \leq r_p \leq R_p\}$ and $\{(\omega_1^{(r_s)}, \omega_2^{(r_s)}),\ 1 \leq r_s \leq R_s\}$, respectively. Note that minimizing the ζ_{tl}, ζ_{tp}, and ζ_{ts} separately here amounts to minimizing their sum. As such, the equiripple least-square SOCP design for 2-D linear-phase Mth-band filters is finally given by

$$\text{minimize} \quad \mathbf{q}^T \mathbf{x} \tag{4.37a}$$

$$\text{subject to} \quad \begin{bmatrix} \mathbf{G}_t \\ \mathbf{C}_{tl} \\ \mathbf{C}_{tm} \end{bmatrix} \mathbf{x} - \begin{bmatrix} \mathbf{O}_n \\ \mathbf{V}_t \\ \mathbf{A}_t \end{bmatrix} \in \left(\text{Fcone}_m \times \text{Scone}_{N_s+2} \times \text{Scone}_2^{(R_p^2+R_s^2)}\right) \tag{4.37b}$$

where $\mathbf{x} = [\zeta_l \ \ \zeta_p \ \ \zeta_s \ \ \mathbf{h}_{ta}^T]^T$ is the optimization variable, $\mathbf{q} = [1 \ 1 \ 1 \ 0 \ \cdots \ 0]^T$, and $\mathbf{O}_n = [0 \ 0 \ \cdots \ 0]$. The second-order cone constraint with respect to the quadratic least-square error is given by

$$\mathbf{C}_{tl} = \begin{bmatrix} \mathbf{q}_1^T \\ [\mathbf{O}_3 \ \mathbf{U}_t^{1/2}] \\ 0 \end{bmatrix}, \qquad \mathbf{V}_t = \begin{bmatrix} 0 \\ \mathbf{U}_t^{-1/2}\mathbf{u}_t \\ (-\lambda_t)^{1/2} \end{bmatrix} \tag{4.37c}$$

where $\mathbf{q}_1 = [1 \ 0 \ 0 \ \cdots \ 0]^T$, $\mathbf{O}_3 = [0 \ 0 \ 0]$, and $\mathbf{U}_l^{1/2}$, $\mathbf{u}_l$ and λ_l are given in (4.35). The second-order constraints with respect to the passband and stopband errors are expressed as

$$\mathbf{C}_{tm} = \begin{bmatrix} \mathbf{q}_2^T \\ [\mathbf{O}_3 \ \mathbf{c}_a^T(\omega_1^{(r_p)}, \omega_2^{(r_p)})] \\ \mathbf{q}_3^T \\ [\mathbf{O}_3 \ \mathbf{c}_a^T(\omega_1^{(r_s)}, \omega_2^{(r_s)})] \end{bmatrix}, \qquad \mathbf{A}_t = \begin{bmatrix} 0 \\ A_d(\omega_1^{(r_p)}, \omega_2^{(r_p)}) \\ 0 \\ A_d(\omega_1^{(r_s)}, \omega_2^{(r_s)}) \end{bmatrix} \tag{4.37d}$$

where $\mathbf{q}_2 = [0 \ 1 \ 0 \ \cdots \ 0]^T$, $\mathbf{q}_3 = [0 \ 0 \ 1 \ \cdots \ 0]^T$.

In summary, the SOCP problems for the design of linear-phase Mth-band filters based on the mini-max and least-square error criteria have been thus far established. Although the SOCP approach as we mentioned earlier is supposed to be better than the SDP approach owing to its better worst-case complexity for the second order cone constraint, it is observed from the above analysis that the SOCP formulation for the filter design is more complex than that of the SDP. All the constraints in a SOCP problem should be formulated in a

structure, which could increase the computational complexity, especially for the 2-D Mth-band filter design. We will verify if the SOCP approach is better than the SDP approach through several examples.

4.4 Numerical Examples

In this section, several linear-phase Mth-band filters are designed via the proposed SOCP approach. Some of the design results are compared with those achieved via the SDP approach in terms of the maximum error as well as the computational complexity. The designed filters will also be used as interpolation filters for image resizing.

The SOCP optimization problems are also implemented by the SeDuMi package under the MATLAB circumstance [27]. When a SOCP filter design problem is modeled as the standard form of (4.13), (4.25), (4.30), or (4.37), SeDuMi provides a structure K to accommodate all the cone constraints and differentiate them through the following instructions:

(1) $K.f$ denotes the dimensions of the free vector constraints (4.15).

(2) $K.l$ denotes the dimensions of the linear inequality constraints (4.2).

(3) $K.q$ denotes the dimensions of the second-order cone constraints (4.1).

(4) $K.r$ denotes the dimensions of the rotated quadratic cone constraints (4.4).

(5) $K.s$ denotes the dimensions of the positive semidefiniteness constraints.

Notice that the free vector constraint is always put on the top in the whole constraint structure, such as in (4.13), (4.25), (4.30), and (4.37). With this constraint structure, several convex optimization problems can be cast as the SOCP problems and then solved efficiently

by the SeDuMi. However, the SOCP formulation is much difficult than that of the SDP in the SeDuMi, since all the constraints in the K structure should be stacked in order and without overlaping or dislocation.

Example 4.1

In this example, we employ both the SOCP and the SDP approach to design the same fifth-band filter with different taps to demonstrate the priority of the SOCP approach. The designed filter has the frequency specifications as: $\omega_p = 0.15\pi$ and $\omega_s = 0.25\pi$. The maximum errors and execution time of the half-band filters with different taps designed via the SOCP and the SDP approaches are given in Table 4.1. As expected, the SOCP approach gives the same maximum errors but with the considerable savings on the computational time as compared to the SDP approach. The amplitude response of the 55-tap filter designed via the SOCP are depicted along with the ideal amplitude response in Fig. 4.2(a) and 4.2(b). The plots of the amplitude response in dB and linear phase response in rad are given in Fig. 4.3(a) and 4.3(b), respectively.

Table 4.1: Comparison of maximum errors and execution time for fifth-band filters designed via the SDP and the SOCP approaches

	Maximum error		Execution time (seconds)	
Filter length	SDP	SOCP	SDP	SOCP
$N = 37$	0.0121	0.0121	1.1560	0.3438
$N = 57$	0.0022	0.0022	1.2344	0.3906
$N = 77$	3.9789e-004	3.9789e-004	1.2343	0.6563
$N = 97$	7.7114e-005	7.7034e-005	1.5156	1.0469
$N = 117$	1.5477e-005	1.5399e-005	1.5316	1.0938

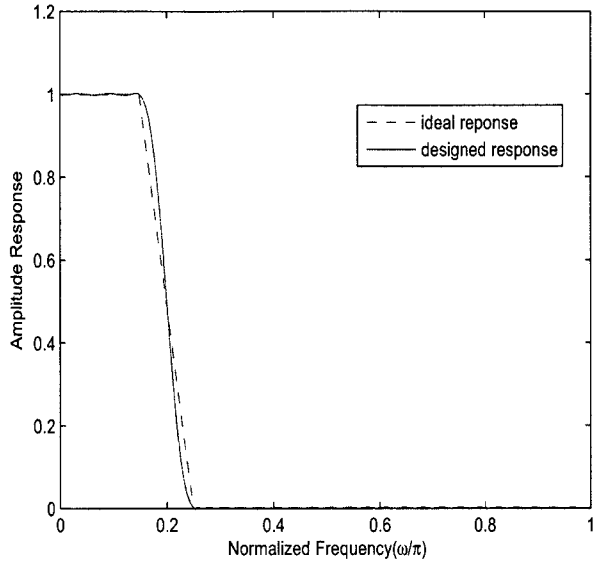

(a)

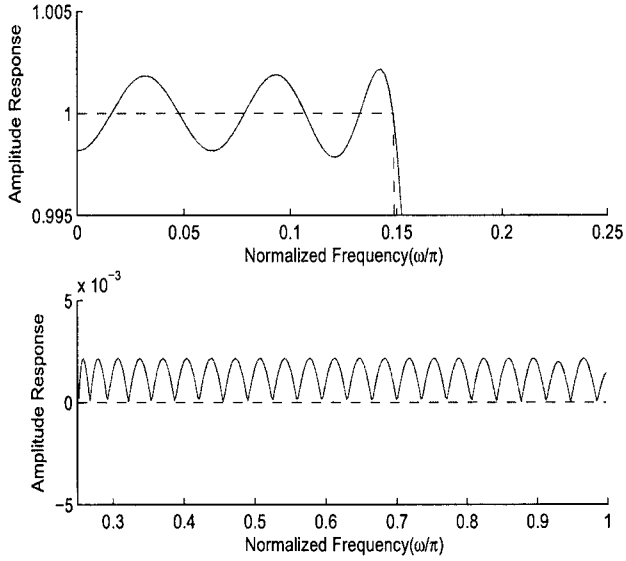

(b)

Figure 4.2: The fifth-band filter designed in *Example 4.1*. (a) Actual amplitude response vs. the ideal specification. (b) Passband and stopband amplitude errors.

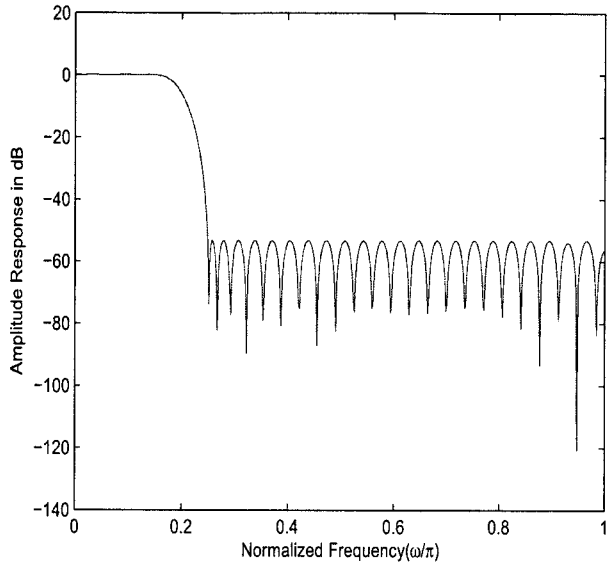

(a)

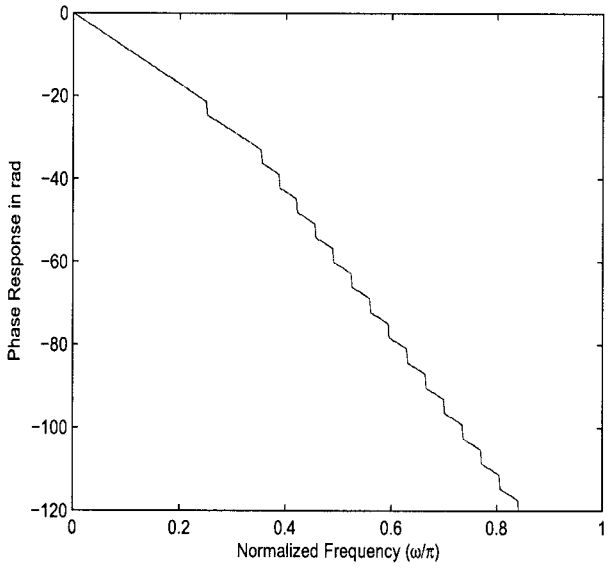

(b)

Figure 4.3: The fifth-band filter designed in *Example 4.1*. (a) Amplitude response in dB. (b) Linear-phase response in rad.

Example 4.2

Here, we employ the SOCP approach to design a 53-tap linear-phase third-band band-pass filter based on the least-square error criterion. According to the cutoff frequency constraint of band-pass Mth-band filter (2.16), i.e., $(\omega_{p1}+\omega_{s1})/2 = \pi/3$ and $(\omega_{p2}+\omega_{s2})/2 = 2\pi/3$, the frequency specifications are set as $\omega_{s1} = \pi/3 - 0.05$, $\omega_{p1} = \pi/3 + 0.05$, $\omega_{p2} = 2\pi/3 - 0.05$, and $\omega_{s2} = 2\pi/3 + 0.05$. The design results are depicted in Fig. 4.4(a), 4.4(b), 4.5(a) and 4.5(b). The maximum least-quare error for this band-pass design is 0.6164 and the maximum pass-band and stop-band approximation errors are 0.0039 and 0.0043, respectively. The execution time is 0.4688 seconds. It can be conclude that the equiripple least-square SOCP design is appropriate for various Mth-band filters.

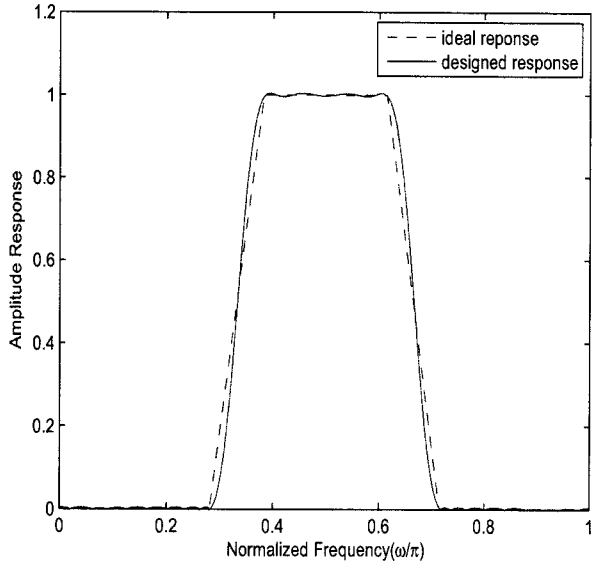

(a)

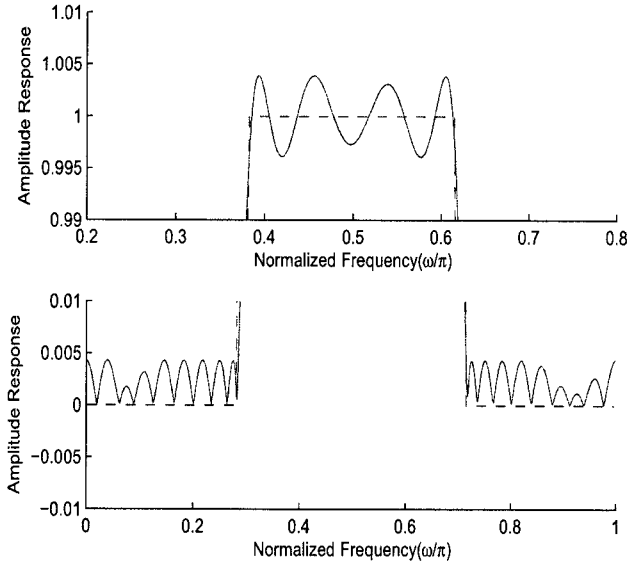

(b)

Figure 4.4: The third-band band-pass filter designed in *Example 4.2*. (a) Actual amplitude response vs. the ideal specification. (b) Passband and stopband amplitude errors.

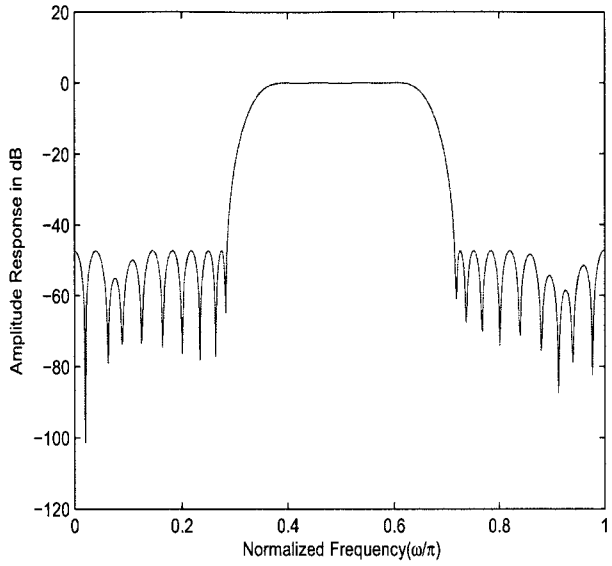

(a)

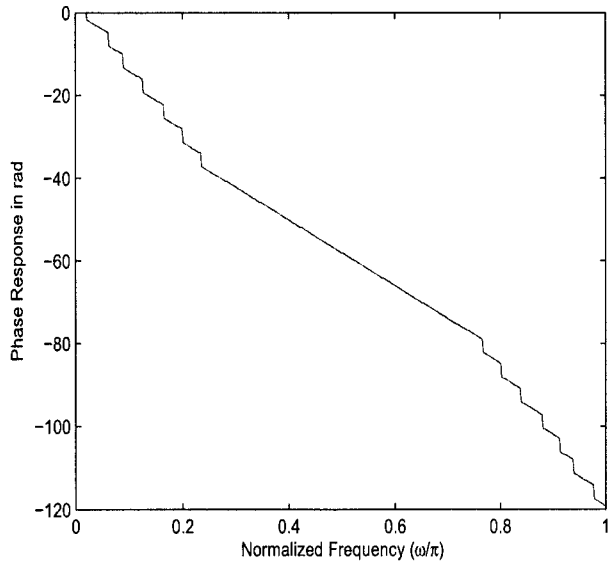

(b)

Figure 4.5: The third-band band-pass filter designed in *Example 4.2*. (a) Amplitude response in dB. (b) Linear-phase response in rad.

Example 4.3

In this example, we would like to demonstrate that the proposed approaches can be used to design 2-D filters with arbitrary amplitude responses. Thus, the 2-D linear-phase 41×37 Mth-band filters with different amplitude responses are directly designed via the mini-max SOCP approach and compared with those met by the mini-max SDP approach. For convenience, we choose the same interpolation coefficients as *Example 3.3*, i.e., $M_1 = 3$ and $M_2 = 5$. The frequency specifications are thus given as $\omega_{1_p} = \pi/3 - 0.05$, $\omega_{1_s} = \pi/3 + 0.05$ and $\omega_{2_p} = \pi/5 - 0.05$, $\omega_{2_s} = \pi/5 + 0.05$. The simulation results confirm that both the SOCP and the SDP approaches are appropriate for the design of 2-D linear-phase Mth-band filters with arbitrary amplitude responses. The plots of the different amplitude responses are depicted in Fig. 4.6 and 4.7, respectively. It is observed from the Table 4.2 that the simulation results of the SDP design is better than the SOCP design. In order

Table 4.2: Comparison of maximum errors and execution time for the 2-D Mth-band filters designed via the SDP and the SOCP approaches

	Maximum error		Execution time (seconds)	
Amplitude response	SDP	SOCP	SDP	SOCP
$A_d = 1$	0.0297	0.0303	31.1459	65.5469
$A_d = 2$	0.0595	0.0606	35.4846	65.5313
$A_d = 3$	0.0892	0.0908	30.5912	65.4688

to further confirm this view, the filter of the unity amplitude response is designed by the two approaches with different sizes. The data in Table 4.3 show that the SDP approach can produce a nearly optimal filter with better maximum errors but less computational times

than the SOCP approach. Furthermore, when the filter size is bigger, the difference of the execution times between these two approaches is more obvious. Based on this analysis, we can conclude that the SOCP is not competitive to design 2-D Mth-band filters from the perspective of the design complexity and the performance of the frequency responses.

Table 4.3: Comparison of maximum errors and execution time for the 2-D Mth-band filters designed via the SDP and the SOCP approaches

	Maximum error		Execution time (seconds)	
Filter size	SDP	SOCP	SDP	SOCP
$N_1 = 10, N_2 = 12$	0.1113	0.1139	8.1717	8.3125
$N_1 = 15, N_2 = 15$	0.0563	0.0580	14.7056	23.4375
$N_1 = 20, N_2 = 18$	0.0297	0.0303	31.3903	65.5469
$N_1 = 25, N_2 = 21$	0.0096	0.0131	41.2541	135.8906

Example 4.4

Although the SOCP does not seem to be better than the SDP in 2-D Mth-band filter design, we still give an example to demonstrate the feasibility of the 2-D equiripple least-square SOCP design. The same filter designed in *Example 3.4* is considered here again, i.e., the interpolation coefficients are $M_1 = 4$ and $M_2 = 2$. The frequency specifications are set as $\omega_{1_p} = 0.2\pi$, $\omega_{1_s} = 0.3\pi$, $\omega_{2_p} = 0.4\pi$, and $\omega_{2_s} = 0.6\pi$. The simulation results are shown in Fig. 4.8. The maximum least-square, passband and stopband errors are 3.0846, 0.0809, and 0.0288, respectively, which are similar to the SDP design. However, it spents more time than the SDP, that is 55.8906 seconds.

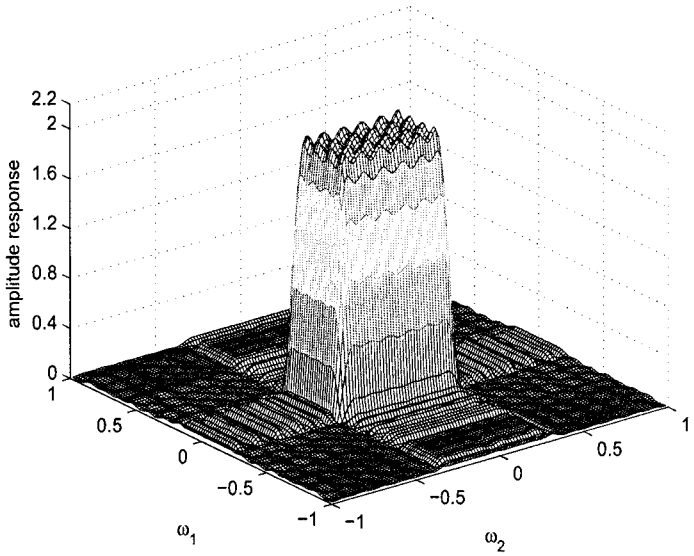

(a)

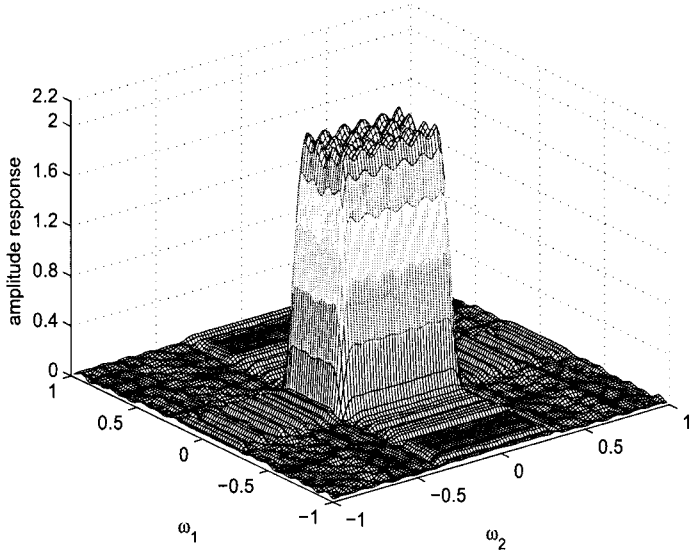

(b)

Figure 4.6: Amplitude response of 2 for the 2-D Mth-band filter in *Example 4.3*. (a) Using the SOCP approach. (b) Using the SDP approach.

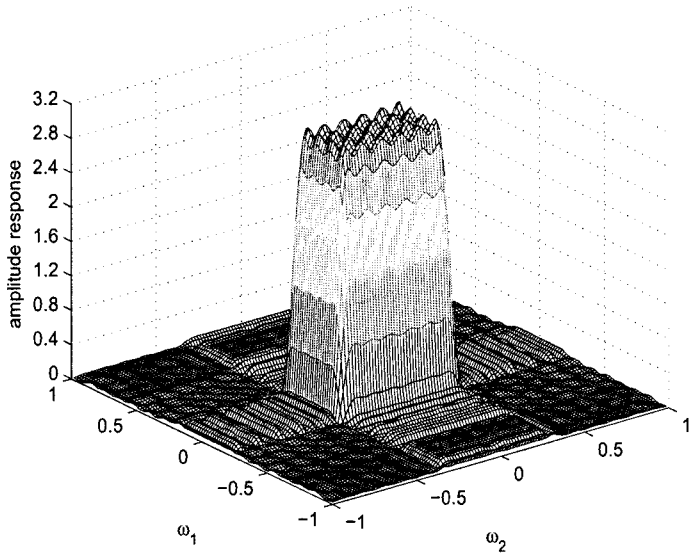

(a)

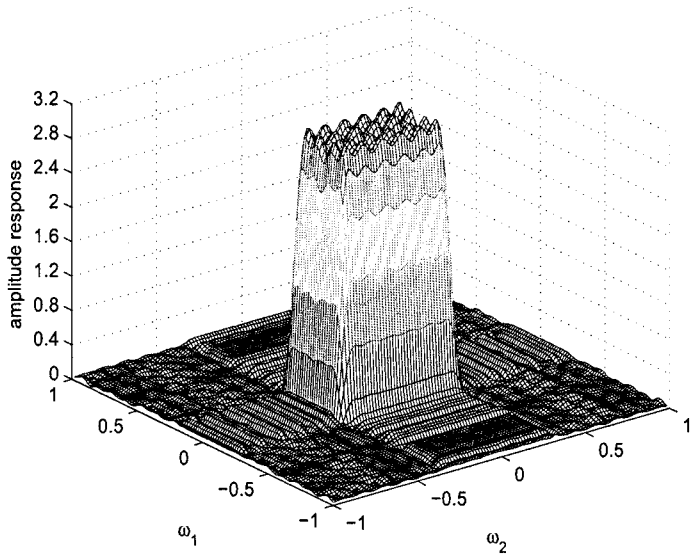

(b)

Figure 4.7: Amplitude response of 3 for the 2-D Mth-band filter in *Example 4.3*. (a) Using the SOCP approach. (b) Using the SDP approach.

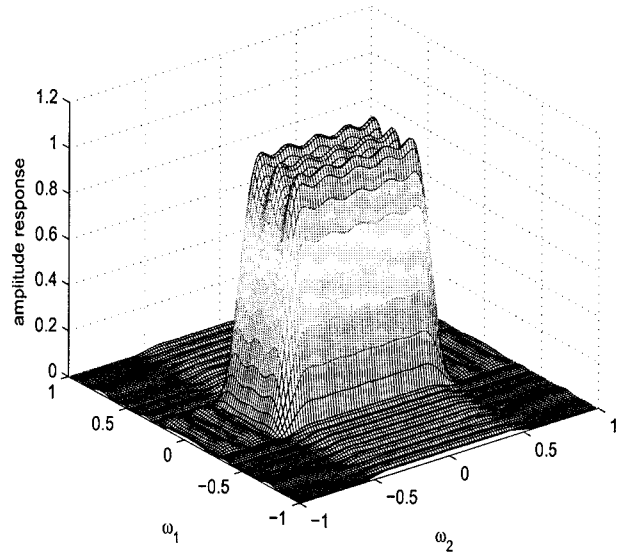

(a)

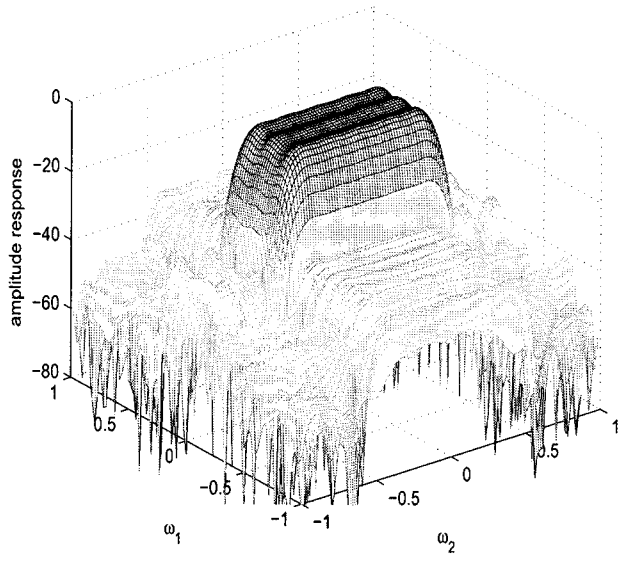

(b)

Figure 4.8: The Mth-band filter designed in *Example 4.4* via the SOCP. (a) Amplitude response in linear value. (b) Amplitude response in dB.

Example 4.5

Here, both the 1-D and 2-D Mth-band filters designed via the SOCP approach are applied in the multirate system in Fig. 1.1 to resize a test image. We employ the same frequency specifications and test images as in Chapter 3. The PSNR of the interpolated images in Table 4.4 confirms that the Mth-band filters designed via the SOCP approach also have a good interpolation property. The interpolated images are depicted in Fig. 4.9, 4.10 and 4.11, respectively.

Table 4.4: Comparison of PSNR for the interpolated images achieved through the 1-D and 2-D Mth-band filter designed via the SOCP approach

	The peak signal-to-noise ratio (PSNR)	
Test image	1-D Mth-band filter	2-D Mth-band filters
Lena	35.1429	35.1318
Girl (Elaine)	32.9976	33.0011
Fishing Boat	30.9903	30.9746

4.5 Conclutions

In this chapter, the SOCP optimization method has been studied for the design of Mth-band filters, showing its better computational complexity for solving the second-order cone constraint. The SOCP optimization problems have been modeled based on both the minimax and least-square error criteria. The performance of this approach in the design of 1-D and 2-D Mth-band filters has been evaluated, and the simulation results have been compared with the SDP approach. It has been demonstrated that the SOCP approach can

(a)

(b)

Figure 4.9: The interpolated image with a low level of detail. (a) Using 1-D Mth-band filter. (b) Using 2-D Mth-band filter.

(a)

(b)

Figure 4.10: The interpolated image with a medium level of detail. (a) Using 1-D Mth-band filter. (b) Using 2-D Mth-band filter.

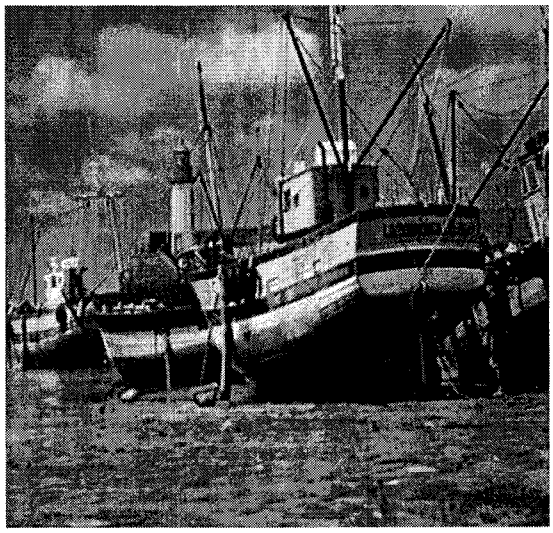

(a)

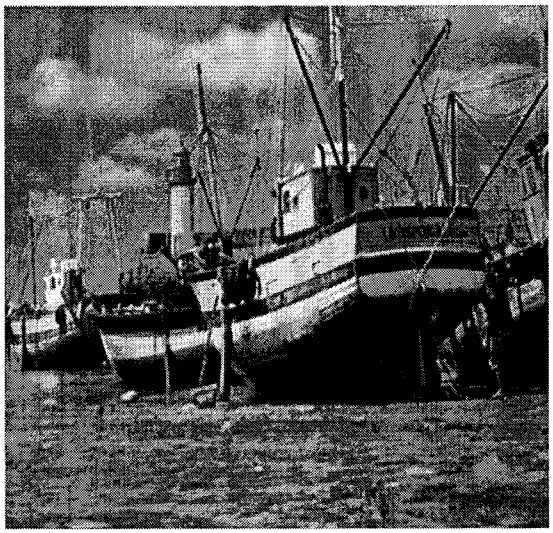

(b)

Figure 4.11: The interpolated image with a relatively large amount of detail. (a) Using 1-D Mth-band filter. (b) Using 2-D Mth-band filter.

achieve the same maximum error but needs much less execution times for the 1-D Mth-band filter design as compared to the SDP approach. On the other hand, the SDP approach is preferable in the design of 2-D Mth-band filters due to its high efficiency and easy formulation. Finally, it has been shown that both 1-D and 2-D linear-phase Mth-band filters designed via the SOCP approach have good interpolation property.

Chapter 5

Conclusions and Future Work

5.1 Summary

In this thesis, the convex cone optimization technique has been investigated for the design of linear-phase Mth-band FIR filters, owing to its powerful optimization capability as well as flexibility in accommodating the time-domain interpolation condition. The designed filters have been evaluated in terms of the approximation accuracy of their frequency responses and their application in image interpolation. It has been verified through computer simulations that the proposed approaches result in a designed filter having optimal or nearly optimal frequency responses and satisfying the exact interpolation condition.

The first chapter has reviewed some existing optimization methods for the design of FIR digital filters. It has been shown that neither the Parks and Mclellan program nor the eigenfilter approach can offer a direct design of Mth-band filters, which is the main motivation of the proposed work.

Chapter 2 has introduced fundamentals of three classes of Mth-band filters, including the time-domain interpolation condition and the cutoff frequency constraint. The relations between the interpolation condition and the frequency specifications for each class have been explained in detail. Besides, the restriction of the interpolation matrix $\mathbf{M}$ for the 2-D linear-phase diamond-shaped Mth-band filters have been given based on the interpolation condition and the symmetry of 2-D impulse responses.

In Chapter 3, a semidefinite programming (SDP) optimization approach has been developed for the design of linear-phase Mth-band FIR filters with an emphasis on accommodating the interpolation condition. The SDP optimization design problem has been formulated based on both the mini-max and the least-square error criteria. It has been shown through several design examples that the SDP approach can offer optimal or nearly optimal frequency responses of designed filters with a considerably reduced computational complexity. Besides, the designed Mth-band filters have been applied to image interpolation. The high perceptual quality of the interpolated images indicates that both 1-D and 2-D linear-phase Mth-band filters designed via the SDP approach have good interpolation property.

Finally in Chapter 4, a second-order cone programming (SOCP) approach has been studied as an alternative for the design of linear-phase Mth-band FIR filters. The SOCP optimization problem has been also modeled based on both the mini-max and the least-square error criteria. The design performance as well as the computational complexity of the SOCP approach as compared to the SDP approach have been investigated through numerical examples. It has been demonstrated that the SOCP approach can achieve the

same maximum error but needs much less execution time in the 1-D Mth-band filter design as opposed to the SDP approach. However, the SDP approach is preferable in the design of 2-D Mth-band filters due to its high efficiency and easy formulation. Moveover, the Mth-band filters designed via the SOCP approach have also shown a high subjective interpolation quality in image resizing.

5.2 Future Research

On the basis of the SDP and the SOCP optimization problems modeled for the design of linear-phase Mth-band filters, the future work could target on how to extend the SDP and the SOCP approaches for the design of nonlinear-phase Mth-band filters, or even other classes of filters with specific requirements. Moreover, employing the SDP and the SOCP to directly design the multidimensional **M**th-band filters is perhaps another interesting but challenging task.

References

[1] A. Antoniou, *Digital signal processing*. McGraw-Hill Companies, Inc., 2005.

[2] A. Antoniou, "New improved method for the design of weighted- chebyshev, nonrecursive, digital filters," *IEEE Transactions on. Circuits and Systems*, vol. 30, pp. 740 – 750, Oct. 1983.

[3] J. McClellan, T. Parks, and L. Rabiner, "A computer program for designing optimum fir linear phase digital filters," *IEEE Transactions on. Audio and Electroacoustics*, vol. 21, pp. 506 – 526, Dec. 1973.

[4] F. Mintzer, "On half-band, third-band, and nth-band fir filters and their design," *IEEE Transactions on. Acoustics, Speech and Signal Processing*, vol. 30, pp. 734 – 738, Oct. 1982.

[5] P. Vaidyanathan and T. Nguyen, "A 'trick' for the design of fir half-band filters," *IEEE Transactions on. Circuits and Systems*, vol. 34, pp. 297 – 300, Mar. 1987.

[6] P. Vaidyanathan and T. Nguyen, "Eigenfilters: A new approach to least-squares fir filter design and applications including nyquist filters," *IEEE Transactions on. Circuits*

and Systems, vol. 34, pp. 11 – 23, Jan. 1987.

[7] T. Nguyen, "The design of arbitrary fir digital filters using the eigenfilter method," *IEEE Transactions on. Signal Processing*, vol. 41, pp. 1128 –1139, Mar. 1993.

[8] Y. Wisutmethangoon and T. Nguyen, "A method for design of mth-band filters," *IEEE Transactions on. Signal Processing*, vol. 47, pp. 1669 –1678, Jun 1999.

[9] L. Vandenberghe and S. Boyd, "Semidefinite programming," *SIAM Review*, vol. 38, pp. 49–95, Mar. 1996.

[10] R. S. H. Wolkowicz and L. Vandenberghe, *Handbook of Semidefinite Programming: Theory, Algorithms, and Applications*. Kluwer Academic, New York, 2000.

[11] T. T. H. Frenk, K. Roos and S. Z. Zhang, *High performance optimization*. Kluwer Academic, New York, 2000.

[12] S. B. M. S. Lobo, L. Vandenberghe and H. Lebret, "Applications of second-order cone programming," Jua. 1998.

[13] F. Alizadeh and D. Goldfarb, *Second-order cone programming*, vol. 95. Springer Berlin / Heidelberg, 2003.

[14] S. Oraintara and T. Nguyen, "A simple mapping between mth-band fir filters using cosine modulation," *IEEE Transactions on. Signal Processing Letters*, vol. 10, pp. 125 – 128, May 2003.

[15] O. Gustafsson and H. Johansson, "Complexity comparison of linear-phase mth-band and general fir filters," *IEEE International Symposium on. Circuits and Systems*, pp. 2335 –2338, May. 2007.

[16] J. Nohrden and T. Nguyen, "Constraints on the cutoff frequencies of mth-band linear-phase fir filters," *IEEE Transactions on. Signal Processing*, vol. 43, pp. 2401 –2405, Oct. 1995.

[17] M. Swamy and P. Rajan, *Symmetry in two-dimensional filters and its applications*, pp. 401–468. Multidimensional Systems: Techniques and Applicaitons, s.g. tzafestas ed., 1986.

[18] W. Zhu, Z. He, M. Ahmad, and M. Swamy, "Design of centrally symmetric 2-d fir fan filters using the mcclellan transform," *1992 IEEE International Symposium on. Circuits and Systems*, vol. 3, pp. 1428 –1431, May. 1992.

[19] H. Reddy, I. Khoo, and P. Rajan, "2-d symmetry: theory and filter design applications," *IEEE Transactions on. Circuits and Systems Magazine*, vol. 3, no. 3, pp. 4 – 33, 2003.

[20] D. E. Dudgeon and R. M. Mersereau, *Multidimensional digital signal processing.* Englewood Cliffs, NJ: Prentice Hall, 1984.

[21] W.-S. Lu, "A unified approach for the design of 2-d digital filters via semidefinite programming," *IEEE Transactions on. Circuits and Systems I: Fundamental Theory and Applications*, vol. 49, pp. 814 –826, Jun 2002.

[22] P. P. Vaidyanathan, *Multirate Systems and Filter Banks*, vol. 95. Englewood Cliffs, NJ: Prentice Hall, 1993.

[23] P. Patwardhan and V. Gadre, "Design of 2-d mth-band lowpass fir eigenfilters with symmetries," *IEEE Transactions on. Signal Processing Letters*, vol. 14, pp. 517 –520, Aug. 2007.

[24] Q. Saifee, P. Patwardhan, and V. Gadre, "On parallelepiped-shaped passbands for multidimensional nonseparable **m** th-band low-pass filters," *IEEE Transactions on. Circuits and Systems II: Express Briefs*, vol. 55, pp. 786 –790, Aug. 2008.

[25] T. Roh, B. Dumitrescu, and L. Vandenberghe, "Interior-point algorithms for sum-of-squares optimization of multidimensional trigonometric polynomials," *IEEE International Conference on. Acoustics, Speech and Signal Processing*, vol. 3, pp. III–905 –III–908, Apr. 2007.

[26] A. Karmakar, A. Kumar, and R. Patney, "Design of an optimal two-channel orthogonal filterbank using semidefinite programming," *IEEE Transactions on. Signal Processing Letters*, vol. 14, pp. 692 –694, Oct. 2007.

[27] J. F. Sturm, "Using SeDuMi 1.02, a matlab toolbox for optimization over symmetric cones (update for version 1.05)." `http://www.optimization-online.org/DB_HTML/2001/10/395.html`.

[28] "Dual linear program." `http://en.wikipedia.org/wiki/Dual_linear_program`.

[29] W.-S. Lu, "Semidefinite programming: a versatile tool for analysis and design of digital filters," *1999 IEEE Canadian Conference on. Electrical and Computer Engineering*, vol. 2, pp. 745 –750, 1999.

[30] Z. Lin and Y. Liu, "Fir filter design with group delay constraint using semidefinite programming," *2006 IEEE International Symposium on. Circuits and Systems*, 2006.

[31] C. Wu, W.-P. Zhu, and M. Swamy, "Some new results in the design of mth-band fir filters," *The 2004 47th Midwest Symposium on. Circuits and Systems*, vol. 2, pp. II–53 – II–56, 2004.

[32] W.-S. Lu, "Design of fir digital filters with discrete coefficients via convex relaxation," *IEEE International Symposium on. Circuits and Systems*, vol. 2, pp. 1831 – 1834, May. 2005.

[33] X. Lai, J. Wang, and Z. Xu, "A new minimax design of two-dimensional fir filters with reduced group delay," *IEEE Transactions on. Asian Control Conference*, pp. 610 –614, Aug. 2009.

[34] K. Fanian, H. Tuan, and T. Nguyen, "Efficient design of 2-d nonseparable filters of low complexity," *2009 16th IEEE International Conference on. Image Processing (ICIP)*, pp. 4001 –4004, Nov. 2009.

[35] Y. D. Peaucelle, D. Henrion and K. Taitz, "User's Guide for SEDUMI INTERFACE 1.04." `http://homepages.laas.fr/peaucell/software/sdmguide.pdf`.

[36] R. C. Gonzalez and R. E. Woods, *Digital image processing.* Prentice-Hall, New Jersey, 2002.

[37] S. Yang and T. Nguyen, "Interpolated mth-band filters for image size conversion," *IEEE Transactions on. Signal Processing*, vol. 50, pp. 3028 – 3035, Dec. 2002.

[38] C. Wu, *Polyphase Structure-Based Approaches for FIR Mth-band Filters and Constrained Filter Bank: Design, Implementation and Applications.* 2007.

[39] "Conic Optimization." `http://www.solver.com/probconic.htm`.

[40] A. Mutapcic, S.-J. Kim, and S. Boyd, "Robust chebyshev fir equalization," *IEEE Transactions on. Global Telecommunications Conference*, pp. 3074 –3079, Nov. 2007.

[41] Y. Nesterov and A. Nemirovsky, *Interior-Point polynomial methods in convex programming*, vol. 13. SIAM, Philadelphia, 1994.

[42] W.-S. Lu and T. Hinamoto, "Optimal design of fir frequency-response-masking filters using second-order cone programming," *2003 International Symposium on. Circuits and Systems*, vol. 3, pp. III–878 – III–881, May. 2003.

[43] K. Tsui, S. Chan, and K. Yeung, "Design of fir digital filters with prescribed flatness and peak error constraints using second-order cone programming," *IEEE Transactions on. Circuits and Systems II: Express Briefs*, vol. 52, pp. 601 – 605, Sept. 2005.

[44] S. Yan and Y. Ma, "A unified approach for optimal design of fir filters with arbitrary frequency response," *2004 7th International Conference on. Signal Processing*, vol. 1, pp. 93 – 96, Aug. 2004.

[45] W.-S. Lu and T. Hinamoto, "Design of frequency-response-masking fir filters using socp with coefficient sensitivity constraint," *IEEE International Symposium on. Circuits and Systems*, pp. 2442 –2445, May. 2008.

[46] D. Scholnik, "Mixed-norm fir filter optimization using second-order cone programming," *IEEE International Conference on. Acoustics, Speech, and Signal Processing*, vol. 2, pp. 1525 –1528, 2002.

[47] W.-S. Lu and T. Hinamoto, "A second-order cone programming approach for minimax design of 2-d fir filters with low group delay," *2006 IEEE International Symposium on. Circuits and Systems*, 2006.